Engineered Materials for Improving Cancer Immunotherapy

Engineered Materials for Improving Cancer Immunotherapy

A dissertation presented

by

Alexander Sing Cheung

to

The John A. Paulson School of Engineering and Applied Sciences

in partial fulfillment of the requirements

for the degree of

Doctor of Philosophy

in the subject of

Engineering Sciences

Harvard University

Cambridge, Massachusetts

December 2016

Professor David J. Mooney Alexander Sing Cheung

Engineered Materials for Improving Cancer Immunotherapy

Abstract

Immunotherapy, the treatment of disease through targeted activation of the immune system, has recently shown unprecedented clinical success for diverse malignancies. In contrast to traditional cancer treatments, which are associated with widespread off-target toxicity and frequent disease recurrence, successful cancer immunotherapies promote an adaptive immune response that is both cancer-specific and highly durable. Nevertheless, many cancer immunotherapy approaches elicit suboptimal responses or are nonfunctional for a large patient population. Although there are many reasons for this that are tied to our incomplete understanding of the immune system, a key limitation common to many cancer immunotherapy approaches relates to the lack of spatiotemporal control with which immune-directing cues are presented to the immune system. Designing biomaterials to interface these cues with the immune system in a spatiotemporally controlled manner is a promising way to improve current cancer immunotherapies.

The general goal of this thesis was to develop materials to improve the spatiotemporal presentation of cues to the immune system as a means of eliciting a more robust response. Specifically, this thesis describes two approaches for improving distinct types of cancer immunotherapy: (1) a method for processing cancer cells that co-localizes native cancer antigens and adjuvants in particles that can be used for cancer vaccination, and (2) the use of an antigen-presenting cell-mimetic material that rapidly expands functional T cells for adoptive T cell transfer. We demonstrate that by designing these systems to present the respective immune-

directing cues in a spatiotemporal pattern that mimics how the cues are naturally presented, a stronger response can be elicited from the immune system. Broadly, the results presented in this thesis illustrate the importance of presenting cues to the immune system in an appropriate spatiotemporal context, and show how biomaterials can be designed to facilitate this. Specifically, this thesis describes two potentially translatable systems that could be used to improve current approaches for therapeutic cancer vaccination and adoptive T cell transfer.

Table of Contents

Acknowledgements

Graduate school was a challenging time for me, and I would not have made it through without the support of my family and friends. To everyone that supported me at some point during this journey: Thank You.

In particular, I want express my sincerest gratitude to Dr. David Mooney. Dave, I don't know how you do it. Through your insanely busy schedule and constant travel, you make time for every one of your students on a regular basis. You care about us all not only as scientists, but as people. Meeting with you always renewed my enthusiasm for research, even when my own work wasn't going well. Throughout graduate school, I experienced long durations of failed experiments, but you always encouraged me to continue trying. During a particularly difficult time, the advice you gave me helped me move past the noise. Dave, thank you for seeing my potential, and giving me the opportunity to work in your lab. Thank you for the mentorship and friendship you gave me over the past 8 years.

Secondly, I want to express my gratitude to Sandeep Koshy. Sandeep, you are awesome. I would not have made it through graduate school without your advice and friendship. Like many people, you were there to celebrate with me during the good times, but unlike most, you also supported me during the difficult times. I also want to thank Lata Grover. Lata, you are an amazing human being. During a time when I felt pessimistic about many things, getting to know you restored my optimism.

Thirdly, I want to thank all the members of the Mooney Lab. I have been through many generations of the lab, and have enjoyed working with every one. Everyone that Dave brings into the lab is a talented scientist, but beyond that, also an amazing person. I appreciate all the

extremely insightful scientific discussions we had, as well as the times we spent together outside of the lab. In particular, I want to thank David Zhang for helping with very large, critical experiments during my last few months in the lab. David, your work ethic is admirable, and your unwavering optimism is truly inspiring. I would also like to thank Dr. Rajiv Desai, Dr. Pascal Joly, Dr. Simon Young, Dr. Omar Ali, Dr. Manav Mehta, Dr. Adam Celiz, Dr. Luo Guo, Dr. Catia Verbeke, Aileen Li, Maxence Dellacherie, Angelo Mao, Dr. Nisarg Shah, Dr. Lan Cao, Dr. Jaeyun Kim, Brian Kwee, Dr. Deniz Yuksel, Dr. Anne-Laure Papa, Dr. Ovi Chaudhuri, Dr. Kyle Vining, Adriana Martinez Ledo, and Dr. Daniel Rubin for valuable scientific discussions, and invaluable friendship. I am also thankful to all the other members of the lab and denizens of the Wyss Institute that I had the pleasure to get to know, and to work with over the years: Dr. Eduardo Silva, Dr. Erin Anderson, William Whyte, Sarah Lewin, Alexander Stafford, Ed Doherty, Chris Johnson, Des White, Garry Cuneo, David Luna, Dr. Robert Staruch, Dr. Steve Perrault, Sauveur Jeanty, Dr. Maartje Bastings, Dr. Gail Chan, Dr. Nathaniel Huebsch, Dr. Warren Sands, Dr. Cathal Kearney, Dr. Darinka Klumpers, Dr. Praveen Arany, Dr. Christine Cezar, Dr. Dima Shvartsman, Dr. Thomas Braschler, Max Darnell, Dr. Yevgeny Brudno, Dr. Jae-Won Shin, Dr. Xuanhe Zhao, Dr. Cristiana Cunha, Dr. Steve Kennedy, Anu Kodiyan, Dr. Kangwon Lee, Dr. Evi Lippens, Dr. Beverly Lu, Theresa Raimondo, Ting-Yu Shih, Dr. Hadas Skaat, Dr. Will Yuen, Dr. Sidi Bencherif, Dr. Hua Wang, Kwasi Adu-Berchie, and Alexander Najibi.

I also want to thank my committee members, Dr. Neel Joshi and Dr. Michael Goldberg, for making time to attend my committee meetings and defense, and for providing insightful feedback and guidance along the way. Additionally, I want to thank Dr. Shannon Turley and Dr. David Edwards, who served on my qualifying exam committee, for providing thoughtful

feedback as well as helpful general advice for graduate school. I also want to thank Katie Parodi, Joan Cassidy, and Kurt Schellenberg who have all been indispensible in allowing our lab to function and run smoothly.

Lastly, I want to thank my parents and my brother for being the constants in my life. No matter what happens, I am lucky to know that I always have the three of you as shelter when I need it. To my mom and dad, my entire life you both believed in me even during times when I doubted myself. Everything I am able to accomplish today is the direct consequence of the love and support you have always given me. To my brother, thank you for being my best friend for the past 25 years. All the challenges you think you have, I have them too. If you let them limit you, you are selling yourself short.

Alexander Sing Cheung

December 2016

To my dad, who always encouraged me to reach for more,

To my mom, who always believed in me,

To my brother, who is capable of so much more than he thinks he is.

You know very well who you are. Don't let 'em hold you down, reach for the stars.

- The Notorious B.I.G.

Chapter 1: Introduction

1.1 Background and Motivation

Immunotherapy, the treatment of disease through targeted activation of the immune system, has recently shown unprecedented clinical success for a range of different types of cancers[1-5]. Unlike traditional treatments for cancer, such as radiation or chemotherapy, which indiscriminately kill rapidly dividing cells, immunotherapy engages the immune system to facilitate tumor elimination. This results in a response that is cancer-specific, due to the antigen-specific nature of the adaptive immune system, and durable, due to the induction of immunological memory[3-5].

Despite the promising outlook of immunotherapy for cancer, many treatments elicit suboptimal immune responses[6], and are nonfunctional for a large patient population[7]. On the opposite end of the spectrum, there are also cancer immunotherapy approaches that are too functional, and elicit severe on-target, off-tumor toxicities[8]. Many potential reasons for these shortcomings have to do with our incomplete understanding of the immune system. However, a common limitation in many current cancer immunotherapies that could also contribute to these shortcomings is the lack of spatiotemporal control with which immune-directing cues are presented to the immune system. The immune system is evolutionarily optimized to recognize and respond to cues when they are presented in specific spatiotemporal patterns, and failure to present cues in the appropriate patterns can lead to suboptimal or dysregulated responses, such as in disease states[9]. As such, cancer immunotherapies that can present immune-directing cues to the immune system in appropriate spatiotemporal patterns are likely to elicit more robust responses.

Biomaterials have a long history of use as precision drug delivery devices that facilitate the spatially- and temporally-defined delivery of cues for diverse applications[10, 11]. For example, particulate systems have been designed to compartmentalize or associate payloads[12], to protect bioactive payloads from the body[11, 13] or to protect the body from toxic payloads[13, 14], or to target payloads to specific organs or tissues[15, 16], or specific cells[17-19]. Alternatively, macroscale scaffold materials have been designed to act as synthetic microenvironments that present specific cell programming cues locally[20-23], or to facilitate the controlled release of soluble cues in predefined spatiotemporal patterns[24, 25]. There is a need to better control the spatiotemporal context with which immune-directing cues are presented to the immune system in cancer immunotherapies, and achieving this could lead to the development of improved therapies with increased efficacy and decreased toxicity. The appropriate design of biomaterials could enable this.

1.2 General Hypothesis

The design of biomaterials that present immune-directing cues to the immune system in a spatiotemporal pattern that mimics how these cues are naturally presented could elicit more robust responses.

1.3 Thesis Outline

This thesis is divided into three major parts. The first part (Chapter 2) is an overview of biomaterial systems that have been developed to improve various types of cancer

immunotherapy approaches. The second and third parts describe the development of biomaterials that interface particular immune-directing cues with different components of the immune system in a spatiotemporally controlled manner. Specifically, the second part (Chapter 3) describes a method for processing cancer cells to generate nano- to microscale particles in which repertoires of native cancer antigens and danger signals (adjuvants) are co-localized. The compartmentalization of antigens and danger signals into particles of this size mimics natural pathogens, which the immune system has evolved to robustly respond to. In this work, we characterize the physical and biochemical properties of the particles, and assess the value of presenting antigens and adjuvants in this context by comparing the *in vitro* and *in vivo* functionality of the cues when they are administered either in free form or in particulate form. The third part (Chapter 4) describes a composite material that presents endogenously cell surface-localized T cell cues on the surface of a synthetic lipid bilayer, and that releases soluble T cell cues over time in a controlled manner. This material mimics how antigen-presenting cells (APCs) naturally present these cues to T cells. In this work, we evaluate the ability of the APC-mimetic material to promote polyclonal and antigen-specific T cell expansion, and benchmark its performance against industry-standard commercial T cell expansion beads.

1.4 Specific Hypotheses and Aims

1.4.1 (Chapter 3) Adjuvant-Loaded Subcellular Vesicles Derived from Disrupted Cancer Cells for Cancer Vaccination

Specific Hypothesis:

Cancer cells can be processed to generate subcellular particles that co-localize repertoires of native cancer antigens and adjuvants, that can be used for cancer vaccination.

Specific Aims:

Aim 3.1 Develop a process for generating nano- to microscale particles that co-localize undefined repertoires of native cancer antigens and adjuvant, and characterize the particles.

Aim 3.2 Characterize the *in vitro* functionality of the particles in comparison to admixed soluble antigens and adjuvant, with respect to APC uptake, activation, antigen presentation.

Aim 3.3 Demonstrate that the particles can be used as a vaccine to induce an antigen-specific immune response in mice, and compare to soluble admixed antigens and adjuvant.

1.4.2 (Chapter 4) Antigen-Presenting Cell-Mimetic Scaffolds for ex vivo T Cell Expansion

Specific Hypothesis:

Supported lipid bilayers prepared on mesoporous silica micro-rods, can be used to present T cell activating cues to T cells in a manner similar to natural APCs, and facilitate efficient *ex vivo* T cell expansion.

Specific Aims:

Aim 4.1 Develop and characterize a material that can present T cell activating cues to T cells in a manner similar to how these cues are naturally presented to T cells by APCs.

Aim 4.2 Demonstrate that the material can be used for the efficient polyclonal expansion of primary mouse and human T cells.

Aim 4.3 Demonstrate that the material can be used for the efficient antigen-specific expansion of primary mouse and human T cells.

1.5 Significance

Broadly, the work described in this thesis demonstrate how materials can be designed to more optimally interface immune-directing cues with different components of the immune system. In particular, this work illustrates the value of designing systems that can present cues to the immune system in a spatiotemporal context that mimics how the immune system naturally encounters the respective cues.

The systems described in this thesis could potentially be used to improve current therapeutic cancer vaccine and adoptive T cell transfer approaches. In non-targeted cancer vaccines, the standard antigen source is tumor lysate, a mixture of soluble proteins obtained from processing a tumor biopsy[20, 21, 26, 27]. The process presented in Chapter 3 is an alternative approach that could be employed for processing tumor biopsies, or other sources of whole cancer cells, that can compartmentalize prospective tumor antigens into nano- to microscale particles,

and co-localize tumor antigens with adjuvants. These particles could be used as a substitute for soluble mixtures of lysate and adjuvants in such non-targeted cancer vaccine approaches.

The material described in Chapter 4 is a flexible drug delivery system that can present cues on the surface of a synthetic lipid bilayer, and release soluble cues over time in a controlled manner. In this thesis, we demonstrate that when the material is formulated to present a small set of T cell activating cues, it can promote faster expansion of functional T cells than industry-standard commercial T cell expansion beads presenting the same cues. This simple formulation could be useful for more rapidly generating functional T cells for adoptive T cell transfer approaches. Importantly, the material can be adapted to present significantly larger and more complex repertoires of cues, and surface cues can be presented at very precise densities. This could enable the generation of T cells with better, or very specialized functionalities, or allow us to gain fundamental insight on how T cells sense and respond to specific cell surface cues as a function of density. More broadly, this material could potentially also serve as a framework for the development of alternative cell-mimetic formulations for diverse applications beyond immunotherapy.

1.6 References

1. Dudley, M.E. et al. Cancer regression and autoimmunity in patients after clonal repopulation with antitumor lymphocytes. *Science* **298**, 850-854 (2002).
2. Davila, M.L. et al. Efficacy and toxicity management of 19-28z CAR T cell therapy in B cell acute lymphoblastic leukemia. *Science translational medicine* **6**, 224ra225-224ra225 (2014).
3. Hodi, F.S. et al. Improved survival with ipilimumab in patients with metastatic melanoma. *New England Journal of Medicine* **363**, 711-723 (2010).

4. Wolchok, J.D. et al. Nivolumab plus ipilimumab in advanced melanoma. *New England Journal of Medicine* **369**, 122-133 (2013).

5. Robert, C. et al. Nivolumab in previously untreated melanoma without BRAF mutation. *New England journal of medicine* **372**, 320-330 (2015).

6. Rosenberg, S.A., Yang, J.C. & Restifo, N.P. Cancer immunotherapy: moving beyond current vaccines. *Nature medicine* **10**, 909-915 (2004).

7. Sharma, P. & Allison, J.P. The future of immune checkpoint therapy. *Science* **348**, 56-61 (2015).

8. Rosenberg, S.A. & Restifo, N.P. Adoptive cell transfer as personalized immunotherapy for human cancer. *Science* **348**, 62-68 (2015).

9. Joyce, J.A. & Fearon, D.T. T cell exclusion, immune privilege, and the tumor microenvironment. *Science* **348**, 74-80 (2015).

10. Kearney, C.J. & Mooney, D.J. Macroscale delivery systems for molecular and cellular payloads. *Nature materials* **12**, 1004-1017 (2013).

11. Park, J. et al. Combination delivery of TGF-β inhibitor and IL-2 by nanoscale liposomal polymeric gels enhances tumour immunotherapy. *Nature materials* **11**, 895-905 (2012).

12. Moon, J.J. et al. Interbilayer-crosslinked multilamellar vesicles as synthetic vaccines for potent humoral and cellular immune responses. *Nature materials* **10**, 243-251 (2011).

13. Tasciotti, E. et al. Mesoporous silicon particles as a multistage delivery system for imaging and therapeutic applications. *Nature nanotechnology* **3**, 151-157 (2008).

14. Blanco, E. et al. Multistage delivery of chemotherapeutic nanoparticles for breast cancer treatment. *Cancer letters* **334**, 245-252 (2013).

15. Qian, X. et al. In vivo tumor targeting and spectroscopic detection with surface-enhanced Raman nanoparticle tags. *Nature biotechnology* **26**, 83-90 (2008).

16. Park, J.H. et al. Systematic surface engineering of magnetic nanoworms for in vivo tumor targeting. *small* **5**, 694-700 (2009).

17. Cruz, L.J. et al. Targeting nanoparticles to CD40, DEC-205 or CD11c molecules on dendritic cells for efficient CD8+ T cell response: a comparative study. *Journal of Controlled Release* **192**, 209-218 (2014).

18. Yang, L. et al. Single chain epidermal growth factor receptor antibody conjugated nanoparticles for in vivo tumor targeting and imaging. *Small* **5**, 235-243 (2009).

19. Martinez, J.O. et al. The effect of multistage nanovector targeting of VEGFR2 positive tumor endothelia on cell adhesion and local payload accumulation. *Biomaterials* **35**, 9824-9832 (2014).

20. Ali, O.A., Huebsch, N., Cao, L., Dranoff, G. & Mooney, D.J. Infection-mimicking materials to program dendritic cells in situ. *Nature materials* **8**, 151-158 (2009).

21. Ali, O.A., Emerich, D., Dranoff, G. & Mooney, D.J. In situ regulation of DC subsets and T cells mediates tumor regression in mice. *Science translational medicine* **1**, 8ra19-18ra19 (2009).

22. Kim, J. et al. Injectable, spontaneously assembling, inorganic scaffolds modulate immune cells in vivo and increase vaccine efficacy. *Nature biotechnology* **33**, 64-72 (2015).

23. Bencherif, S.A. et al. Injectable cryogel-based whole-cell cancer vaccines. *Nature communications* **6** (2015).

24. Silva, E. & Mooney, D. Spatiotemporal control of vascular endothelial growth factor delivery from injectable hydrogels enhances angiogenesis. *Journal of Thrombosis and Haemostasis* **5**, 590-598 (2007).

25. Chen, R.R., Silva, E.A., Yuen, W.W. & Mooney, D.J. Spatio–temporal VEGF and PDGF delivery patterns blood vessel formation and maturation. *Pharmaceutical research* **24**, 258-264 (2007).

26. John, S.Y. et al. Vaccination with tumor lysate-pulsed dendritic cells elicits antigen-specific, cytotoxic T-cells in patients with malignant glioma. *Cancer research* **64**, 4973-4979 (2004).

27. Geiger, J.D. et al. Vaccination of pediatric solid tumor patients with tumor lysate-pulsed dendritic cells can expand specific T cells and mediate tumor regression. *Cancer research* **61**, 8513-8519 (2001).

Chapter 2: Overview of Biomaterials for Cancer Immunotherapy

The work described in this chapter was originally published in Nano Today: Cheung AS and Mooney DJ. *Nano Today* 2015; 10 (4): 511-531.

2.1 Introduction

In this chapter, we provide an overview of biomaterials for various types of cancer immunotherapy applications, and explain how these systems could potentially improve current cancer immunotherapies. Cancers are among the leading causes of morbidity and mortality worldwide with incidence expected to rise by 70% over the next two decades [1]. Current treatments for cancer, such as chemotherapy and radiation therapy which are characterized by a lack of specificity and response durability, are insufficient. There is a need for therapies that can target cancer cells with a high degree of specificity, leading to lower treatment-related morbidity, and that can facilitate long-term remission.

Cancer immunotherapy refers to any intervention that leverages the immune system to eliminate a malignancy. Successful cancer immunotherapies generate an anti-cancer response that is systemic, specific, and durable, overcoming the primary limitations of traditional cancer treatment modalities. Recent progress in our understanding of the immune system has enabled the development of effective platforms for promoting anti-cancer immunity, particularly in the areas of biologics for reversing immunosuppression in the tumor microenvironment (TME) [2, 3], therapeutic cancer vaccines [4-6], and adoptive T cell therapies (ACT) [7-9]. For example, checkpoint inhibitors, monoclonal antibodies that block cell surface co-inhibitory receptors that disable the ability of T cells to destroy cancer cells, have shown unprecedented clinical success in a wide range of advanced stage malignancies [2, 3, 10-12]. To date, monoclonal antibodies for cytotoxic T-

lymphocyte-associated protein 4 (CTLA-4; Ipilimumab) and programmed cell death protein 1 (PD-1; Pembrolizumab and Nivolumab) have been FDA approved for metastatic melanoma with the PD-1 antibodies given "breakthrough therapy" designation by the FDA. The discovery of key molecular players in the generation of immune responses, including pattern recognition receptors (PRRs) such as Toll-like receptors (TLRs) and their respective ligands, has provided us with a vast toolbox of danger signals for precisely tuning the immune response. These cues, in combination with an improved understanding of dendritic cells (DCs), the most potent antigen-presenting cells (APCs), have enabled the design of promising therapeutic cancer vaccines, many of which are under investigation in various stages of clinical trials [4-6]. Importantly, these developments also lead to the first approval of a therapeutic cancer vaccine by the FDA in 2010 (Sipuleucel-T) [13]. Although Sipuleucel-T showed only modest therapeutic benefit and was associated with a high treatment cost, its approval set a precedence in the therapeutic cancer vaccine field and will likely lead to the development of more effective and efficient cancer vaccine approaches in the future. Advancements in our understanding of the cellular and molecular biology of T cells and antigen recognition has allowed for the development of highly efficacious ACTs, including tumor-infiltrating lymphocyte (TIL)-based therapies for advanced melanoma [9], and high-affinity/avidity T cell receptor (TCR)- [8] and chimeric antigen receptor (CAR)-transduced T cell-based therapies [7] for a wide range of hematologic malignancies.

Despite these advancements, drawbacks to current cancer immunotherapy strategies remain. Therapeutics are commonly administered as soluble injections, typically necessitating high doses and frequent re-dosing to achieve biologically relevant concentrations in target tissues, which often results in systemic toxicities [14, 15]. Soluble bolus-based vaccine formulations typically elicit weak cellular immune responses [16, 17], limiting their effective use for cancer.

Current methods for *ex vivo* cell expansion for ACT are suboptimal and do not always facilitate the generation of high quality T cells [18, 19], and achieving high T cell persistence and sustained functionality with limited systemic toxicity following transfer remains challenging [20, 21]. The use of biomaterials as platforms for cancer immunotherapy could allow for some of these limitations to be overcome. Although beyond the scope of this review, there are also promising virus-based approaches for cancer vaccination being explored, and this is described elsewhere [22, 23].

To date, a wide range of material systems have been developed as molecular and cellular delivery vehicles in biomedical applications ranging from diagnostics [24-26] to therapeutics [27-29]. As delivery vehicles, biomaterials allow for a level of spatiotemporal control over payload delivery that is difficult to recapitulate with a bolus. For example, nanomaterials can be used to deliver diverse combinations of bioactive payloads to specific tissues [25, 30], cell types [31, 32], and intracellular compartments [33-35] in a controlled manner and with a high degree of specificity, curtailing off-target toxicity and allowing for dose-sparing. Micro- to macroscale materials can be designed as depots for the sustained local delivery of bioactive payloads with high spatiotemporal resolution [36-38], or as artificial cellular microenvironments displaying complex combinations of cues [39-43]. This review will point out some of the challenges associated with various current immunotherapy modalities, and will discuss how the application of biomaterials as delivery vehicles or engineered microenvironments can potentially aid in overcoming some of these challenges. Specifically, this review will discuss the use of nano- to microscale materials for modulation of immunosuppression in the TME, therapeutic vaccination, and for promoting *in vitro* and *in vivo* T cell survival and expansion, and the use of 3-D macroscale materials as engineered microenvironments for programming immune cells, and as cellular delivery devices.

2.2 Brief Review of Cancer and the Immune System

The generation of a productive anti-cancer immune response resulting in the elimination of cancer cells is dependent on a coordinated series of events that must take place in an iterative and self-sustaining manner (Fig. 2.1). This process, termed the "cancer-immunity cycle", has been reviewed in detail elsewhere [44]. Briefly, antigens are released from cancer cells and captured by DCs, the primary mediators of adaptive immunity (step 1). DC activation, which is associated with the upregulation of cell surface co-stimulatory molecules and cytokine production, is necessary for efficient downstream priming of a T cell response, and may be promoted in the endogenous situation by factors released by dying cancer cells, broadly termed "danger associated molecular patterns". DC activation facilitates efficient processing of the uptaken antigen and subsequent presentation of antigenic peptides on cell surface MHC molecules (step 2). In the draining lymph nodes, activated DCs present cancer antigens to naïve T cells, resulting in the priming and activation of cancer antigen-specific T cells, a subset of which will differentiate into long-lived memory cells (step 3). Activated T cells, in particular, effector CD8+ cytotoxic T lymphocytes (CTLs), subsequently traffic to (step 4) and infiltrate the tumor (step 5), recognize cancer cells presenting the cognate antigenic determinants (step 6), and kill the cancer cells (step 7).

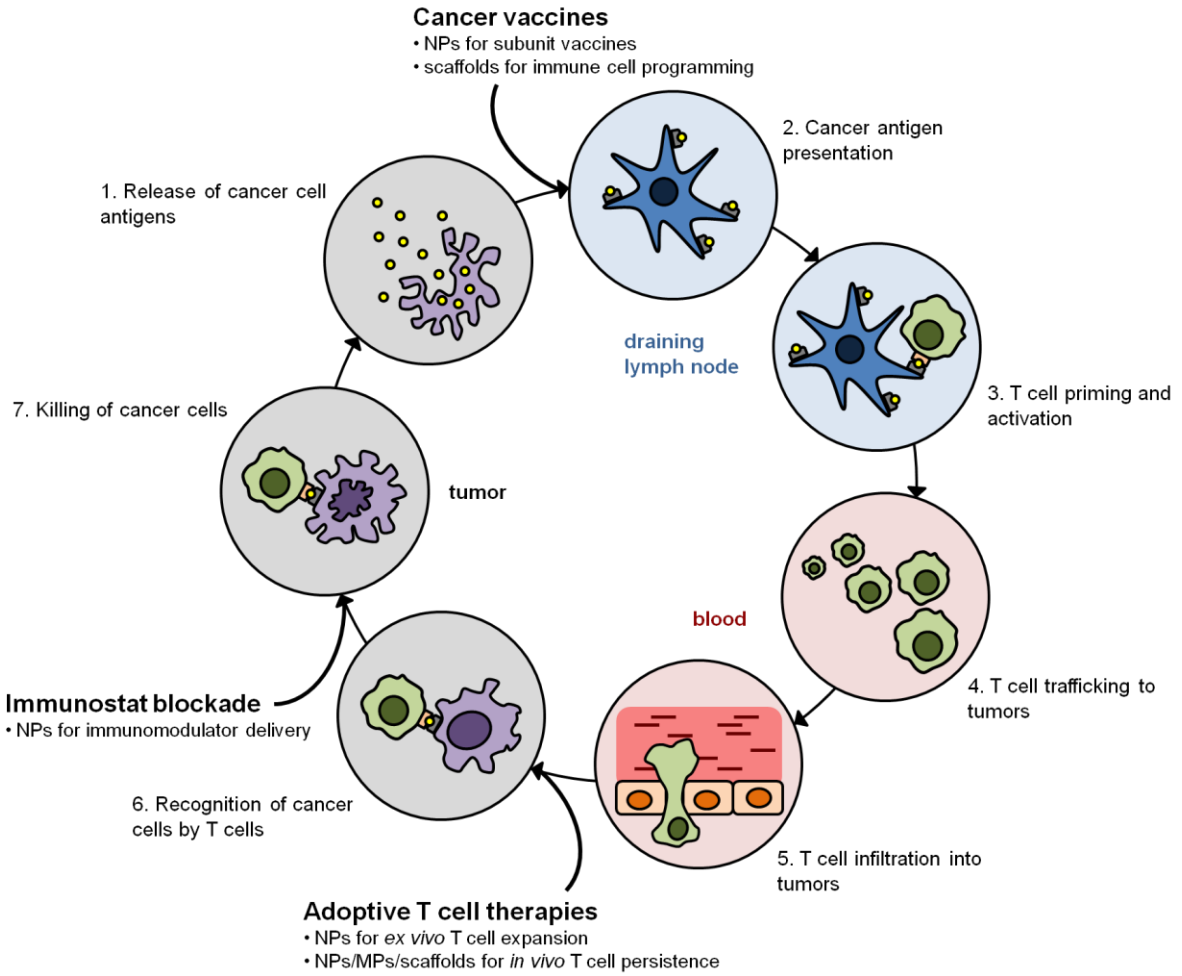

Figure 2.1. The Cancer-Immunity Cycle. Diagram illustrating the steps involved in the cancer-immunity cycle that take place in distinct spatiotemporal compartments in a sequential manner. Cancer immunotherapy approaches augment various steps in the cycle (bolded). Biomaterials can potentially be used to make these approaches more effective (bullet points). Adapted from [44].

In cancer patients, the cancer-immunity cycle is blocked at one or more of these steps, dampening the anti-cancer immune response and allowing for immune escape. Cancer immunotherapies seek to promote anti-cancer immunity by augmenting specific steps in the cycle (Fig. 1). For example, PD-1/PD-L1 axis inhibitors or other agents that seek to reverse immune dysregulation in the TME are aimed at improving the killing of cancer cells by pre-existing CTLs (step 7). Therapeutic vaccines target DCs to facilitate cancer antigen presentation

(step 2) in order to promote more robust T cell priming and activation (step 3) and subsequent CTL effector function. In ACTs, large populations of cancer-specific CTLs are generated *ex vivo* that can efficiently recognize cancer cells (step 6) following transfer into the patient. Materials can be used to overcome some of the limitations of current cancer immunotherapy approaches, and could allow for the development of immunotherapies that fulfill their respective endpoints more effectively and efficiently.

2.3 Nanomaterials for Modulating Immune Dysregulation in the Tumor Microenvironment

The TME of most solid tumors is characterized by immune privilege and pro-tumorigenic inflammation [45, 46]. These properties are facilitated by the concerted activity of the cancer cells themselves [47], tumor-associated stromal cells such as cancer-associated fibroblasts (CAFs) [48], and tumor-infiltrating immune cells including regulatory T cells (T_{reg} cells) [49, 50], tumor-associated macrophages (TAMs) [51], and myeloid-derived suppressor cells (MDSCs) [52, 53]. Through various mechanisms, these cells preferentially exclude effector T cells from the tumor parenchyma [53], inhibit local cytotoxic effector function [49], promote tumor growth and metastasis [46], and reinforce the tolerogenic bias [46, 54, 55]. Modulating this tumor-proximal immune dysregulation, for example, by inhibiting molecular or cellular tolerogenic mediators or activating local cytotoxic effector cells, can sometimes be sufficient to induce anti-cancer immunity [12], and will likely have significant synergy with approaches that promote the generation or expansion of cancer-specific T cells. Immunotherapies that reverse immunosuppression in the TME are likely to be particularly relevant in immunogenic cancer types in which a significant anti-cancer T cell population already exists but is functionally

inhibited in the TME [55, 56]. Of note, although the TME represents the source of these tolerogenic mediators, they are often not confined to this site and can accumulate in sinks such as the tumor draining lymph nodes (tdLNs) [57, 58], and in some cases, lead to systemic effects in patients as well [59]. As such, addressing the tolerogenic effects of the tumor more broadly, for example, by targeting peripheral sinks or tolerogenic mediators in circulation, represent potential alternative treatment strategies. However, such approaches will have to be appropriately designed to minimize systemic inflammatory toxicities, particularly since many of the inflammatory mediators used in such approaches (e.g. cytokines) can induce potent and serious systemic side-effects [21]. In this review, we focus on addressing mechanisms of immune dysregulation in the TME, which leverages the extensive amount of research that has been done on the use of nanomaterials as drug delivery vehicles to the tumor.

Designing a system to address immune suppression in the TME presents numerous challenges for soluble bolus-based delivery approaches, specifically with respect to delivering combinations of immune modulating payloads in a bioactive state to the tumor site while minimizing systemic toxicity. To overcome these challenges, nanomaterials can be used to facilitate the preferential accumulation of associated payloads in the TME, by being designed to either passively accumulate in the TME via the enhanced permeability and retention (EPR) effect [60], or to actively target the TME via diverse targeting strategies including the use of peptides [30], aptamers [26, 61], small molecules [62], or single-chain variable fragments of antibodies (scFv) [32], that may either interact directly with tumor cells or other components of the TME. Alternatively, stimulus-responsive systems have been designed that release sequestered payloads in response to triggers that are enriched in the TME, such as moderately low pH [63] or proteases, such as the

matrix metalloproteinases (MMP) MMP-2 and MMP-9 [64], or in response to exogenous triggers that are selectively directed at the tumor, for example light [65], magnetic field [66, 67], or heat [67].

In the design of such systems, it is important to consider the spatial and temporal pattern of delivery that would be optimal for the activity of the particular payload. For the delivery of immune modulators such as cytokines or antagonistic agents that target cell surface receptors, the vehicle should be designed to minimize interactions with phagocytic cells in order to release the payload in the TME extracellularly. For example such vehicles can be surface modified with bioinert polymeric coatings such as poly(ethylene) glycol (PEG) or PEG derivatives [68], or with anti-phagocytic signals such as CD47 [69]. Physical properties of the vehicle such as size [70], aspect ratio [71, 72], or stiffness [73, 74] can also be tuned to decrease cell uptake. Alternatively, for the delivery of immune modulators such as certain PRR ligands or siRNA targeting immune regulatory pathways, the vehicle should be designed to target the appropriate intracellular compartment. As examples, endolysomal targeting can be enhanced by tuning the surface [75] or physical properties [70-74] of the particle to promote endocytosis, or by modifying the particle surface with ligands that actively target endocytosis-associated receptors [76]. Release of payloads in the endolysosomal environment can be achieved, for example, through the use of a stimulus-responsive vehicle [37] or through conjugation of the payload to the vehicle via a stimulus-responsive linker (e.g. one responsive to acidic pH or proteases) [77]. Cytosolic targeting could be facilitated, for example, through modification of the particle surface with cell penetrating peptides [78], or polycationic polymers that act as proton sponges [79] and promote endosomal escape following endocytosis. The temporal pattern of payload release can be tuned by varying system parameters including the method of payload loading (e.g. encapsulation versus chemical

conjugation), the porosity and degradability of the material, and the relative physicochemical properties of the payload and the vehicle.

Nanomaterials have been designed to deliver diverse immunomodulatory payloads to the TME in order to address various mechanisms of TME immunosuppression. One attractive therapeutic target that has been pursued is the transcription factor STAT3, which has been identified as a key regulator of immune dysregulation in the TME. More specifically, expression of STAT3 in tumor-infiltrating immune cells has been shown to promote Th2-biased inflammation, thereby inhibiting a Th1 response, and to promote the survival of T_{reg} cells [80]. STAT3 inhibition in the TME was reported using systemically administered tumor-targeting liposome nanoparticles loaded with a hydrophobic small molecule STAT3 inhibitor [62]. Of note, such hydrophobic agents are rapidly removed when administered as a soluble bolus and are therefore challenging to efficiently deliver to a target tissue systemically in free form. The targeted nanoparticles facilitated the delivery of the STAT3 inhibitor to the tumor and promoted the upregulation of a large panel of Th1-associated proinflammatory cytokines, and the concomitant downregulation of Th2-biased cytokines. This translated to slower tumor growth in murine breast cancer models in prophylactic and therapeutic settings, with an enhanced response observed when the inhibitor was delivered in the targeted liposomes versus in free form or via non-targeted liposomes. Importantly, the targeted delivery of the STAT3 inhibitor to the TME was shown to improve the effects of a therapeutic cancer vaccine in a murine breast cancer model [62]. Similar studies have been performed using other methods of antagonizing the STAT3 pathway, including the use of STAT3 siRNA [81], and other small molecule inhibitors [82, 83].

Multifunctional nanomaterials have also been designed to simultaneously inhibit suppression and promote immunity in the TME. For example, 120 nm lipid-enveloped nanoparticles composed of PEG-crosslinked polylactide, termed "nanolipogels", were designed to co-deliver a hydrophobic small molecule inhibitor of the immunosuppressive cytokine TGF-β, and the T cell mitogenic cytokine interleukin 2 (IL-2) [84] (Fig. 2.2a). Notably, these particles were specifically designed to facilitate the co-delivery of these payloads in a single vehicle, which is generally challenging due to the distinct physicochemical properties of these payloads. Nanolipogels facilitated the release of both payloads in a sustained manner for at least a week *in vitro*. Comparative biodistribution studies using nanolipogels bearing a fluorescein-labeled lipid shell and loaded with a rhodamine payload demonstrated that both vehicle and payload accumulated in subcutaneous tumors and lung metastases (Fig. 2.2b) following systemic administration. In a therapeutic murine model of metastatic melanoma, systemic administration of the TGF-β inhibitor and IL-2 co-loaded nanolipogels resulted in attenuated tumor growth and enhanced survival (Fig. 2.2c). Notably, co-delivery of both components in a single carrier resulted in improved outcomes over the delivery of each component alone in soluble or nanolipogel-associated form (Fig. 2.2c).

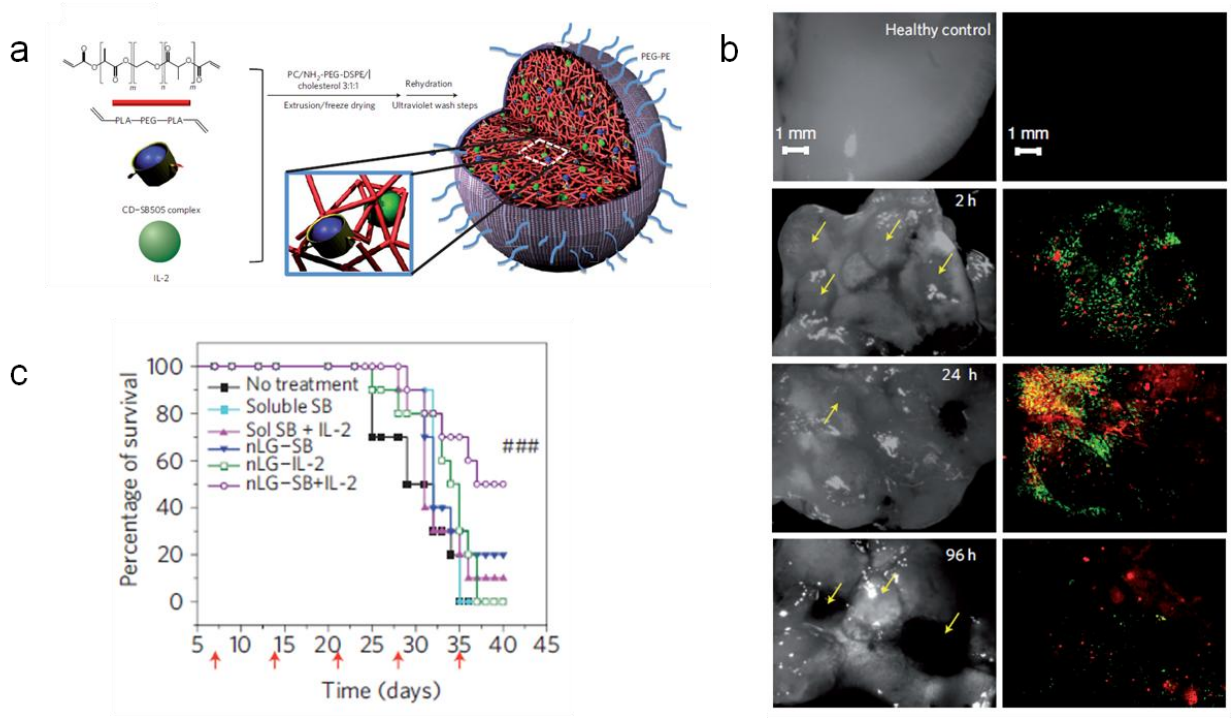

Figure 2.2. Nanolipogels for modulating immunosuppression in the TME. (a) Diagram of nanolipogel formulation. (b) Analysis of healthy lung tissues (top row) or lung tissues bearing metastases (yellow arrows) at 2 h, 24 h, and 96 h following a single injection of nanolipogels loaded with rhodamine and containing fluorescein-labeled phospholipid in the lipid bilayer shell. Tissues are visualized under bright field (left) and fluorescence microscopy (right), showing the presence of both lipid carrier (green) and rhodamine payload (red) around individual lung tumors at these time points. (c) Survival of mice bearing melanoma lung metastases either untreated or treated via systemic injections of soluble TGF-β inhibitor (soluble SB), soluble TGF-β inhibitor with soluble IL-2 (sol SB + IL-2), nanolipogels loaded with TGF-β inhibitor (nLG-SB), nanolipogels loaded with IL-2 (nLG-IL-2), or nanolipogels loaded with both TGF-β inhibitor and IL-2 (nLG-SB+IL-2). Red arrows denote treatment days. From [84].

Alternatively, nanomaterials can also be designed to locally present agonistic cues to cell surface molecules, or to act as depots for sequestering payloads at the tumor site following administration into the vicinity of the tumor, enhancing the local bioavailability of the payload and minimizing systemic toxicity. For example, nanoscale liposomes were prepared that simultaneously displayed an agonistic CD40 antibody, and released unmethylated CpG

oligodeoxynucleotides (CpG), a TLR ligand, in a sustained manner for over a week *in vitro* [85]. These agents have been shown to be have synergistic anti-tumorigenic effects in preclinical models [86, 87], but have been associated with off-target inflammatory effects following systemic over-exposure. In a murine melanoma model, anti-CD40 and CpG delivered intratumorally, either as a soluble bolus or co-delivered in the liposomal formulation, inhibited tumor growth to a comparable degree. Notably, however, serum levels of anti-CD40 and CpG were significantly attenuated when the agents were delivered in the liposomal formulation [85]. Consistent with this observation, compared to animals that received the agents as a soluble bolus, animals treated with the liposomal formulation exhibited minimal weight loss, and significantly decreased serum levels of hepatic ALT enzyme and the proinflammatory cytokines TNF-α and IL-6.

2.4 Nanomaterials as Therapeutic Cancer Vaccines

Nanomaterials are being developed as efficient and versatile mediators of therapeutic cancer vaccination. Fundamentally, an immune response is generated when DCs acquire antigen in the context of a danger signal such as a PRR ligand, and subsequently prime a cancer-specific T cell response. One family of PRRs that is particularly important in vaccine design is the TLRs, due to their frequent use as adjuvants in vaccine formulations. Examples of TLR ligands include lipopolysaccharide (LPS) and its derivate monophosphoryl lipid A (MPLA), found in the outer membrane of gram-negative bacteria, polyinosinic:polycytidylic acid (poly I:C), a synthetic mimic of double-stranded RNA found in some viruses, and CpG oligodeoxynucleotides, which resemble DNA motifs found in microbial genomes. A primary challenge in designing cancer vaccines is consolidating DCs, danger signal, and antigen into a single spatiotemporal

compartment. To this end, nanomaterials can be employed as colloidal scaffolds to associate antigen with danger signal, and designed to target migratory peripheral or lymph node-resident DCs. Alternatively, adjuvanted nanomaterials can be designed to target DC-rich cancer antigen experienced sites such as the tdLNs or potentially the tumor itself.

2.4.1 Targeting the Draining Lymph Nodes

DCs are the most potent APCs for initiating an immune response [88, 89]. However, DCs are comprised of diverse subpopulations that vary with respect to their residence and function [90]. The discussion in this review will be limited to therapeutic vaccines that are administered in the skin. In this context, we draw a general and simplistic distinction between just two DC subpopulations: the migratory DCs that reside in peripheral tissues and migrate to the tissue-draining lymph nodes following activation, and the non-migratory lymphoid tissue-resident DCs. Of note, among the lymphoid tissue-resident DCs is a subset that expresses the cell surface marker CD8 in mouse and is specialized for cross-presentation, a process critical for CTL induction. As such, targeting the lymph nodes is, in general, of particular interest for nanoparticulate-based therapeutic vaccines.

Nanoparticulate vaccines that are administered in the skin, that is, either intradermally or subcutaneously, can be designed to either interact with migratory DCs at the injection site, or to drain passively to the lymph node for acquisition and presentation by lymph node-resident DCs. The former relies on cell trafficking to reach the draining lymph node, and takes place with relatively slower kinetics. The latter depends on lymphatic flow without the need for an active cell trafficking mechanism, and takes place with relatively faster kinetics. In general, the primary feature determining whether a colloid will spontaneously drain or be taken up by migratory DCs

is size, although surface properties have been shown to play a role as well [91]. When trafficking of polystyrene particles between 20-2000 nm was evaluated following subcutaneous administration, it was observed that 20 nm particles rapidly and efficiently arrived in the draining lymph node two hours post-injection (Fig. 2.3a) with initial localization in the subcapsular sinus (Fig. 2.3b), a pattern consistent with lymphatic-mediated drainage [92]. In contrast, 1000 nm particles were not observable in the draining lymph node until 24-48 hours post-injection (Fig. 2.3a), and were excluded from the subcapsular sinus (Fig. 2.3b), suggesting a cell trafficking-mediated mechanism of lymph node accumulation. Consistent with this, depletion of DCs abrogated the trafficking of 500 nm particles to the draining lymph node but had minimal effects on the trafficking pattern of 20 nm particles. Taken together, these findings demonstrate that particles of 500 nm or larger likely depend on active DC-mediated trafficking to reach the lymph node. Notably, particle size and CD8+ DC uptake were found to be negatively correlated, with 20 nm particles found to be frequently associated with CD8+ DCs. A similar observation was made following intradermal administration of polypropylene sulfide (PPS) nanoparticles wherein 20 nm particles accumulated in draining lymph nodes more rapidly and at a higher magnitude than larger 100 nm particles (Fig. 2.3c). A significantly larger fraction of the small particles were also taken up by lymph node DCs (Fig. 2.3d).

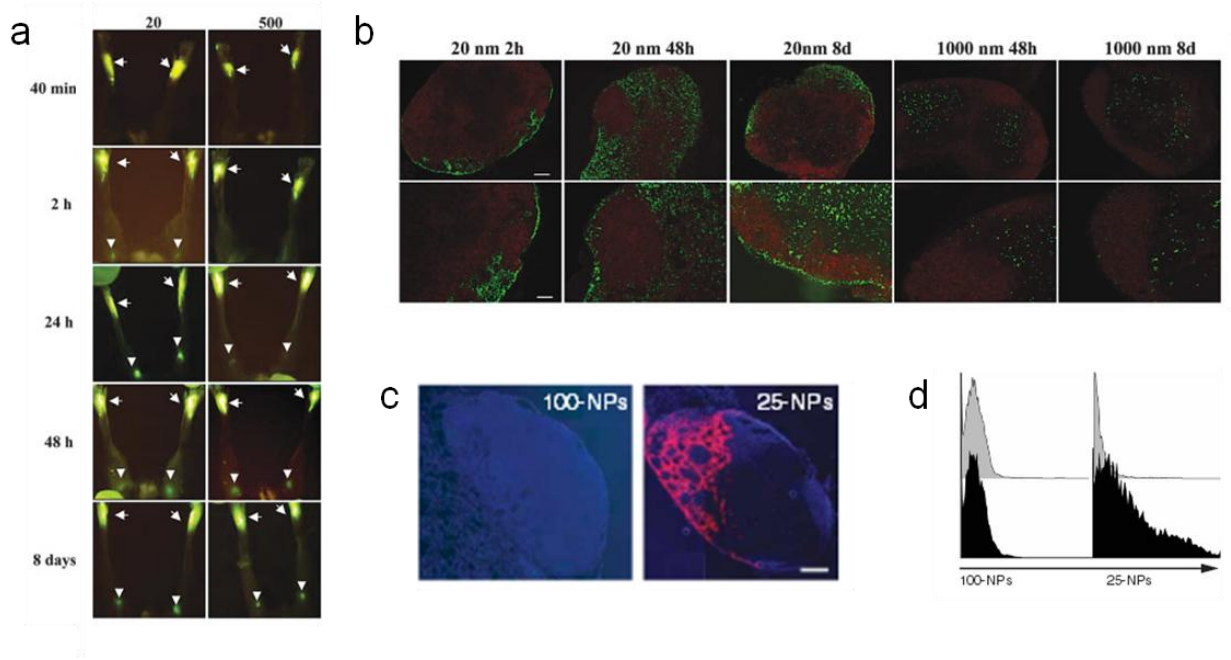

Figure 2.3. Effects of particle properties on lymph node accumulation. (a) Accumulation of 20 nm and 500 nm fluorescent polystyrene nanoparticles to the draining popliteal lymph nodes at 40 min, 2 h, 24 h, 48 h, and 8 days following subcutaneous injection in the footpad. Arrows point to injection site in footpad and arrowheads point to draining popliteal lymph nodes. (b) Localization of 20 nm and 1000 nm polystyrene nanoparticles (green) in the draining popliteal lymph node at 2 h, 48 h, and 8 days following subcutaneous injection in the footpad. B220 staining shows lymph node B cell follicles in red. (c) Accumulation of 100 nm and 25 nm fluorescent PPS nanoparticles (red) in the draining lymph node at 24 h after intradermal injection. Cell nuclei stained with DAPI are shown in blue. Scale bar = 200 μm. (d) Flow cytometry histograms showing CD11c+ DCs isolated from the draining lymph nodes after intradermal injection of fluorescent 100 nm and 25 nm particles (black) or mock (gray). a, b from [92]. c, d from [93].

2.4.2 Nanomaterials for Subunit Vaccines

A considerable focus in recent cancer vaccine development has been on subunit vaccines that contain purified tumor antigens or antigenic epitopes as an antigen source, often in combination with an adjuvant such as a TLR agonist. Although roles for Th1-biased anti-cancer antibodies [16] and cancer-specific CD4+ T cells [94] have been implicated, it is generally understood that the primary determinant of successful cancer immunotherapies is the generation of a large,

functional cancer-specific CTL pool [95, 96]. However, soluble bolus-based subunit vaccines typically induce weak CTL responses [16, 17], which limit their utility for cancer, and this is likely due to the inefficient cross-presentation of soluble, nonimmunogenic antigens [97-101]. To overcome this, nanoscale colloids can be used to promote more efficient antigen presentation by acting as phagocytic substrates that physically associate antigen and adjuvant.

Nanoparticulate subunit vaccines that co-deliver these cues have been prepared using a wide range of synthetic [37, 102-104] and natural materials [105-107]. For example, virus-mimicking 25 nm protein dodecahedrons, based on the E2 subunit of pyruvate dehydrogenase, were immobilized with the TLR9 agonist CpG and a peptide antigen (Fig. 2.4a) [77]. Importantly, CpG was immobilized onto the capsules via acid-labile hydrazone bonds, facilitating its release in the endolysosomal compartment where TLR9 is localized. Attachment of CpG to the E2 particles enhanced the activation of primary bone marrow-derived dendritic cells (BMDCs) compared to free CpG, likely by enhancing cellular uptake of CpG. E2 particles presenting both CpG and peptide antigen facilitated more robust activation of antigen-specific T cells compared to the cues presented separately (Fig. 2.4b), illustrating the benefit of consolidating both antigen and danger signal on a single carrier.

Beyond solid colloids, subunit vaccines can also be prepared using polymersomes [108, 109] and liposomes [110]. However, a limitation to the use of standard liposomes for this purpose is their relatively low stability in serum. One approach that has been reported to improve the stability of liposomes is to prepare multilamellar liposomes with cross-linked layers, termed interbilayer-crosslinked multilamellar vesicles (ICMVs) [108, 111, 112]. PEGylated ICMV subunit vaccines were prepared that contained the model antigen ovalbumin (OVA) in the aqueous interior of the particles, and the lipophilic TLR 4 agonist MPLA embedded in the ICMV lipid walls (Fig. 2.4c).

ICMV vaccines demonstrated enhanced extracellular stability compared to unilamellar and uncrosslinked multilamellar counterparts, but underwent rapid particle degradation and cargo release in response to enzymes present in the endolysosomal compartment.

When mice were vaccinated subcutaneously with the ICMV vaccine, robust induction of antigen-specific CD8+ T cells was observed. Using the optimal ICMV formulation, a maximum frequency of 28% antigen-specific T cells among total CD8+ T cells in the peripheral blood was generated (Fig. 2.4d). This was equivalent to a 14-fold enhancement compared to soluble OVA and MPLA at the same dose, and this magnitude of response could not be recapitulated with the soluble formulation even using a 10-fold higher MPLA dose, suggesting that there are inherent limitations to using soluble subunit vaccine formulations. The induced antigen-specific CTLs included a CD44+CD62L+ subset, which has been reported to be indicative of a memory phenotype. In addition, a significant portion of the antigen-specific CTLs were observed to be functional, producing the inflammatory Th1 cytokine IFNγ following *in vitro* peptide restimulation. To date, the magnitude of the antigen-specific CTL response induced using the ICMV system is one of the most potent achieved with a non-viral vaccine, albeit against a model antigen. Understanding the specific mechanisms by which the ICMVs, and similarly robust vaccines, derive their potent CTL-inducing activity, will be important for the design of even more effective systems in the future.

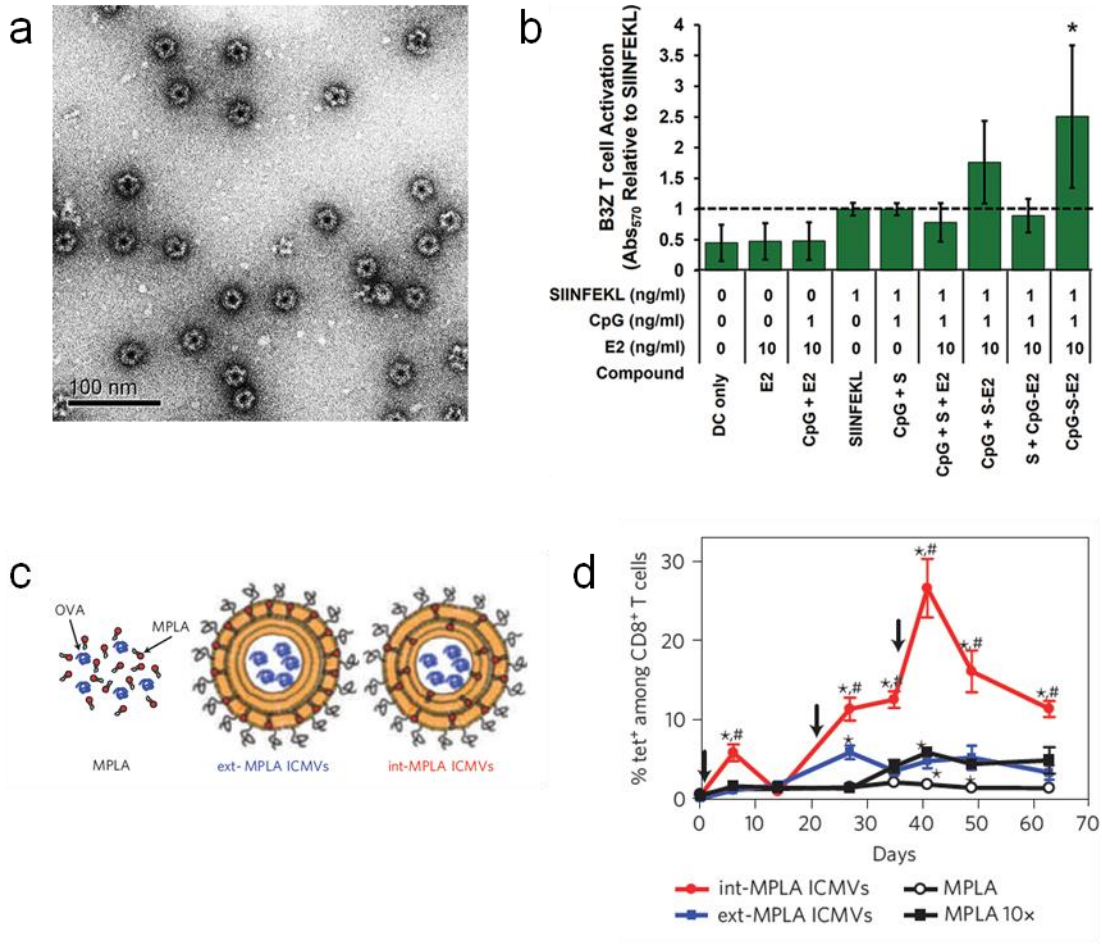

Figure 2.4. Nanoparticulate subunit vaccines. (a) TEM image of negatively-stained protein-based vaccines showing virus mimicking dodecahedral geometry. (b) Activation of B3Z antigen-specific T cell hybridoma cell line by BMDCs either unloaded (DC only), or loaded with E2 vehicle (E2), soluble CpG with E2 vehicle (CpG + E2), soluble peptide antigen (SIINFEKL), soluble CpG with soluble peptide antigen (CpG + S), soluble CpG with soluble peptide antigen and E2 vehicle (CpG + S + E2), soluble CpG with peptide antigen-conjugated E2 (CpG + S-E2), soluble peptide antigen with CpG-conjugated E2 (S + CpG-E2), or peptide antigen and CpG co-loaded E2 (CpG-S-E2). (c) Diagram showing OVA-loaded ICMV vaccine formulations containing MPLA only in the outer vesicle layer (ext-MPLA ICMVs) or containing MPLA throughout the multilayers (int-MPLA ICMVs). (d) Time-dependent quantification of antigen-specific CTLs in peripheral blood after subcutaneous vaccination of naive mice with soluble MPLA in combination with soluble OVA (MPLA), ICMVs loaded with the same amount of OVA and MPLA with the MPLA either in the outer vesicle layer only (ext-MPLA ICMVs) or distributed throughout the multilayers (int-MPLA ICMVs), or with soluble OVA in combination with a 10-fold higher dose of soluble MPLA. Black arrows represent vaccination timepoints. a, b from [77], c, d from [111].

An alternative approach to using inert nanomaterials to simply consolidate antigen and adjuvant is to design the material itself to act as an immune directing cue. For example, OVA-conjugated αAl_2O_3 nanoparticles were found to target autophagosomes following uptake by BMDCs, promoting highly efficient cross-presentation of OVA-derived peptides via an autophagy-dependent mechanism [35]. In another example, degradable PPS nanoparticles were surface polyhydroxylated, which facilitated their opsonization by ubiquitous serum complement components, specifically, by C3b which typically reacts with hydroxyl groups on surface carbohydrates of pathogens [93]. Following intradermal administration, 25 nm polyhydroxylated nanoparticles were found to efficiently activate draining lymph node dendritic cells, whereas 25 nm polymethoxylated nanoparticles, which do not interact with complement, did not. In addition, OVA-conjugated polyhydroxylated nanoparticles promoted robust expansion of antigen-specific T cell *in vivo* whereas the polymethoxylated nanoparticles promoted only minimal expansion. In a follow-up study, the effect of surface chemistries on complement activation was further explored, specifically with respect to the ratio of surface deposited C3b to inactivated C3b (iC3b), which has been shown to have an immunosuppressive function [113]. It was shown that the C3b:iC3b ratio could be tuned by altering the ratio of carboxylated to hydroxylated groups on the nanoparticle surface. Consistent with the suppressive function of iC3b, a higher C3b:iC3b ratio was found to correlate with the induction of higher antigen-specific antibody titers and enhanced Th1-biased cytokine production following *ex vivo* peptide restimulation of splenocytes from vaccinated animals.

2.4.3 Adjuvanted Nanomaterials for Targeting Cancer Antigen Experienced Sites as Therapeutic Cancer Vaccines

Despite the promise of engineered subunit vaccines, there are limitations to such targeted approaches. First, targeted vaccines generally immunize against prototypic cancer antigens, which precludes their use in cancers for which a such a target has not been identified, or in patients refractory for the particular known target. Of note, however, recent work on the patient-specific identification of cancer-associated neoantigens [114, 115] may allow for the use of targeted vaccines as personalized therapies, and this is discussed later in this review. Second, targeted approaches do not capture the complex antigen repertoire of tumors, and suboptimal vaccines that do not induce efficient antigen spread can potentially facilitate cancer immunoediting favoring the selection of lowly immunogenic subpopulations, leading to immune escape [116]. Based on these observations, there is interest in the development of non-targeted vaccine approaches that immunize against a range of different tumor-associated antigens. Examples of such approaches include vaccines based on inactivated whole tumor cells, autologous tumor lysate, and endogenous cancer antigens. The latter, in which the presence of cancer antigens at antigen experienced sites is leveraged through *in situ* vaccination at those sites, is particularly attractive in that such approaches do not require biopsies or tumor samples, and do not involve the *ex vivo* manipulation or processing of cancer cells.

To this end, adjuvanted nanoparticles have recently been described for targeting the tdLNs, which are known to be cancer antigen experienced sites, for *in situ* vaccination against endogenous cancer antigens [57, 58]. In addition to being antigen experienced, tdLNs are unique in several other aspects that make them both attractive as well as challenging sites for successful vaccination. tdLNs are enriched in immunosuppressive factors from the TME, as indicated by the increase in PD-L1+ DCs and PD-1+CD8+ T cells in the tdLNs compared to non-tdLNs [58]. In addition, tdLNs generally have fewer T cells and CD8+ DCs [58]. However, the potential for the

endogenous generation of cancer-specific T cells in the tdLNs is supported by the observation that there is a time-dependent increase in functional OVA-peptide specific CD8+ T cells in the tdLNs of E.G7-OVA (OVA-transduced lymphoma cell line) tumor-bearing mice [58]. Additionally, the pre-existence of endogenous cancer-specific T cells in untreated cancer patients is well established [95]. Collectively, it is unclear in general whether the tdLNs necessarily represent beneficial or detrimental sites of vaccination although the success of tdLN-targeting vaccines is likely to be dependent both on the progression and nature of the malignancy as well as the robustness of the vaccine.

The potential for inducing an anti-cancer immune response using adjuvanted nanoparticles targeting the tdLNs was recently interrogated using 30 nm pyridyl disulfide (PDS) conjugated to CpG via a reduction-sensitive bond (PDS-CpG) [57]. These particles were shown to activate DCs *in vitro*, owing to the endolysosomal-triggered release of the CpG payload, facilitating CpG-TLR 9 interactions, and to efficiently drain to the lymph nodes following intradermal administration. Induction of intradermal B16-F10 melanoma tumors on one side of the animal resulted in the selective drainage of tumor antigen exclusively to ipsilateral (i.l.), but not to contralateral (c.l.) lymph nodes, as evaluated based on the drainage pattern of intratumorally administered fluorescent dextran (Fig. 2.5a,b). Intradermal administration of the PDS nanoparticles i.l. or c.l. also resulted in drainage of the particles primarily to LNs on the respective side of the animal (Fig. 2.5a,c). Notably, treatment of mice i.l. with PDS-CpG led to significantly slower tumor growth compared to the same particle formulation administered c.l., which showed no therapeutic effect (Fig. 2.5d). Co-administration of PDS nanoparticles with free CpG either i.l. or c.l. also yielded no therapeutic effect. The therapeutic benefit of the i.l. administered PDS-CpG was associated with an increased frequency of CD40+CD11c+ cells in

the tdLNs, that may represent DCs with an activated phenotype, as well as in the frequency of activated CD25+ CD8+ T cells and the CD8:CD4 T cell ratio. In addition, only i.l. treatment with PDS-CpG promoted an increase in the frequency of tumor-infiltrating CD8+ T cells specific for the melanoma-associated antigen TRP-2.

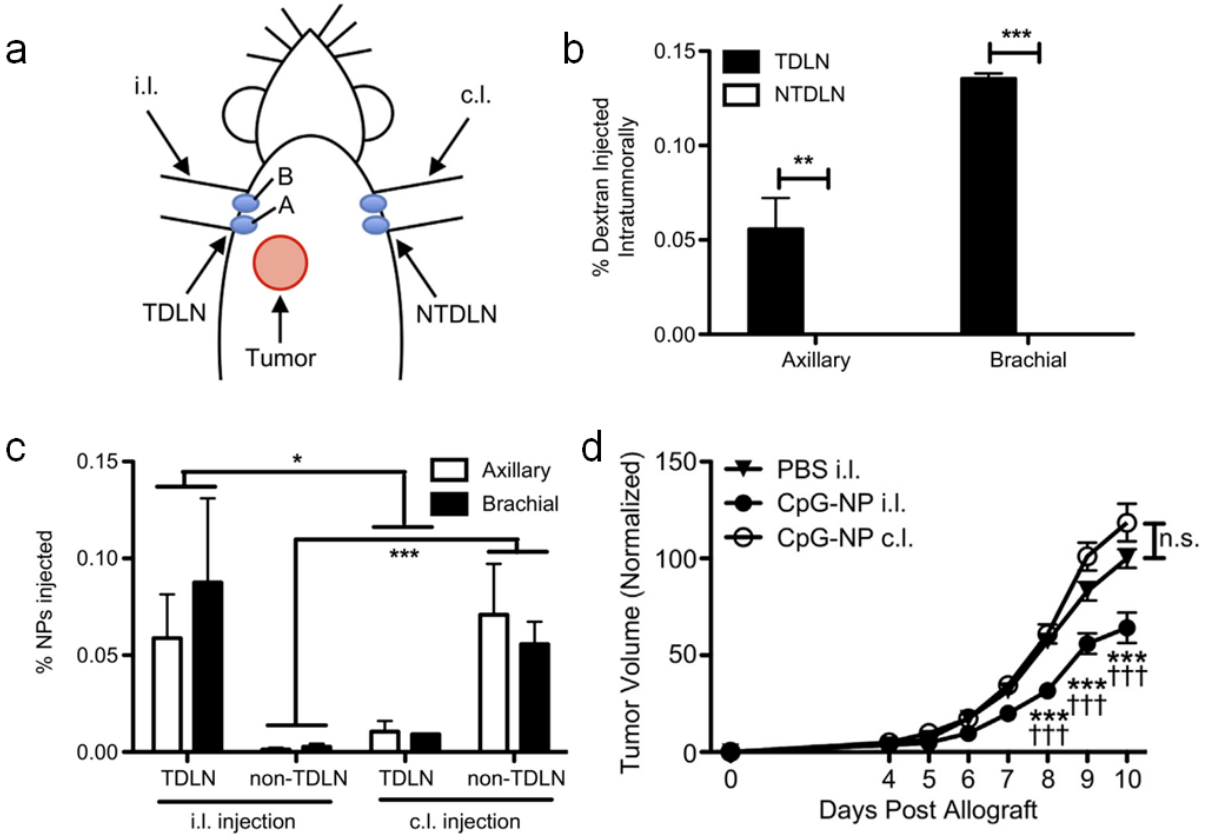

Figure 2.5. Adjuvanted nanoparticles targeting the tdLNs as a therapeutic cancer vaccine. (a) Diagram showing location of tumor inoculation in relation to the i.l. (TDLN) and c.l. (NTDLN) axillary (A) and brachial (B) draining LNs. (b) Quantification of dextran in axillary and brachial draining LNs following intratumoral administration of dextran. (c) Quantification of PDS nanoparticles (NPs) in draining LNs following either i.l. or c.l. intradermal administration of PDS nanoparticles. (d) Quantification of tumor volume as a function of time post tumor allograft following treatment with PBS or PDS-CpG administered either i.l. or c.l.. From [57].

Interestingly, it was also recently shown that, in the context of both E.G7-OVA and wild-type B16-F10 melanoma tumor-bearing mice, nanoparticulate subunit vaccines were more effective in the therapeutic setting (i.e. after the tumor has affected the tdLNs) at slowing tumor growth and promoting survival when they were targeted to tdLNs versus non-tdLNs [58]. Consistent with this, it was observed that delivery of these vaccines to the tdLNs versus the non-tdLNs resulted in the generation of a greater cancer-specific CTL response both locally in the tdLNs as well as systemically. Collectively, these observations suggests that not only can appropriately designed vaccines overcome the immunosuppressive mechanisms in the tdLNs and thereby leverage the cancer antigen experience of these sites for vaccination, but also that vaccines that target the tdLNs and are able to overcome this immunosuppression could induce particularly potent effects. Based on this idea, the TME itself represents another potentially attractive cancer antigen experienced site for vaccination. However, overcoming the active immunosuppressive mechanisms in the TME will likely be more challenging than overcoming those at the tdLNs, requiring that such vaccines be highly potent, and possibly necessitating combinatorial treatment with TME immunomodulators.

2.5 Engineered Microenvironments for Dendritic Cell Programming as Therapeutic Cancer Vaccines

An alternative approach to preparing colloidal vaccines that target relatively infrequent populations of peripheral or draining lymph node DCs is to design micro- to macroscale materials to act as microenvironments that recruit large numbers of DCs to the material, and program them *in situ*. In such an approach, a biomaterial scaffold is designed to release a

recruitment factor to promote mass immune cell trafficking to the scaffold site, where danger cues and antigen are presented locally within a microenvironment permissive for cell infiltration. Activated, antigen-loaded DCs can subsequently traffic to the draining lymph nodes to facilitate T cell priming and activation (Fig. 2.6). Compared to DC-based cancer vaccine approaches such as Sipuleucel-T, such material systems bypass the need for *ex vivo* cell culture. This may decrease the substantial financial and regulatory burdens typical for cell therapies, and also avoid inconsistent and suboptimal cell products.

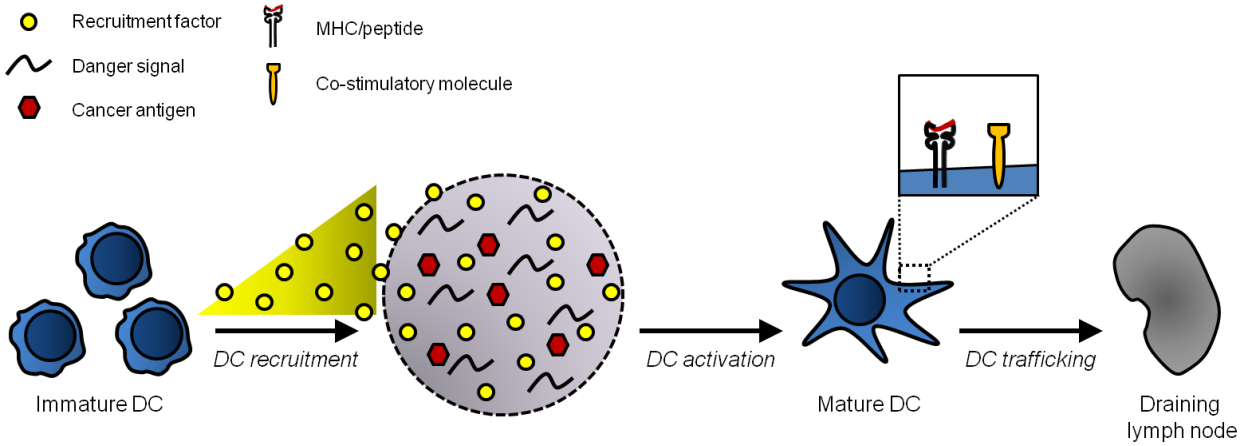

Figure 2.6. Porous scaffolds can act as microenvironments for programming dendritic cells *in situ*. Immature DCs accumulate within the porous scaffold in response to a recruitment factor gradient. Inside the scaffold microenvironment, immature DCs acquire cancer antigen and become activated by danger signals presented by the scaffold matrix. Activated DCs present cancer antigen-derived peptides on cell surface MHC molecules and upregulate surface co-stimulatory molecules. Activated DCs subsequently traffic from the scaffold to the draining lymph nodes where they can initiate a T cell response.

Based on this paradigm, highly porous bulk scaffolds fabricated from the degradable copolymer PLG, loaded with GM-CSF as an immune cell attractant, CpG as a danger signal, and tumor lysate as an antigen source were employed as *in situ* DC programming devices (Fig. 2.7a) [40, 41, 117, 118]. PLG scaffolds released GM-CSF in a sustained manner, resulting in robust GM-CSF

dose-dependent accumulation of CD11c+ DCs within the scaffold following subcutaneous implantation (Fig. 2.7b). Notably, DC numbers within the device were on the order of 10^6, comparable to the number of DCs commonly expanded and deployed in *ex vivo* protocols [117]. CpG nanoparticles presented locally within the PLG matrix promoted the activation of infiltrating DCs, facilitating their subsequent trafficking to the draining lymph nodes. In a murine melanoma model, vaccines promoted robust tumor-specific CTL responses (Fig. 2.7c), which translated to 90% survival in the prophylactic setting, and 50% survival in the therapeutic setting (Fig. 2.7d) [117]. The PLG vaccine was found to recruit diverse DC subsets to the scaffold site, including CD8+ DCs, which are important for cross-presentation, and plasmacytoid DCs, which produce type I interferons that could further promote local DC activation [117]. Importantly, vaccine persistence for greater than a week was found to be necessary for the induction of a durable response [119]. In follow-up studies, these matrices were alternatively used to deliver the cytokine Flt3L, the chemokine CCL20 [40], and the TLR ligands poly I:C and MPLA [41], demonstrating the versatility of this system as a platform approach that can be used for the controlled delivery of different immune modulating payloads.

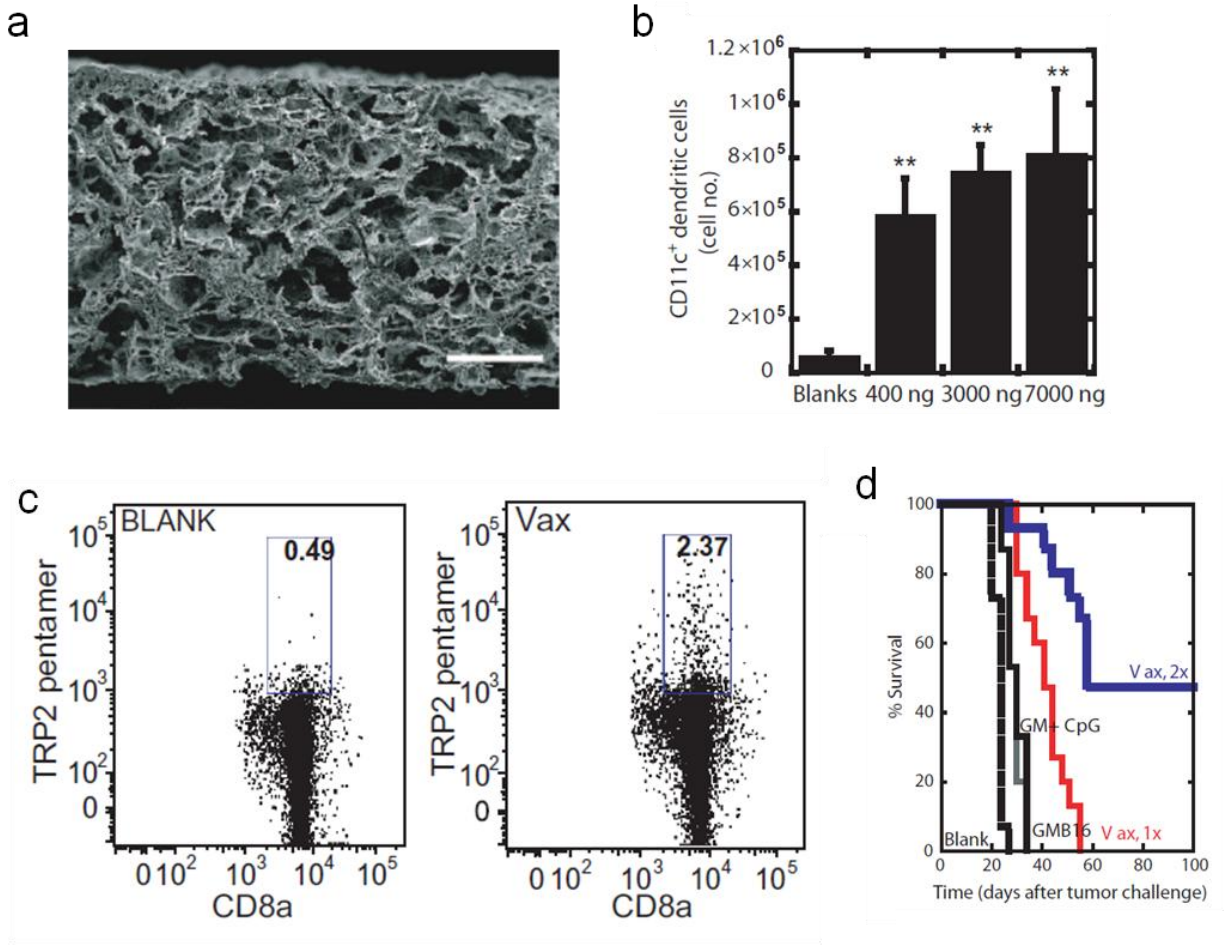

Figure 2.7. Porous PLG scaffolds as engineered microenvironments for therapeutic cancer vaccination. (a) SEM of porous PLG scaffold showing pores on the size scale of cells. Scale bar = 200 μm. (b) Quantification of CD11c+ DC accumulation in scaffolds at 14 days post-implantation in response to 0 ng, 400 ng, 3000 ng, and 7000 ng GM-CSF. (c) FACS plots of tumor antigen (TRP2)-specific CTLs in the spleens of mice on day 16 post-vaccination with blank PLG scaffolds, or PLG scaffolds containing 3000 ng GM-CSF, 100 μg CpG, and tumor lysate. (e) Survival of mice bearing subcutaneous melanoma tumors that were therapeutically vaccinated 9 days post-inoculation with blank PLG scaffolds (blank), $5x10^5$ irradiated GM-CSF-transduced melanoma cells (GMB16), 3000 ng soluble GM-CSF with 100 μg soluble CpG (GM + CpG), or PLG vaccines containing 3000 ng GM-CSF, 100 μg CpG and tumor lysate either once (Vax, 1x) or twice (vaccinated day 9 and day 19; Vax, 2x). a from [119], b-d from [118].

This PLG scaffold-based vaccine, referred to as WDVAX, is currently being investigated in a phase I clinical trial for the treatment of advanced melanoma (NCT01753089). Nine patients

have been treated at the time of this review. In general, erythema has been observed in the vicinity of the implant that has increased with subsequent implantations, suggesting general immune activity in response to the vaccine [120]. In addition, a post-treatment tumor biopsy has been obtained from one patient. Histological and flow cytometric analysis of the sample indicates a general increase in T cells in the TME relative to pre-treatment, associated with the upregulation of markers indicative of an activated phenotype. Although preliminary, the results thus far indicate that at the current dose, the vaccine is safe, and suggests that WDVAX may be contributing, at least in this particular patient, to the generation or expansion of a population of activated T cells in the TME. These early results support the potential of biomaterial scaffolds as *in situ* sites for DC recruitment and programming, and their use for therapeutic cancer vaccination.

The use of high aspect ratio mesoporous silica rods (MSRs) has recently also been reported as DC-programming scaffolds for cancer vaccination, based on the same paradigm [42] (Fig. 2.8a). In contrast to preformed bulk scaffolds that must be implanted, MSRs can be injected through a conventional needle, allowing for minimally invasive vaccine administration. Following injection, the MSRs nonspecifically assemble *in situ* to form structures with inter-particle spaces permissive for cell trafficking (Fig. 2.8a). The MSRs used in this study have nanopores on the order of approximately 10 nm, giving them an extremely high surface area for surface modification or payload adsorption. MSRs loaded with GM-CSF, CpG and OVA facilitated the sustained release of GM-CSF and CpG for upwards of 28 days *in vitro,* and enhanced the persistence of OVA compared to a soluble bolus *in vivo*. Notably, MSR vaccines were able to recruit on the order of $25x10^6$ total cells by day 7, with roughly of $3x10^6$ CD11c+ DCs, significantly more than the PLG-based vaccines. The MSR vaccines also promoted robust

humoral and cellular anti-cancer immune responses, including immunoglobulin class switching to the Th1-like isotype IgG2a, which the conventional adjuvant alum was unable to facilitate (Fig. 2.8b), and the induction of antigen-specific CD8+ T cells. This translated to significant prophylactic protection from an OVA-expressing lymphoma cell line in a murine model (Fig. 2.8c).

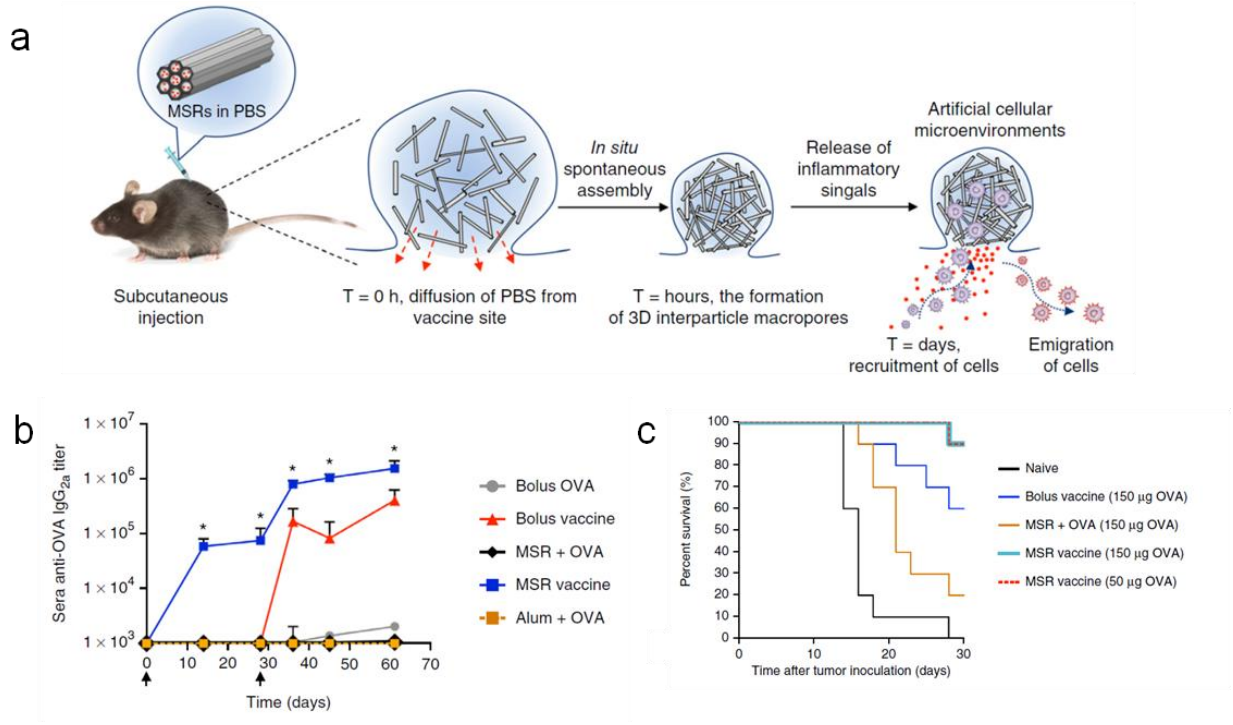

Figure 2.8. MSRs as engineered microenvironments for therapeutic vaccination. (a) Diagram illustrating mechanism of MSR *in situ* self assembly and *in vivo* function. (b) ELISA analysis of sera OVA-specific IgG2a after immunization with soluble OVA (bolus OVA), soluble GM-CSF, CpG, and OVA (bolus vaccine), soluble OVA with Imject Alum (Alum + OVA), MSRs with OVA (MSR + OVA), or MSR vaccines loaded with GM-CSF, OVA, and CpG (MSR vaccine). Black arrows indicate vaccination days. (c) Survival of naive mice or mice that were prophylactically vaccinated with 150 μg soluble OVA in combination with soluble GM-CSF and CpG (bolus vaccine), MSRs with OVA (MSR + OVA), or MSR vaccines loaded with GM-CSF, CpG, and either 50 μg or 150 μg OVA (MSR vaccine), and challenged with an OVA-expressing murine lymphoma model 10 days later. From [42].

2.6 Engineered Materials for Adoptive T Cell Therapy

In ACT, autologous T cells are isolated from the patient, either enriched for natural cancer-reactive clones or genetically modified with a cancer-specific TCR or CAR, and then transferred back into the patient to elicit an anti-cancer immune response. Naturally occurring polyclonal populations of cancer-reactive T cells can be enriched from various sources including peripheral blood and tumor biopsies. The isolation of cancer-reactive TILs from tumor samples represents a particularly promising approach for the treatment of various cancers [9, 121], and has shown exceptional efficacy in the clinic for the treatment of advanced melanoma [122]. However, the *ex vivo* culture of TILs still represents a bottleneck in TIL-based ACT, wherein, using standard methods, it is challenging to expand the cells in a rapid and cost-efficient manner while maintaining them in an undifferentiated and functional state, and in which a consistent product is obtained following the *ex vivo* culture protocol [18, 19]. In addition, challenges also remain with respect to maintaining cell persistence and sustained effector functionality following bolus cell administration, wherein lymphodepletion regimens and systemic co-administration of survival factors, which are associated with significant morbidity and inflammatory toxicities, respectively, are necessary for effective TIL-based ACT [20, 21].

TCR- and CAR-transduced T cell-based ACT has also shown extremely promising results in the clinic, in particular, for B cell malignancies, using transgenic T cells specific for CD19 [7], which is expressed by most malignant B cells. The use of such genetically engineered T cells for a range of other malignancies is also being actively explored [8, 123], although their widespread use has thus far been limited by their extreme potency, wherein the use of high-

affinity/avidity TCR or CAR T cells specific for cancer antigens expressed even at low levels in normal tissues has resulted in significant, even fatal, off-tumor on-target toxicities [124, 125]. Consistent with this, treatment of patients with CD19-specific TCR- or CAR-transduced T cells also results in the T cell-mediated elimination of normal B cells, necessitating immunoglobulin infusions following therapy [126]. Also, despite these potent effects, similar to the use of TILs, genetically-transduced T cells can also suffer from limited survival, persistence, and sustained functionality following bolus transfer, typically necessitating preparative lymphodepletion regimens to be performed prior to cell transfer, and in some cases, systemic cytokine administration [127, 128].

Biomaterials can potentially help to overcome some of the challenges currently associated with ACT. Specifically, the following topics will be discussed: (1) the design of materials as biomimetic substrates for the efficient *ex vivo* expansion of "high quality" T cells, (2) engineered particles that support the *in vivo* expansion of transferred T cells, and (3) engineered microenvironments as cell delivery vehicles that support the *in situ* expansion and sustained functionality of transferred T cells.

Efficient *ex vivo* cell expansion is one of the primary bottlenecks in TIL-based ACT. Early approaches for ACT used autologous monocyte-derived APCs for T cell expansion [129]. However, the use of autologous APCs is associated with numerous limitations, specifically, (1) the autologous cells could be affected by the patient's disease state or could respond to cues produced by the lymphocytes, resulting in the generation of a suboptimal and inconsistent T cell product [130, 131], and (2) the need to generate and culture these cells on a patient-specific basis makes the process cumbersome and costly. An alternative approach that is currently used in the clinical setting is the "rapid expansion protocol" (REP) which employs inactivated allogeneic

feeder cells in the presence of a CD3 antibody and the mitogenic cytokine IL-2 [122]. However, the use of allogeneic cells can also lead to suboptimal and inconsistent T cell products [18]. Genetically engineered "artificial APCs" (aAPCs) have also been developed to facilitate more efficient *ex vivo* T cell expansion, and this is described elsewhere [132].

An alternative approach to the use of live cells as mediators for *ex vivo* T cell expansion is the use of synthetic aAPCs, acellular materials that present the cues for promoting T cell activation and proliferation. At a minimum, synthetic aAPCs must present two critical signals: (signal 1) TCR activation via peptide-MHC complexes (antigen specific) or TCR clustering using CD3 antibodies (antigen nonspecific), and (signal 2) co-stimulation via agonistic CD28 antibodies. The coordinated provision of both signals is important because signal 1 in the absence of signal 2 has been shown to induce T cell anergy [133]. Mitogenic cytokines such as IL-2, IL-15, or IL-21 can also be added, and have been shown to fulfill the role of a "signal 3" important for optimal T cell expansion [18, 134]. The benefits of using synthetic aAPCs for T cell expansion are the design versatility, reproducibility, cost-efficiency, and scalability of synthetic systems. Standard acellular protocols for the *ex vivo* expansion of T cells typically involve the use of commercial high-throughput automated systems employing synthetic anti-CD3/CD28-immobilized beads (e.g. Dynabeads). Although convenient, these systems provide a limited set of cues to the T cells, and therefore likely promote T cell expansion with suboptimal efficiency. In addition, recent studies have highlighted the fact that the quality of the resultant T cells, with respect to their persistence and sustained functionality following transfer, is highly dependent on the *in vitro* environment in which they are expanded, and that protocols based on standard anti-CD3/CD28 beads and REP fail to produce high quality CTLs [18]. This may be due to an effect of the expansion protocol on properties of the resultant population including CD4:CD8 ratio [135],

differentiation state [136], or the "age" (telomere length) of the cells [127]. Synthetic aAPC systems that present the appropriate combinations of cues (signals 1-3) in a context that recapitulates natural APC-T cell interactions may more efficiently promote the expansion of high quality CTLs. Important contextual considerations that are discussed below include the spatial distribution of mitogen, and the avidity of the aAPC-T cell interaction, which is affected by the surface area of aAPC-T cell contact and the density of T cell stimuli.

During interactions between natural APCs and cognate T cells, APCs produce T cell mitogenic cytokines, such as IL-2, in a paracrine manner, which promote the expansion of reactive T cell clones. To mimic this process, synthetic aAPCs have been prepared using spherical PLG cores immobilized with either anti-CD3 or peptide-MHC, and anti-CD28, and loaded with soluble IL-2 for local release to interacting T cells [134] (Fig. 2.9a). These synthetic aAPCs were found to promote efficient expansion of T cells *in vitro* compared to the same cues in soluble form, and a 10-fold lower dose of encapsulated IL-2 was found to promote a comparable degree of T cell expansion as soluble factor (Fig. 2.9b). Based on a similar design, it could be possible to prepare synthetic aAPCs that release multiple soluble cues, including polarizing signals, such as IL-12 or IFNγ, which may enhance the quality of the resultant T cells [18]. It was additionally found with this system that spherical microbeads on the size scale of natural APCs were more effective aAPCs than spherical nanobeads bearing the same signals, likely due to the inability of T cells to form high surface area interfaces with the spherical nano-aAPCs due to their high angles of curvature. Related to this is the finding that the shape of the aAPC also impacts the effectiveness of T cell activation wherein higher aspect ratio ellipsoidal microparticle aAPCs promoted more efficient *in vitro* T cell expansion than lower aspect ratio or spherical counterparts of the same volume. Time-lapsed microscopy demonstrated this is likely

due to a larger surface area of contact between the particles and the T cells along the long axis of the particles, as T cells were observed to actively reposition themselves along this axis and generate higher surface area contacts with the aAPCs [137].

Although solid microbead-based systems roughly mimic the size and geometry of natural APCs, the immobilization of surface cues on a static substrate precludes the molecular reorganization that takes place during natural APC-T cell interactions, in which an immunological synapse (IS) is formed. The formation of the IS facilitates the assembly of high-density TCR microdomains on the size scale of cells, and this process has been shown to be critical for efficient T cell signaling [138]. To more closely mimic this process, liposomes bearing MHC II-enriched lipid rafts [139] and 3D supported lipid bilayers incorporating purified MHC I molecules [140] have been prepared, which allow for dynamic reorganization of the respective surface-associated cues. An alternative approach is the use of aAPC "nanoworms" comprised of a semi-flexible 200 nm poly(isocyano peptide) polymer modified with anti-CD3 [141]. Anti-CD3-modified nanoworms activated T cells more efficiently than free or PLG microparticle-immobilized anti-CD3. This likely owes to the ability of the semi-flexible polymeric backbone to facilitate dynamic high avidity interactions with T cells.

An alternative approach for *ex vivo* T cell expansion is the use of high surface area materials, such as carbon nanotubes (CNTs), that can present T cell stimuli at extremely high local densities [142, 143]. Chemical treatment of CNTs can be used to introduce surface defects and improve protein adsorption, further increasing the density at which stimuli can be presented. Specifically, such treatment was found to facilitate the formation of local antibody clusters on the size scale of cells, approximately 5-6 μm in diameter, with an inter-antibody distance of approximately 4.5 nm, allowing for high avidity interactions with T cells over a contact surface

area that has been shown to be in the range optimal for IS formation (Fig. 2.9c) [138]. Notably, based on IL-2 production, T cells cultured with chemically treated CNTs immobilized with anti-CD3 and anti-CD28 showed enhanced activation compared to untreated CNTs or polystyrene microbeads bearing the same cues (Fig. 2.9d).

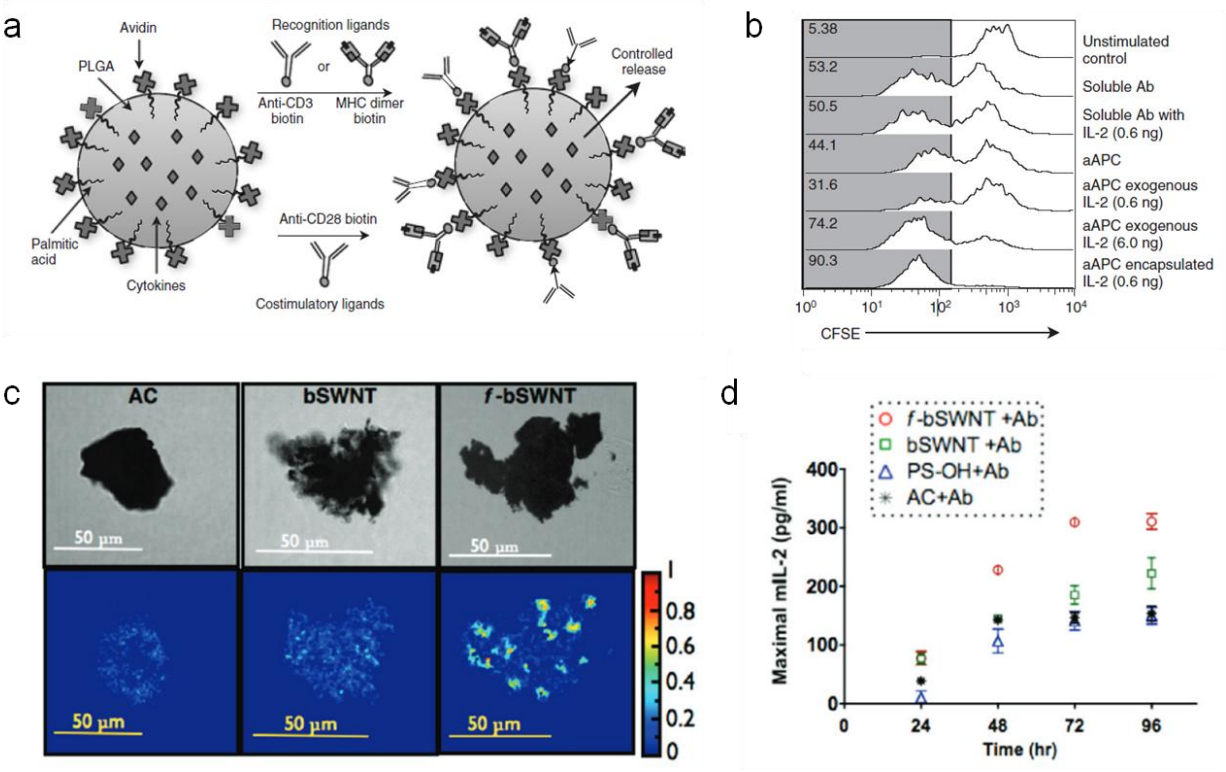

Figure 2.9. Material strategies for *ex vivo* T cell expansion. (a) Diagram of PLG bead-based aAPCs that are surface immobilized with either anti-CD3, for polyclonal T cell expansion, or peptide-presenting MHC dimers, for monoclonal T cell expansion. Beads also surface present anti-CD28 as a co-stimulatory signal, and can release soluble mitogenic factors in a controlled manner. (b) Flow cytometry histograms showing T cell expansion, as measured by CFSE dilution, when T cells are either left unstimulated, or stimulated with soluble anti-CD3 and anti-CD28 (soluble Ab), soluble anti-CD3 and anti-CD28 with 0.6 ng soluble IL-2 (Soluble Ab with IL-2), PLG microbeads presenting anti-CD3 and anti-CD28 (aAPC), PLG microbeads presenting anti-CD3 and anti-CD28 supplemented with either 0.6 ng or 6 ng soluble IL-2 (aAPC exogenous IL-2), or PLG microbeads presenting anti-CD3 and anti-CD28 and encapsulated with 0.6 ng IL-2 (aAPC encapsulated IL-2). The numbers represent the percentage of divided cells in that condition as defined by the gray gate. (c) Confocal (top row), and FRET efficiency images (bottom row) showing cell-scale antibody clusters on chemically activated carbon (AC), untreated bundled SWNTs (bSWNT), and chemically treated "functionalized" bundled SWNTs

(f-bSWNT). Colored legend represents degree of FRET efficiency in lower row images. (d) Quantification of T cell activation based on maximal IL-2 production, as measured over a range of stimuli concentrations, following T cell culture for various amounts of time on anti-CD3- and anti-CD28-immobilized chemically activated carbon (AC), untreated bundled SWNTs (bSWNT), chemically treated "functionalized" bundled SWNTs (f-bSWNT), or hydroxylated polystyrene beads (PS-OH). a, b from [134]. c, d from [143].

Recently, an approach has been described for the generation of a carbon nanotube-polymer composite (CNP) that combines these T cell stimulatory CNTs with IL-2-releasing, magnetite-loaded PLG nanoparticles (Fig. 2.10a,b) [144]. By combining the high avidity antigen presentation afforded by the CNTs with the paracrine release of IL-2 facilitated by the PLG nanoparticles, extremely robust expansion of functional T cells was observed *in vitro*. In addition, the magnetite-loaded PLG nanoparticles allowed the CNPs to be efficiently separated from the expanded T cells prior to cell transfer, an important step for clinical translation. Following two-weeks of *ex vivo* culture, the magnitude of T cell expansion, and the effector function of the resultant T cells as evaluated by IFNγ and granzyme B production, were both significantly higher with CNPs than with CNTs, commercial Dynabeads, or soluble tetramer. This finding was similar with or without the addition of exogenous IL-2. Importantly, throughout the duration of the culture, CNPs facilitated the greatest maintenance of CD27+CD8+ T cells. CD27 is an early-differentiation T cell marker that has been strongly correlated with clinical response to ACT [136]. ACT using CNP-expanded CTLs significantly slowed tumor growth in a therapeutic murine melanoma model compared to mock treatment, and this effect was associated with an increase in tumor T cell infiltration. Notably, in order to obtain a comparable therapeutic effect with Dynabeads-expanded CTLs, a 1000-fold greater concentration of IL-2 during *ex vivo* culture was required. CNPs were also used for the expansion of human Epstein–Barr virus (EBV)-specific CD8+ T cells from healthy donor PBMCs or leukopaks using either EBV

peptide-loaded MHC or anti-CD3. Strikingly, either CNP-mediated approach led to the more efficient expansion of EBV peptide-specific CD8+ T cells than EBV peptide-loaded primary DCs with exogenous IL-2, the clinical gold standard for T cell expansion (Fig. 2.10c). This work illustrates the potential of more closely recapitulating natural APC-T cell interactions through the design of systems that collectively provide multiple cues in an appropriate context. Specifically, this work demonstrates how the use of such composite systems can translate to the more efficient *ex vivo* expansion of higher quality T cells, and speaks to the potential of using materials to engineer novel synthetic approaches for *ex vivo* T cell expansion for ACT.

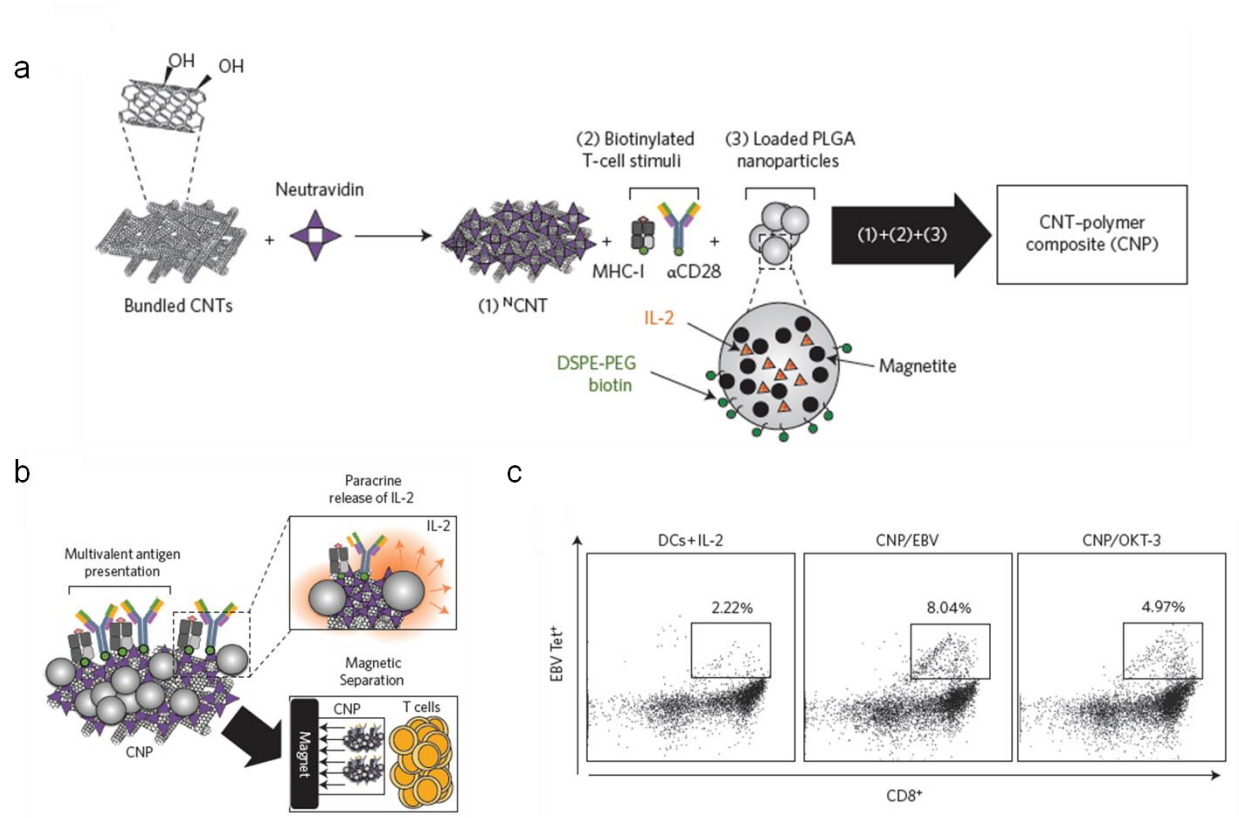

Figure 2.10. Carbon nanotube-polymer composite (CNP) for *ex vivo* T cell expansion. (a) Schematic of CNP assembly. Neutravidin-adsorbed CNTs (^{N}CNT) are associated with biotinylated T cell stimuli and biotin-presenting PLG nanoparticles encapsulating IL-2 and magnetite. (b) Schematic of CNP functionality. CNPs present high density surface-adsorbed T cell stimuli, facilitate paracrine IL-2 release, and can be separated from T cells using magnetic

separation. (c) Flow cytometry plots showing enhanced expansion of human EBV-specific CD8+ human T cells using CNPs presenting EBV peptide in MHC or anti-CD3 (OKT-3), compared to primary DCs loaded with EBV peptide and cultured in soluble IL-2. From [144].

Limited cell persistence following bolus cell administration represents another challenge to effective ACT, and necessitates preparative lymphodepletion regimens prior to cell transfer, as well as the systemic co-administration of exogenous survival cues such as IL-2, leading to patient morbidity and systemic toxicities, respectively. Relevant to this, the use of synthetic aAPCs to improve *in vivo* T cell survival has also been explored. For example, subcutaneous administration of synthetic aAPCs based on PLG microparticles were reported to improve the outcome of prophylactic ACT in a murine melanoma model based on tumor growth kinetics and overall survival [137]. Interestingly, high aspect ratio ellipsoidal microparticle aAPCs were found to be more effective than their spherical counterparts at slowing tumor growth, consistent with the observation that elongated particles facilitate more efficient T cell expansion *in vitro*.

Although it has been shown that spherical cell-sized microparticles are more efficient aAPCs than spherical nanoscale counterparts, the generally unfavorable bioavailability profiles of microparticles following systemic administration makes the effective *in vivo* translation of microparticle- based aAPCs challenging. Based on these observations, nanoellipsoidal PLG aAPCs were prepared to leverage the improved bioavailability of nanoparticles following systemic administration, while achieving a larger radius of curvature to support a larger contact surface area with T cells [145]. Nanoellipsoidal aAPCs were found to resist uptake by macrophages *in vitro* to a greater extent, and to have a prolonged blood half-life following systemic administration compared to spherical counterparts. Nanoellipsoidal aAPCs were also observed to promote the *in vitro* expansion of responder T cells more efficiently than spherical counterparts

loaded with the same amount of peptide-MHC and anti-CD28, demonstrating the beneficial effect of nano-aAPCs with larger radii of curvature. Notably, the systemic co-administration of nanoellipsoidal aAPCs with responder T cells into immunocompetent mice promoted the *in vivo* proliferation of the administered T cells, with enhanced persistence of the administered T cells observed in the blood, lymph nodes, and spleen at 10 days post-injection. In contrast, spherical nano-aAPCs showed no improvement with respect to *in vivo* T cell expansion compared to mock treatment. The nanoellipsoidal aAPCs could have significant synergy with current ACT protocols by enhancing the *in vivo* survival and persistence of administered cells, and could potentially also have utility as a therapeutic vaccine platform.

An alternative approach to improving cell persistence in ACT is the design of nanomaterials as cell-associated depots for the sustained pseudo-autocrine delivery of survival and proliferative cues [146]. In such an approach, stabilized multilamellar liposomes were attached to cell surfaces via endogenous cell-surface thiol groups. The degree of uptake of cell surface-associated particles was previously found to be dependent on the size and surface properties of the particle [147]. When 300 nm liposomes were attached to CD8+ T cells, it was observed that the particles remained at the cell surface, and that up to 100 particles could be conjugated to the T cells without affecting their overall proliferative capacity, cytotoxic effector functionality, or *in vivo* migratory potential. When these depots were loaded with IL-15 superagonist (IL-15Sa) and IL-21, which have been shown to promote T cell expansion and function *in vivo*, sustained release of the cytokines was observed over 7 days *in vitro.* In a therapeutic murine model of metastatic melanoma, the conjugation of cytokine-loaded particles to tumor-specific CTLs was found to significantly enhance their persistence compared to systemic cytokine administration, and a subset of the transferred T cells homed to the spleen and lymph nodes and adopted a

central memory phenotype. Consistent with this, all mice that received T cells conjugated with the particulate cytokine depots exhibited long-term survival in this model. Such systems, broadly referred to as "cellular backpacks" have also been explored for the targeted delivery of cell-associated payloads to specific tissues, leveraging the carrier cells as tissue-homing vectors [148]. Such an approach could be similarly used with T cells for the delivery of microenvironment-polarizing factors to the TME that may enhance the activity of local effector cells, including the transferred cells themselves.

The accumulation of cancer-reactive T cells in the TME following systemic administration represents another challenge to effective ACT, and biomaterial scaffolds can be used to facilitate the sustained delivery of T cells to the vicinity of accessible or resected tumors. A macroporous alginate scaffold, modified with a lymphocyte adhesion peptide, and entrapping lipid-enveloped mesoporous silica microspheres loaded with soluble IL-15Sa and surface presenting anti-CD3 and anti-CD28 was recently described [43]. The scaffold facilitated time-dependent migration of seeded T cells out of the device (Fig. 2.11a) and promoted enhanced T cell expansion and survival compared to unloaded scaffolds *in vitro* (Fig. 2.11b). In therapeutic murine models of resected breast cancer and nonresectable ovarian cancer, delivery of tumor-targeting CTLs in the device (either primary 4T1 breast cancer-responsive T cells or NKG2D CAR-transduced T cells, respectively) promoted enhanced T cell persistence, likely due to time-dependent *in vivo* cell expansion, which took place over the course of at least 12 days (Fig. 2.11c). In contrast, bolus T cell delivery via various administration routes, with or without *in vitro* prestimulation and systemic exogenous mitogen administration, resulted in a time-dependent decrease in T cell load over the same timeframe (Fig. 2.11c). The enhanced T cell persistence translated to significantly enhanced survival in both tumor models (Fig. 2.11d). Of

particular note is the observation that T cells deployed as a bolus directly into the tumor resection cavity showed limited proliferation and upregulated markers associated with exhaustion, whereas T cells delivered into the resection cavity via the scaffold device proliferated robustly, maintained a non-exhausted phenotype, and migrated from the implant into the peritumoral tissue. These observations highlight the critical importance of the local microenvironment for T cell function, and support the use of biomaterial scaffolds as cell delivery devices in ACT. The versatility of the general paradigm will allow for the potential development of next-generation systems, for example, based on injectable hydrogels [28, 149], or materials that deliver additional signals such as T cell polarizing factors, or chemokines for recruiting endogenous cells such as DCs or other myeloid cells that can favorably interact with the transplanted T cells within the scaffold.

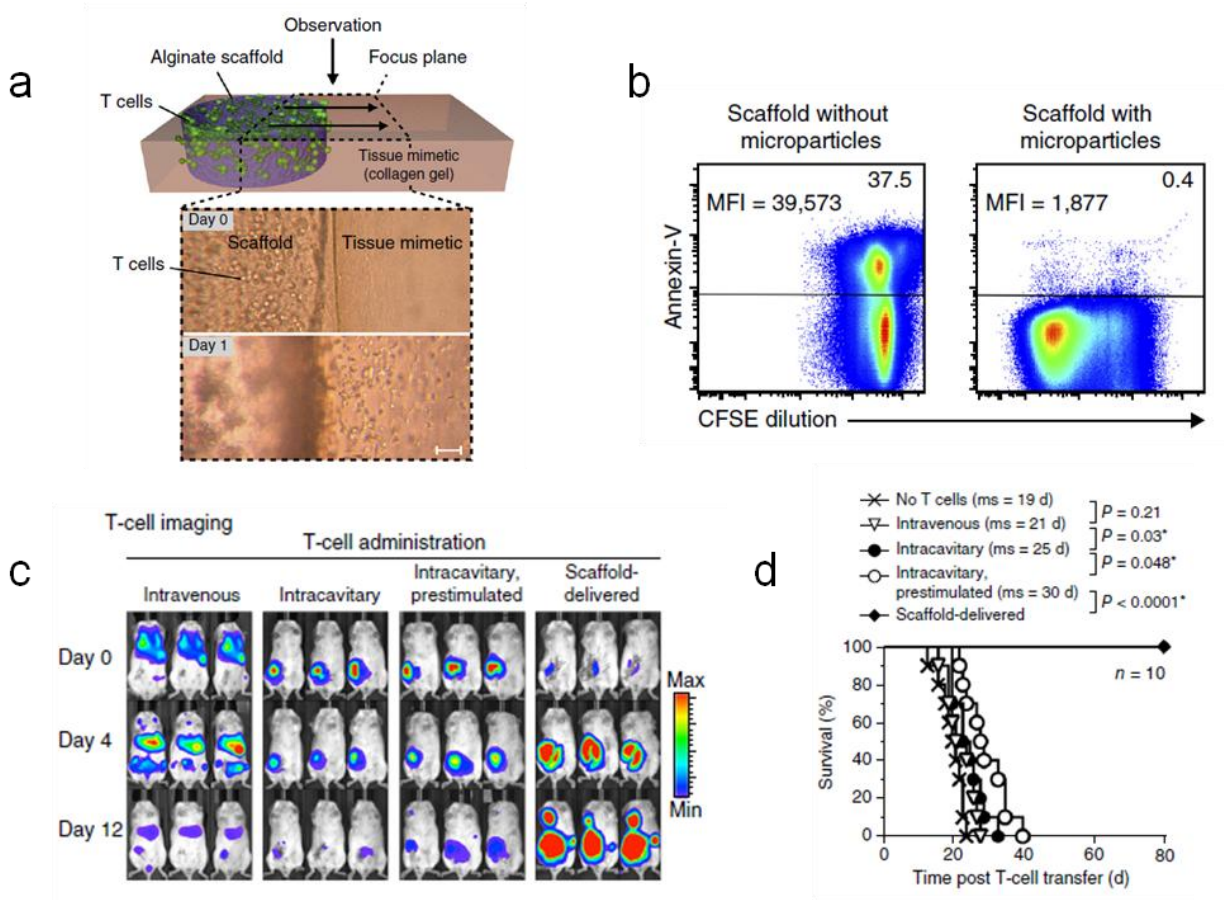

Figure 2.11. Biopolymer implants for *in situ* T cell expansion. (a) Top, schematic of the *in vitro* assay used to quantify cell migration out of the scaffold (purple) and into a collagen gel tissue mimetic (pink). Bottom, time-lapsed light micrographs showing lymphocyte migration out of adhesion peptide-modified scaffolds after one day. Scale bar = 100 μm. (b) Flow cytometry plots showing robust T cell proliferation, as measured by CFSE dilution, and maintenance of T cell viability, as measured by negative expression of the apoptosis marker annexin-V, after *in vitro* culture in microparticle-loaded but not blank scaffolds for 7 days. CFSE MFI is indicated on the left and percent of cells positive for annexin-V is indicated on the right for each plot. (c) *In vivo* bioluminescence imaging of breast tumor-specific T cells retrovirally transduced with CBR-luc 0 days, 4, days, and 12 days post-transfer in resected breast cancer model. $7x10^6$ cells were administered intravenously, into the resection cavity (intracavitary) with or without *in vitro* prestimulation with IL-15Sa, anti-CD3, anti-CD28, and anti-CD137, or delivered via the scaffold device into the resection cavity. Colored legend indicates bioluminescence intensity. (d) Survival of mice in resected breast cancer model either untreated (no T cells) or treated with $7x10^6$ T cells administered either intravenously, intracavitary, intracavitary following *in vitro* prestimulation as defined in (c), or via the scaffold device into the resection cavity. Mean survival of each group is indicated in the legend (ms). From [43].

2.7 Conclusion

The recent clinical successes of checkpoint inhibitor therapies in a wide range of solid and hematologic malignancies, and CAR T cell therapies in diverse hematologic malignancies, have significantly heightened the enthusiasm for cancer immunotherapy. However, despite these successes, the vast majority of immunotherapies in clinical trials fail to meet their endpoints. Further, even checkpoint inhibitor therapies, which have shown unprecedented clinical success for a wide range of cancers, are only effective to date for a minority of the patient population [10, 12, 150]. In order to design more effective cancer immunotherapies in the future, it is important to consider why current therapies fail, both in the context of therapies that elicit generally suboptimal effects, and in the context of immunotherapies that are highly efficacious for a subset of the patient pool, but show minimal effects in the remainder. Broadly, the reason cancer immunotherapies fail in either context is likely because, (1) the immunotherapy fails to elicit a robust enough response, or (2) the response elicited by the immunotherapy is irrelevant or suboptimal for the particular patient. Overcoming these limitations will require both an improved understanding of the immunobiology of cancer, as well as the design of therapies that allow for the more precise and robust induction of the desired response. In other words, we must be able to (1) accurately assess what type of response needs to be generated in the particular patient, (2) define specific immunotherapeutic subgoals (e.g. generating *de novo* cancer-specific T cells, expanding pre-existing cancer-specific T cell number, or enhancing the effector functions of cancer-specific T cells through regulation of tumor-imposed immunosuppression), and (3) design systems that can precisely and effectively achieve those subgoals. Engineered materials will likely play an important role in facilitating the latter.

Being able to define optimal immunotherapy regimens on a patient-specific basis has thus far proven challenging because, currently, we have a relatively limited understanding of the specific determinants that contribute to a robust anti-cancer response, and of the biomarkers that indicate what types of immune interventions are optimal for fulfilling those determinants. The significance of a large range of factors including the frequency, demographic, phenotype, and spatial distributions of tumor-infiltrating and peripheral immune cell populations has been demonstrated [95, 151], but the ability to translate these readouts into an efficacious therapeutic regimen remains elusive. A better understanding of the specific determinants underlying a robust anti-cancer response will inform the design of more effective immunotherapies by providing a more accurate set of design criteria. In addition, it is only when we are able to translate these determinants into specific immunotherapeutic subgoals that the spatiotemporal precision afforded by the use of engineered materials is likely to be exceptionally constructive. On the other hand, to be able to effectively apply materials for the development of cancer immunotherapies, it will be important to gain a better understanding of how material systems interact with the immune system. In this respect, a systematic characterization of how immunologic components interact with, and respond to material systems at relevant timescales, and how these interactions are affected by the physical, mechanical, and physicochemical properties of the particular material system, is necessary. Such characterization will need to be coupled with studies aimed at understanding the mechanisms by which these material-immune system interactions take place. Indeed, the development of such a framework represents the primary challenge to the establishment of a "materials toolbox" that will enable the widespread application of biomaterials in cancer immunotherapy design in the future.

In any case, the application of materials to the development of cancer immunotherapies holds significant promise, as demonstrated by the work highlighted in this review. Advancements in immuno-oncology will continue to fuel the development of new materials-based cancer immunotherapy strategies in the future. For example, targeted delivery strategies using nanomaterial vehicles could be used for the delivery of anti-CTLA-4 antibodies, which function by promoting indiscriminate T cell activation and expansion, often leading to systemic inflammatory toxicities. Indeed, the magnitude of the increase in peripheral T cell TCR diversity in patients following treatment with an anti-CTLA-4 antibody was shown to be correlated with patient inflammatory toxicity but not with clinical outcome [152]. Using materials to promote the preferential accumulation or sequestration of the antibody in target sites, such as the tdLNs or the TME, could curtail systemic toxicities and potentially increase the therapeutic window of the drug. Work is underway to develop agents that target other co-inhibitory [153] as well as co-stimulatory [154] pathways, and nanomaterial-mediated targeted delivery strategies could similarly be useful for some of these agents.

Recently, workflows have been described for the patient-specific identification of neoantigens [114, 115], antigens produced in tumors due to random nonsynonymous somatic mutations. Neoantigens represent particularly attractive vaccine targets because they are not subject to central tolerance mechanisms that promote the deletion of high-affinity reactive T cell clones, and the utility of such neoantigen-targeting vaccines has recently been demonstrated in preclinical models [155]. Material subunit vaccines could be tremendously effective mediators of neoantigen-based vaccination, particularly those that were developed using model antigens that are also not subject to central tolerance and may consequently be optimized for inducing responses against such antigens. The design of biomaterials for neoantigen vaccines is likely to

be an extremely promising area in the future. Alternatively, materials-based approaches for promoting *ex vivo* T cell expansion and survival using antigen-presenting synthetic aAPCs could be employed, for example, for efficiently expanding neoantigen-reactive TILs for ACT.

As we gain a better understanding of the optimal conditions for expanding high quality T cells *ex vivo*, synthetic materials that can facilitate the combinatorial release or presentation of multiple cues in a spatiotemporally-defined manner are likely to become increasingly important. Future studies exploring the use of synthetic aAPCs for T cell expansion will likely focus on the quality of the resultant T cells following *in vivo* transfer rather than just the efficiency of *ex vivo* T cell expansion and function. The use of biomaterial scaffolds for the delivery of high-affinity/avidity TCR- and CAR-transduced T cells could potentially also be useful in the future not only as devices to promote the enhanced survival and expansion of these cells *in vivo*, as has already been demonstrated [43], but potentially also as physical microenvironments that sequester these T cells in the vicinity of the tumor, curtailing the off-tumor on-target toxicity that has largely precluded the use of these highly potent cells for the treatment of solid malignancies [124, 125].

In conclusion, biomaterials represent a broad and versatile toolbox with which to design tailored cancer immunotherapies that may overcome many limitations of current approaches. In particular, this review discussed the use of nano- to microscale materials as targeted delivery vehicles for immune modulating payloads, as colloidal scaffolds in subunit vaccine formulations, and as synthetic aAPCs for *ex vivo* T cell expansion. The use of macroscale materials as microenvironments for recruiting and programming cells *in situ*, and for facilitating the survival and expansion of adoptively transferred cells, was also discussed. The ways in which engineered materials can productively interface with cancer immunotherapy are vast, and as we gain a better

understanding of cancer immunobiology and of material-immune system interactions, this interface is likely to become even more prolific.

2.8 Acknowledgments

The authors acknowledge support from the NIH (R01 EB015498) and the Wyss Institute.

2.9 References

1. Organization, W.H. World Cancer Report 2014 (ePUB). *WHO. int. http://apps. who. int/bookorders/anglais/detart1. jsp* (2014).
2. Hamid, O. et al. Safety and tumor responses with lambrolizumab (anti–PD-1) in melanoma. *New England Journal of Medicine* **369**, 134-144 (2013).
3. Brahmer, J.R. et al. Safety and activity of anti–PD-L1 antibody in patients with advanced cancer. *New England Journal of Medicine* **366**, 2455-2465 (2012).
4. Sampson, J.H. et al. An epidermal growth factor receptor variant III–targeted vaccine is safe and immunogenic in patients with glioblastoma multiforme. *Molecular cancer therapeutics* **8**, 2773-2779 (2009).
5. Kantoff, P.W. et al. Overall survival analysis of a phase II randomized controlled trial of a Poxviral-based PSA-targeted immunotherapy in metastatic castration-resistant prostate cancer. *Journal of Clinical Oncology* **28**, 1099-1105 (2010).
6. Walter, S. et al. Multipeptide immune response to cancer vaccine IMA901 after single-dose cyclophosphamide associates with longer patient survival. *Nature medicine* **18**, 1254-1261 (2012).
7. Kochenderfer, J.N. et al. Eradication of B-lineage cells and regression of lymphoma in a patient treated with autologous T cells genetically engineered to recognize CD19. *Blood* **116**, 4099-4102 (2010).
8. Robbins, P.F. et al. Tumor regression in patients with metastatic synovial cell sarcoma and melanoma using genetically engineered lymphocytes reactive with NY-ESO-1. *Journal of Clinical Oncology* **29**, 917-924 (2011).
9. Tran, E. et al. Cancer immunotherapy based on mutation-specific CD4+ T cells in a patient with epithelial cancer. *Science* **344**, 641-645 (2014).

10. Hodi, F.S. et al. Improved survival with ipilimumab in patients with metastatic melanoma. *New England Journal of Medicine* **363**, 711-723 (2010).

11. Sheridan, C. Immune-checkpoint inhibitors march on, now in combinations. *Nature biotechnology* **32**, 297-299 (2014).

12. Postow, M.A. et al. Nivolumab and ipilimumab versus ipilimumab in untreated melanoma. *New England Journal of Medicine* (2015).

13. Kantoff, P.W. et al. Sipuleucel-T immunotherapy for castration-resistant prostate cancer. *New England Journal of Medicine* **363**, 411-422 (2010).

14. Hussein, M. et al. A phase I multidose study of dacetuzumab (SGN-40; humanized anti-CD40 monoclonal antibody) in patients with multiple myeloma. *haematologica* **95**, 845-848 (2010).

15. Bouchlaka, M.N. et al. Aging predisposes to acute inflammatory induced pathology after tumor immunotherapy. *The Journal of experimental medicine* **210**, 2223-2237 (2013).

16. Heimberger, A.B. et al. Epidermal growth factor receptor VIII peptide vaccination is efficacious against established intracerebral tumors. *Clinical Cancer Research* **9**, 4247-4254 (2003).

17. Ramanathan, R.K. et al. Phase I study of a MUC1 vaccine composed of different doses of MUC1 peptide with SB-AS2 adjuvant in resected and locally advanced pancreatic cancer. *Cancer Immunology, Immunotherapy* **54**, 254-264 (2005).

18. Jin, C. et al. Allogeneic lymphocyte-licensed DCs expand T cells with improved antitumor activity and resistance to oxidative stress and immunosuppressive factors. *Molecular Therapy—Methods & Clinical Development* **1** (2014).

19. Zeng, W., Su, M., Anderson, K.S. & Sasada, T. Artificial antigen-presenting cells expressing CD80, CD70, and 4-1BB ligand efficiently expand functional T cells specific to tumor-associated antigens. *Immunobiology* **219**, 583-592 (2014).

20. Dudley, M.E. et al. Adoptive cell transfer therapy following non-myeloablative but lymphodepleting chemotherapy for the treatment of patients with refractory metastatic melanoma. *Journal of Clinical Oncology* **23**, 2346-2357 (2005).

21. Chou, S.H. et al. Palmitate-derivatized human IL-2: a potential anticancer immunotherapeutic of low systemic toxicity. *Cancer Immunology, Immunotherapy* **62**, 597-603 (2013).

22. Larocca, C. & Schlom, J. Viral Vector–based Therapeutic Cancer Vaccines. *Cancer journal (Sudbury, Mass.)* **17**, 359 (2011).

23. Lichty, B.D., Breitbach, C.J., Stojdl, D.F. & Bell, J.C. Going viral with cancer immunotherapy. *Nature Reviews Cancer* **14**, 559-567 (2014).

24. Liong, M. et al. Multifunctional inorganic nanoparticles for imaging, targeting, and drug delivery. *ACS nano* **2**, 889-896 (2008).

25. Qian, X. et al. In vivo tumor targeting and spectroscopic detection with surface-enhanced Raman nanoparticle tags. *Nature biotechnology* **26**, 83-90 (2008).

26. Fan, Z. et al. Multifunctional plasmonic shell–magnetic core nanoparticles for targeted diagnostics, isolation, and photothermal destruction of tumor cells. *ACS nano* **6**, 1065-1073 (2012).

27. Zhang, L., Guo, R., Yang, M., Jiang, X. & Liu, B. Thermo and pH Dual-Responsive Nanoparticles for Anti-Cancer Drug Delivery. *Advanced Materials* **19**, 2988-2992 (2007).

28. Koshy, S.T., Ferrante, T.C., Lewin, S.A. & Mooney, D.J. Injectable, porous, and cell-responsive gelatin cryogels. *Biomaterials* **35**, 2477-2487 (2014).

29. Chiappini, C. et al. Biodegradable silicon nanoneedles delivering nucleic acids intracellularly induce localized in vivo neovascularization. *Nature materials* (2015).

30. Park, J.H. et al. Systematic surface engineering of magnetic nanoworms for in vivo tumor targeting. *small* **5**, 694-700 (2009).

31. Cruz, L.J. et al. Targeting nanoparticles to CD40, DEC-205 or CD11c molecules on dendritic cells for efficient CD8+ T cell response: a comparative study. *Journal of Controlled Release* **192**, 209-218 (2014).

32. Yang, L. et al. Single chain epidermal growth factor receptor antibody conjugated nanoparticles for in vivo tumor targeting and imaging. *Small* **5**, 235-243 (2009).

33. Verma, A. et al. Surface-structure-regulated cell-membrane penetration by monolayer-protected nanoparticles. *Nature materials* **7**, 588-595 (2008).

34. Marrache, S., Tundup, S., Harn, D.A. & Dhar, S. Ex vivo programming of dendritic cells by mitochondria-targeted nanoparticles to produce interferon-gamma for cancer immunotherapy. *ACS nano* **7**, 7392-7402 (2013).

35. Li, H., Li, Y., Jiao, J. & Hu, H.-M. Alpha-alumina nanoparticles induce efficient autophagy-dependent cross-presentation and potent antitumour response. *Nature nanotechnology* **6**, 645-650 (2011).

36. Macdonald, M.L. et al. Tissue integration of growth factor-eluting layer-by-layer polyelectrolyte multilayer coated implants. *Biomaterials* **32**, 1446-1453 (2011).

37. Fabiilli, M.L. et al. Acoustic droplet–hydrogel composites for spatial and temporal control of growth factor delivery and scaffold stiffness. *Acta biomaterialia* **9**, 7399-7409 (2013).

38. Cezar, C.A. et al. Biphasic ferrogels for triggered drug and cell delivery. *Advanced healthcare materials* **3**, 1869-1876 (2014).

39. Gauvin, R. et al. Microfabrication of complex porous tissue engineering scaffolds using 3D projection stereolithography. *Biomaterials* **33**, 3824-3834 (2012).

40. Ali, O.A., Tayalia, P., Shvartsman, D., Lewin, S. & Mooney, D.J. Inflammatory Cytokines Presented from Polymer Matrices Differentially Generate and Activate DCs In Situ. *Advanced functional materials* **23**, 4621-4628 (2013).

41. Ali, O.A. et al. Identification of Immune Factors Regulating Antitumor Immunity Using Polymeric Vaccines with Multiple Adjuvants. *Cancer research* **74**, 1670-1681 (2014).

42. Kim, J. et al. Injectable, spontaneously assembling, inorganic scaffolds modulate immune cells in vivo and increase vaccine efficacy. *Nature biotechnology* **33**, 64-72 (2015).

43. Stephan, S.B. et al. Biopolymer implants enhance the efficacy of adoptive T-cell therapy. *Nature biotechnology* **33**, 97-101 (2015).

44. Chen, D.S. & Mellman, I. Oncology meets immunology: the cancer-immunity cycle. *Immunity* **39**, 1-10 (2013).

45. Ruffell, B. et al. Macrophage IL-10 blocks CD8+ T cell-dependent responses to chemotherapy by suppressing IL-12 expression in intratumoral dendritic cells. *Cancer cell* **26**, 623-637 (2014).

46. Coussens, L.M., Zitvogel, L. & Palucka, A.K. Neutralizing tumor-promoting chronic inflammation: a magic bullet? *Science* **339**, 286-291 (2013).

47. Iwai, Y. et al. Involvement of PD-L1 on tumor cells in the escape from host immune system and tumor immunotherapy by PD-L1 blockade. *Proceedings of the National Academy of Sciences* **99**, 12293-12297 (2002).

48. Feig, C. et al. Targeting CXCL12 from FAP-expressing carcinoma-associated fibroblasts synergizes with anti–PD-L1 immunotherapy in pancreatic cancer. *Proceedings of the National Academy of Sciences* **110**, 20212-20217 (2013).

49. Perret, R. et al. Adjuvants that improve the ratio of antigen-specific effector to regulatory T cells enhance tumor immunity. *Cancer research* **73**, 6597-6608 (2013).

50. Stewart, C.A. et al. Interferon-dependent IL-10 production by Tregs limits tumor Th17 inflammation. *The Journal of clinical investigation* **123**, 4859 (2013).

51. Hagemann, T. et al. "Re-educating" tumor-associated macrophages by targeting NF-κB. *The Journal of experimental medicine* **205**, 1261-1268 (2008).

52. Smith, C. et al. IDO is a nodal pathogenic driver of lung cancer and metastasis development. *Cancer discovery* **2**, 722-735 (2012).

53. Molon, B. et al. Chemokine nitration prevents intratumoral infiltration of antigen-specific T cells. *The Journal of experimental medicine* **208**, 1949-1962 (2011).

54. Mantovani, A., Allavena, P., Sica, A. & Balkwill, F. Cancer-related inflammation. *Nature* **454**, 436-444 (2008).

55. Mellman, I., Coukos, G. & Dranoff, G. Cancer immunotherapy comes of age. *Nature* **480**, 480-489 (2011).

56. Le, H.N., Lee, N.C., Tsung, K. & Norton, J.A. Pre-existing tumor-sensitized T cells are essential for eradication of established tumors by IL-12 and cyclophosphamide plus IL-12. *The Journal of Immunology* **167**, 6765-6772 (2001).

57. Thomas, S.N., Vokali, E., Lund, A.W., Hubbell, J.A. & Swartz, M.A. Targeting the tumor-draining lymph node with adjuvanted nanoparticles reshapes the anti-tumor immune response. *Biomaterials* **35**, 814-824 (2014).

58. Jeanbart, L. et al. Enhancing efficacy of anticancer vaccines by targeted delivery to tumor-draining lymph nodes. *Cancer immunology research* **2**, 436-447 (2014).

59. von Bernstorff, W. et al. Systemic and local immunosuppression in pancreatic cancer patients. *Clinical Cancer Research* **7**, 925s-932s (2001).

60. Iyer, A.K., Khaled, G., Fang, J. & Maeda, H. Exploiting the enhanced permeability and retention effect for tumor targeting. *Drug discovery today* **11**, 812-818 (2006).

61. Farokhzad, O.C. et al. Targeted nanoparticle-aptamer bioconjugates for cancer chemotherapy in vivo. *Proceedings of the National Academy of Sciences* **103**, 6315-6320 (2006).

62. Liao, D. et al. Targeted therapeutic remodeling of the tumor microenvironment improves an HER-2 DNA vaccine and prevents recurrence in a murine breast cancer model. *Cancer research* **71**, 5688-5696 (2011).

63. Dreaden, E.C. et al. Bimodal Tumor-Targeting from Microenvironment Responsive Hyaluronan Layer-by-Layer (LbL) Nanoparticles. *ACS nano* **8**, 8374-8382 (2014).

64. Singh, N. et al. Bioresponsive mesoporous silica nanoparticles for triggered drug release. *Journal of the American Chemical Society* **133**, 19582-19585 (2011).

65. Fan, N.C., Cheng, F.Y., Ho, J.a.A. & Yeh, C.S. Photocontrolled Targeted Drug Delivery: Photocaged Biologically Active Folic Acid as a Light-Responsive Tumor-Targeting Molecule. *Angewandte Chemie International Edition* **51**, 8806-8810 (2012).

66. Liu, T.-Y. et al. Instantaneous drug delivery of magnetic/thermally sensitive nanospheres by a high-frequency magnetic field. *Langmuir* **24**, 13306-13311 (2008).

67. Koppolu, B. et al. Temperature-sensitive polymer-coated magnetic nanoparticles as a potential drug delivery system for targeted therapy of thyroid cancer. *Journal of biomedical nanotechnology* **8**, 983-990 (2012).

68. Pignatello, R. et al. Evaluation of new amphiphilic PEG derivatives for preparing stealth lipid nanoparticles. *Colloids and Surfaces A: Physicochemical and Engineering Aspects* **434**, 136-144 (2013).

69. Rodriguez, P.L. et al. Minimal" Self" peptides that inhibit phagocytic clearance and enhance delivery of nanoparticles. *Science* **339**, 971-975 (2013).

70. Foged, C., Brodin, B., Frokjaer, S. & Sundblad, A. Particle size and surface charge affect particle uptake by human dendritic cells in an in vitro model. *International journal of pharmaceutics* **298**, 315-322 (2005).

71. Geng, Y. et al. Shape effects of filaments versus spherical particles in flow and drug delivery. *Nature nanotechnology* **2**, 249-255 (2007).

72. Huang, X., Teng, X., Chen, D., Tang, F. & He, J. The effect of the shape of mesoporous silica nanoparticles on cellular uptake and cell function. *Biomaterials* **31**, 438-448 (2010).

73. Beningo, K.A. & Wang, Y.-l. Fc-receptor-mediated phagocytosis is regulated by mechanical properties of the target. *Journal of Cell Science* **115**, 849-856 (2002).

74. Liu, W. et al. Uptake of hydrogel particles with different stiffness and its influence on HepG2 cell functions. *Soft Matter* **8**, 9235-9245 (2012).

75. Harush-Frenkel, O., Debotton, N., Benita, S. & Altschuler, Y. Targeting of nanoparticles to the clathrin-mediated endocytic pathway. *Biochemical and biophysical research communications* **353**, 26-32 (2007).

76. Kim, H.R. et al. Low-density lipoprotein receptor-mediated endocytosis of PEGylated nanoparticles in rat brain endothelial cells. *Cellular and molecular life sciences* **64**, 356-364 (2007).

77. Molino, N.M., Anderson, A.K., Nelson, E.L. & Wang, S.-W. Biomimetic protein nanoparticles facilitate enhanced dendritic cell activation and cross-presentation. *ACS nano* **7**, 9743-9752 (2013).

78. Asai, T. et al. Cell-penetrating peptide-conjugated lipid nanoparticles for siRNA delivery. *Biochemical and biophysical research communications* **444**, 599-604 (2014).

79. Chen, C.-J. et al. Self-assembly cationic nanoparticles based on cholesterol-grafted bioreducible poly (amidoamine) for siRNA delivery. *Biomaterials* **34**, 5303-5316 (2013).

80. Kortylewski, M. et al. Regulation of the IL-23 and IL-12 balance by Stat3 signaling in the tumor microenvironment. *Cancer cell* **15**, 114-123 (2009).

81. Alshamsan, A. et al. The induction of tumor apoptosis in B16 melanoma following STAT3 siRNA delivery with a lipid-substituted polyethylenimine. *Biomaterials* **31**, 1420-1428 (2010).

82. Molavi, O. et al. Development of a Poly (D, L-lactic-co-glycolic acid) Nanoparticle Formulation of STAT3 Inhibitor JSI-124: Implication for Cancer Immunotherapy. *Molecular pharmaceutics* **7**, 364-374 (2010).

83. Zhang, X. et al. Hydrazinocurcumin encapsuled nanoparticles “re-educate” tumor-associated macrophages and exhibit anti-tumor effects on breast cancer following STAT3 suppression. *PloS one* **8**, e65896 (2013).

84. Park, J. et al. Combination delivery of TGF-β inhibitor and IL-2 by nanoscale liposomal polymeric gels enhances tumour immunotherapy. *Nature materials* **11**, 895-905 (2012).

85. Kwong, B., Liu, H. & Irvine, D.J. Induction of potent anti-tumor responses while eliminating systemic side effects via liposome-anchored combinatorial immunotherapy. *Biomaterials* **32**, 5134-5147 (2011).

86. Buhtoiarov, I.N., Lum, H.D., Berke, G., Sondel, P.M. & Rakhmilevich, A.L. Synergistic activation of macrophages via CD40 and TLR9 results in T cell independent antitumor effects. *The Journal of Immunology* **176**, 309-318 (2006).

87. Ahonen, C.L. et al. Enhanced efficacy and reduced toxicity of multifactorial adjuvants compared with unitary adjuvants as cancer vaccines. *Blood* **111**, 3116-3125 (2008).

88. Palucka, K. & Banchereau, J. Cancer immunotherapy via dendritic cells. *Nature Reviews Cancer* **12**, 265-277 (2012).

89. Paul, W.E. Bridging innate and adaptive immunity. *Cell* **147**, 1212-1215 (2011).

90. Steinman, R.M. Decisions about dendritic cells: past, present, and future. *Annual review of immunology* **30**, 1-22 (2012).

91. Helle, M. et al. Surface chemistry architecture of silica nanoparticles determine the efficiency of in vivo fluorescence lymph node mapping. *ACS nano* **7**, 8645-8657 (2013).

92. Manolova, V. et al. Nanoparticles target distinct dendritic cell populations according to their size. *European journal of immunology* **38**, 1404-1413 (2008).

93. Reddy, S.T. et al. Exploiting lymphatic transport and complement activation in nanoparticle vaccines. *Nature biotechnology* **25**, 1159-1164 (2007).

94. Bos, R. & Sherman, L.A. CD4+ T-cell help in the tumor milieu is required for recruitment and cytolytic function of CD8+ T lymphocytes. *Cancer research* **70**, 8368-8377 (2010).

95. Tumeh, P.C. et al. PD-1 blockade induces responses by inhibiting adaptive immune resistance. *Nature* **515**, 568-571 (2014).

96. Baumgaertner, P. et al. Vaccination-induced functional competence of circulating human tumor-specific CD8 T-cells. *International Journal of Cancer* **130**, 2607-2617 (2012).

97. Blander, J.M. & Medzhitov, R. Toll-dependent selection of microbial antigens for presentation by dendritic cells. *Nature* **440**, 808-812 (2006).

98. Trombetta, E.S., Ebersold, M., Garrett, W., Pypaert, M. & Mellman, I. Activation of lysosomal function during dendritic cell maturation. *Science* **299**, 1400-1403 (2003).

99. Burgdorf, S., Schölz, C., Kautz, A., Tampé, R. & Kurts, C. Spatial and mechanistic separation of cross-presentation and endogenous antigen presentation. *Nature immunology* **9**, 558-566 (2008).

100. Rock, K.L. Presentation of exogenous antigens by macrophages: analysis of major histocompatibility complex class I and II presentation and regulation by cytokines. *European journal of immunology* **24**, 2421-2428 (1994).

101. Li, M. et al. Cell-associated ovalbumin is cross-presented much more efficiently than soluble ovalbumin in vivo. *The Journal of Immunology* **166**, 6099-6103 (2001).

102. Zhang, Z. et al. Induction of anti-tumor cytotoxic T cell responses through PLGA-nanoparticle mediated antigen delivery. *Biomaterials* **32**, 3666-3678 (2011).

103. Lee, I.H. et al. Imageable Antigen-Presenting Gold Nanoparticle Vaccines for Effective Cancer Immunotherapy In Vivo. *Angewandte Chemie* **124**, 8930-8935 (2012).

104. Demento, S.L. et al. TLR9-targeted biodegradable nanoparticles as immunization vectors protect against West Nile encephalitis. *The Journal of Immunology* **185**, 2989-2997 (2010).

105. Borges, O. et al. Immune response by nasal delivery of hepatitis B surface antigen and codelivery of a CpG ODN in alginate coated chitosan nanoparticles. *European Journal of Pharmaceutics and Biopharmaceutics* **69**, 405-416 (2008).

106. Slütter, B. & Jiskoot, W. Dual role of CpG as immune modulator and physical crosslinker in ovalbumin loaded N-trimethyl chitosan (TMC) nanoparticles for nasal vaccination. *Journal of Controlled Release* **148**, 117-121 (2010).

107. Bal, S.M., Slütter, B., Verheul, R., Bouwstra, J.A. & Jiskoot, W. Adjuvanted, antigen loaded N-trimethyl chitosan nanoparticles for nasal and intradermal vaccination: adjuvant-and site-dependent immunogenicity in mice. *European Journal of Pharmaceutical Sciences* **45**, 475-481 (2012).

108. Scott, E.A. et al. Dendritic cell activation and T cell priming with adjuvant-and antigen-loaded oxidation-sensitive polymersomes. *Biomaterials* **33**, 6211-6219 (2012).

109. Stano, A., Scott, E.A., Dane, K.Y., Swartz, M.A. & Hubbell, J.A. Tunable T cell immunity towards a protein antigen using polymersomes vs. solid-core nanoparticles. *Biomaterials* **34**, 4339-4346 (2013).

110. Butts, C. et al. Updated survival analysis in patients with stage IIIB or IV non-small-cell lung cancer receiving BLP25 liposome vaccine (L-BLP25): phase IIB randomized, multicenter, open-label trial. *Journal of cancer research and clinical oncology* **137**, 1337-1342 (2011).

111. Moon, J.J. et al. Interbilayer-crosslinked multilamellar vesicles as synthetic vaccines for potent humoral and cellular immune responses. *Nature materials* **10**, 243-251 (2011).

112. Moon, J.J. et al. Enhancing humoral responses to a malaria antigen with nanoparticle vaccines that expand Tfh cells and promote germinal center induction. *Proceedings of the National Academy of Sciences* **109**, 1080-1085 (2012).

113. Thomas, S.N. et al. Engineering complement activation on polypropylene sulfide vaccine nanoparticles. *Biomaterials* **32**, 2194-2203 (2011).

114. Rajasagi, M. et al. Systematic identification of personal tumor-specific neoantigens in chronic lymphocytic leukemia. *Blood* **124**, 453-462 (2014).

115. Yadav, M. et al. Predicting immunogenic tumour mutations by combining mass spectrometry and exome sequencing. *Nature* **515**, 572-576 (2014).

116. Schreiber, R.D., Old, L.J. & Smyth, M.J. Cancer immunoediting: integrating immunity's roles in cancer suppression and promotion. *Science* **331**, 1565-1570 (2011).

117. Ali, O.A., Huebsch, N., Cao, L., Dranoff, G. & Mooney, D.J. Infection-mimicking materials to program dendritic cells in situ. *Nature materials* **8**, 151-158 (2009).

118. Ali, O.A., Emerich, D., Dranoff, G. & Mooney, D.J. In situ regulation of DC subsets and T cells mediates tumor regression in mice. *Science translational medicine* **1**, 8ra19-18ra19 (2009).

119. Ali, O.A., Doherty, E., Mooney, D.J. & Emerich, D. Relationship of vaccine efficacy to the kinetics of DC and T-cell responses induced by PLG-based cancer vaccines. *Biomatter* **1**, 66-75 (2011).

120. Hodi, F.S. in Tumor Immunology: Multidisciplinary Science Driving Combination Therapy (Banff, Alberta, Canada; 2015).

121. Stevanović, S. et al. Complete regression of metastatic cervical cancer after treatment with human papillomavirus–targeted tumor-infiltrating T cells. *Journal of Clinical Oncology*, JCO. 2014.2058. 9093 (2015).

122. Besser, M.J. et al. Adoptive transfer of tumor-infiltrating lymphocytes in patients with metastatic melanoma: intent-to-treat analysis and efficacy after failure to prior immunotherapies. *Clinical Cancer Research* **19**, 4792-4800 (2013).

123. Louis, C.U. et al. Antitumor activity and long-term fate of chimeric antigen receptor–positive T cells in patients with neuroblastoma. *Blood* **118**, 6050-6056 (2011).

124. Morgan, R.A. et al. Cancer regression and neurologic toxicity following anti-MAGE-A3 TCR gene therapy. *Journal of immunotherapy (Hagerstown, Md.: 1997)* **36**, 133 (2013).

125. Lamers, C.H. et al. Treatment of metastatic renal cell carcinoma with CAIX CAR-engineered T cells: clinical evaluation and management of on-target toxicity. *Molecular Therapy* **21**, 904-912 (2013).

126. Grupp, S.A. et al. T cells engineered with a chimeric antigen receptor (CAR) targeting CD19 (CTL019) produce significant in vivo proliferation, complete responses and long-

term persistence without Gvhd in children and adults with relapsed, refractory ALL. *Blood* **122**, 67-67 (2013).

127. Dudley, M.E. et al. Adoptive cell therapy for patients with metastatic melanoma: evaluation of intensive myeloablative chemoradiation preparative regimens. *Journal of Clinical Oncology* **26**, 5233-5239 (2008).

128. Pegram, H.J. et al. Tumor-targeted T cells modified to secrete IL-12 eradicate systemic tumors without need for prior conditioning. *Blood* **119**, 4133-4141 (2012).

129. Yee, C. et al. Adoptive T cell therapy using antigen-specific CD8+ T cell clones for the treatment of patients with metastatic melanoma: in vivo persistence, migration, and antitumor effect of transferred T cells. *Proceedings of the National Academy of Sciences* **99**, 16168-16173 (2002).

130. Almand, B. et al. Clinical significance of defective dendritic cell differentiation in cancer. *Clinical Cancer Research* **6**, 1755-1766 (2000).

131. Satthaporn, S. et al. Dendritic cells are dysfunctional in patients with operable breast cancer. *Cancer Immunology, Immunotherapy* **53**, 510-518 (2004).

132. Butler, M.O. & Hirano, N. Human cell-based artificial antigen-presenting cells for cancer immunotherapy. *Immunological reviews* **257**, 191-209 (2014).

133. Appel, H., Seth, N.P., Gauthier, L. & Wucherpfennig, K.W. Anergy induction by dimeric TCR ligands. *The Journal of Immunology* **166**, 5279-5285 (2001).

134. Steenblock, E.R. & Fahmy, T.M. A comprehensive platform for ex vivo T-cell expansion based on biodegradable polymeric artificial antigen-presenting cells. *Molecular Therapy* **16**, 765-772 (2008).

135. Peshwa, M.V. et al. Generation of primary peptide-specific CD8 cytotoxic T-lymphocytes in vitro using allogeneic dendritic cells. *Cell transplantation* **7**, 1-9 (1998).

136. Rosenberg, S.A. et al. Durable complete responses in heavily pretreated patients with metastatic melanoma using T-cell transfer immunotherapy. *Clinical Cancer Research* **17**, 4550-4557 (2011).

137. Sunshine, J.C., Perica, K., Schneck, J.P. & Green, J.J. Particle shape dependence of CD8+ T cell activation by artificial antigen presenting cells. *Biomaterials* **35**, 269-277 (2014).

138. Huppa, J.B. & Davis, M.M. T-cell-antigen recognition and the immunological synapse. *Nature Reviews Immunology* **3**, 973-983 (2003).

139. Ding, Q. et al. RAFTsomes containing epitope-MHC-II complexes mediated CD4+ T cell activation and antigen-specific immune responses. *Pharmaceutical research* **30**, 60-69 (2013).

140. Goldstein, S.A. & Mescher, M. Cell-sized, supported artificial membranes (pseudocytes): response of precursor cytotoxic T lymphocytes to class I MHC proteins. *The Journal of Immunology* **137**, 3383-3392 (1986).

141. Mandal, S. et al. Therapeutic nanoworms: towards novel synthetic dendritic cells for immunotherapy. *Chemical Science* **4**, 4168-4174 (2013).

142. Fadel, T.R. et al. Enhanced cellular activation with single walled carbon nanotube bundles presenting antibody stimuli. *Nano letters* **8**, 2070-2076 (2008).

143. Fadel, T.R. et al. Clustering of stimuli on single-walled carbon nanotube bundles enhances cellular activation. *Langmuir* **26**, 5645-5654 (2009).

144. Fadel, T.R. et al. A carbon nanotube–polymer composite for T-cell therapy. *Nature nanotechnology* **9**, 639-647 (2014).

145. Meyer, R.A. et al. Biodegradable Nanoellipsoidal Artificial Antigen Presenting Cells for Antigen Specific T-Cell Activation. *Small* (2014).

146. Stephan, M.T., Moon, J.J., Um, S.H., Bershteyn, A. & Irvine, D.J. Therapeutic cell engineering with surface-conjugated synthetic nanoparticles. *Nature medicine* **16**, 1035-1041 (2010).

147. Doshi, N. et al. Cell-Based Drug Delivery Devices Using Phagocytosis-Resistant Backpacks. *Advanced Materials* **23**, H105-H109 (2011).

148. Anselmo, A.C. et al. Monocyte-mediated delivery of polymeric backpacks to inflamed tissues: a generalized strategy to deliver drugs to treat inflammation. *Journal of Controlled Release* **199**, 29-36 (2015).

149. Bencherif, S.A. et al. Injectable preformed scaffolds with shape-memory properties. *Proceedings of the National Academy of Sciences* **109**, 19590-19595 (2012).

150. Weber, J.S. et al. Nivolumab versus chemotherapy in patients with advanced melanoma who progressed after anti-CTLA-4 treatment (CheckMate 037): a randomised, controlled, open-label, phase 3 trial. *The Lancet Oncology* **16**, 375-384 (2015).

151. Herbst, R.S. et al. Predictive correlates of response to the anti-PD-L1 antibody MPDL3280A in cancer patients. *Nature* **515**, 563-567 (2014).

152. Robert, L. et al. CTLA4 blockade broadens the peripheral T-cell receptor repertoire. *Clinical Cancer Research* **20**, 2424-2432 (2014).

153. Le Mercier, I. et al. VISTA regulates the development of protective antitumor immunity. *Cancer research* **74**, 1933-1944 (2014).

154. Fan, X., Quezada, S.A., Sepulveda, M.A., Sharma, P. & Allison, J.P. Engagement of the ICOS pathway markedly enhances efficacy of CTLA-4 blockade in cancer immunotherapy. *The Journal of experimental medicine* **211**, 715-725 (2014).

155. Gubin, M.M. et al. Checkpoint blockade cancer immunotherapy targets tumour-specific mutant antigens. *Nature* **515**, 577-581 (2014).

Chapter 3: Adjuvant-Loaded Subcellular Vesicles Derived from Disrupted Cancer Cells for Cancer Vaccination

The work described in this chapter was originally published in Small: Cheung AS et al. *Small* 2016; 12 (17): 2321-2333.

3.1 Introduction

In this chapter, we develop a method to prepare native cancer antigen and adjuvant co-loaded particles for cancer vaccination. Therapeutic cancer vaccines immunize the patient against cancer antigens in order to generate immune effector cells that can recognize and eliminate the cancer cells. Cancer vaccination is challenging for several reasons. First, tumors are heterogeneous populations with high degrees of both inter- and intra-tumoral antigen variability[1]. Second, tumors possess tolerogenic mechanisms that enable them to avoid immune destruction[2]. Third, tumors are dynamic populations that can evolve in response to weak selective pressures induced by suboptimal vaccination[3]. In order to overcome these challenges, it is important for a cancer vaccine to elicit a response that is personalized to the patient's unique cancer antigen repertoire, and broad enough to capture the antigenic diversity of the tumor. The vaccine must also facilitate efficient antigen presentation and promote robust cytotoxic effector cell function in order to overcome the immunosuppressive mechanisms imposed by the tumor.

In general, there exist two approaches to cancer vaccination: 1) targeted approaches, which immunize against defined tumor antigens and 2) broad vaccination against a breadth of undefined tumor antigens. Targeted approaches are attractive because they generally target antigenic determinants that are known to be uniquely overexpressed and immunogenic. However, because targeted vaccines do not reflect the antigenic complexity of the tumor,

suboptimal vaccinations that fail to induce efficient antigen spread can potentially facilitate the selection of lowly immunogenic subpopulations, leading to immune escape[3]. Additionally, targeted approaches are commonly non-personalized in that they immunize against prototypic cancer antigens, which precludes the use of such approaches for a large patient population that either has a cancer for which a characteristic target has not been identified, or is refractory for the particular known target. Alternatively, strategies that utilize material derived from the tumor as an antigen source vaccinate against a breadth of prospective tumor antigens in a patient-specific manner. The current standard for such primary antigen preparations is tumor lysate, the soluble fraction obtained after freeze-thawing cancer cells. Lysate-based approaches have the advantage of capturing both the uniqueness and breadth of the tumor antigen repertoire, without the need for pre-knowledge of specific antigen targets. This is particularly advantageous in cancer types with high mutational loads (e.g. melanoma), in which patients frequently have unique and extensive mutanomes encoding neoantigens not subject to central tolerance, that could potentially facilitate efficient vaccination[4, 5]. Despite these advantages, tumor lysate possesses limited immunogenicity, and the soluble lysate constituents are not efficiently taken up by antigen-presenting cells, limiting the immune response generated[6].

Previous work has demonstrated that the physical association of antigen with a molecular danger signal, such as a Toll-like receptor (TLR) agonist, for example through chemical conjugation[7, 8] or co-loading onto a nano- or microscale colloidal scaffold[9-12], significantly increases its presentation efficiency, even when compared to the same amount of soluble antigen and danger cue admixed but not physically associated. Indeed, the presence of danger signal and antigen in the same phagosomal compartment has been shown to be important for the efficient presentation of that antigen[13, 14]. It has also been shown that compared to a soluble counterpart,

antigens associated with a "phagocytic substrate" such as an engineered colloid[9, 10, 15], or cell debris[16], or that is packaged into apoptotic blebs[17], or tumor exosomes[18], are more efficiently presented by antigen presenting cells. The application of nano- or microscale materials as delivery vehicles in cancer vaccines has allowed for the development of many promising targeted vaccines, but non-targeted approaches based on such platforms are much more limited, largely owing to the difficulty of loading complex undefined mixtures of proteins into such systems while maintaining a reasonable degree of colloidal stability. In addition, the use of exogenous materials as colloidal delivery vehicles can potentially lead to challenges associated with scale-up and reproducibility, as well as regulatory hurdles to translation.

In light of these observations, the goal of this work was to develop an alternative method for processing cancer cells in which the antigen diversity of the parent cells is maintained but the antigen content is reformulated to facilitate efficient antigen presentation. To this end, we hypothesized that whole cancer cells could be broken down into membrane-enclosed vesicular compartments and loaded with adjuvant. The benefits of such a system are that (1) the unique antigen repertoire of the parent cells is reflected, (2) the breadth of antigenic diversity of the parent cell population is captured, (3) associated cancer antigens are presented in a highly immunogenic format, in contrast to lysate, the current standard, and (4) endogenous cell material functions as the delivery vehicle, obviating the input of exogenous carrier material. In this work, we investigated two approaches to mechanically disrupt whole cancer cells, extrusion and sonication, in order to generate vesicular compartments we termed "reduced cancer cells" (RCCs). We demonstrate that in contrast to extruded RCCs, sonicated RCCs retain protein from diverse intracellular compartments with a protein distribution that is highly representative of the parent whole cells, and leverage this property for vaccine design. We show that sonicated RCCs

can be loaded with diverse payloads, and that these adjuvant-loaded RCCs are highly immunogenic and facilitate more efficient antigen presentation in vitro than cell lysate or purified soluble antigen. When administered as a vaccine in vivo, RCCs can also be used to stimulate antigen-specific cellular and humoral immune responses. Overall, this work describes an approach for reformulating whole cancer cells into immunogenic antigen-rich particles that may represent a superior alternative to the derivation of lysate.

3.2 Materials and Methods

3.2.1 Animals

All work with C57BL/6J and C57BL/6-Tg(TcraTcrb)1100Mjb/J (OT-I) mice (The Jackson Laboratory) was performed in compliance with National Institutes of Health and institutional guidelines.

3.2.2 Cells and Reagents

The B16-F10 murine melanoma cell line (ATCC) was cultured in DMEM supplemented with 10% heat inactivated FBS (HI-FBS) and 1% penicillin-streptomycin. The MF2.2D murine T cell hybridoma cell line, kindly provided by Dr. Kenneth Rock, was cultured in RPMI 1640 supplemented with 10% HI-FBS, 2 mM L-glutamine, 55 μM beta-mercaptoethanol, 1x non-essential amino acids, 10mM HEPES, and 1% penicillin-streptomycin. The B3Z murine T cell hybridoma cell line, kindly provided by Dr. Nilabh Shastri, was cultured in RPMI 1640 supplemented 10% HI-FBS, 2 mM L-glutamine, 1 mM sodium pyruvate, 50 μM beta-mercaptoethanol, and 1% penicillin-streptomycin.

Primary CD8+ T cells were isolated from the spleens of OT-I mice and enriched using an anti-CD8 MACS isolation kit (Miltenyi Biotec). T cells were used immediately for co-culture experiments and were cultured in RPMI 1640 supplemented with 10% HI-FBS, 1% penicillin-streptomycin, 1 mM sodium pyruvate, 5 mM HEPES, and 50 μM beta-mercaptoethanol.

CpG and CpG-FAM (fluorescent CpG) were synthesized by Integrated DNA Technologies based on the described B class 1826 sequence (tccatgacgttcctgacgtt). MPLA derived from Salmonella minnesota R595 was purchased from Invivogen. Unless otherwise stated, antibodies were purchased from eBioscience.

3.2.3 Derivation of RCCs

B16-F10 or B16-mOVA cells were grown in T150 tissue culture flasks until near-confluency. Cells were non-enzymatically removed by incubating cells with Ca-/Mg- PBS at 4°C for 5 minutes and washed three times with PBS. After the final wash, cells were resuspended at 5e6 cells/ml in PBS supplemented with a protease inhibitor tablet (Roche Life Science) and CpG or OVA, if applicable. Cell suspensions were cooled on ice until disruption. Cell suspensions were maintained at 5e6 cells/ml for eRCC derivation as this concentration has previously been shown to be efficient for whole cell extrusion[19, 20], and higher initial cell concentrations were found to result in significant clogging of the extruder membrane (data not shown). To generate eRCCs, 1 ml aliquots of pre-cooled cell suspensions were serially extruded using a mini extruder (Avanti Polar Lipids) through 10 μm, 5 μm, and 1 μm polycarbonate filters. To generate sRCCs, 1 ml aliquots of pre-cooled cell suspensions were transferred to round-bottom tubes and sonicated (Qsonica Q700 equipped with 3.2 mm stepped microtip probe) for a total process time of 45 seconds in alternating 15 second burst and rest cycles of 60% amplitude and no sonication,

respectively. Raw RCC suspensions were subsequently fractionated in a discontinuous iodixanol (Sigma-Aldrich) gradient containing 10% and 50% iodixanol layers. Following centrifugation at 100,000 rcf for at least 2 hours at 4°C, RCCs were collected from the interface of the layers. Where applicable, RCCs were incubated overnight at room temperature with MPLA. The collected fraction was subsequently washed by diluting at least 20-fold in PBS and pelleted by centrifuging at 95,000 rcf for 20 minutes at 4°C. The supernatant was completely decanted, and the RCC pellets were resuspended by slowly running the collected material through a 29 gauge syringe. For western blot and CpG loading studies, RCCs were lysed in RIPA buffer (Amresco) supplemented with protease inhibitor (Roche). For all other studies, RCCs were resuspended in PBS at approximately 0.9 mg protein/ml, unless otherwise stated. RCCs were stored at 4°C and used within a few days.

3.2.4 Characterization of RCCs

RCC hydrodynamic size and zeta potential were evaluated using a Malvern Nano ZS. Size measurements were taken in PBS with RCCs suspended at ~0.05 mg/ml. Zeta potential measurements were taken in H2O with RCCs suspended at ~0.005 mg/ml.

For quantification of payload loading, payloads were loaded into sRCCs and purified sRCCs were subsequently lysed in RIPA buffer. CpG loading was quantified through a combination of fluorescent measurements of a fluorescently tagged CpG conjugate using a standard plate reader, and quantification with HPLC. HPLC analysis was conducted on an Agilent 1100 HPLC equipped with an XTerra MS C18 5 micron, 4.6x250 mm Column (Waters Cat# 186000494). Samples were analyzed using 0.1M triethylammonium acetate, pH 7 (Mobile Phase A) and 90% acetonitrile in 0.1M triethylammonium acetate, pH 7 (Mobile Phase B) with

the following gradient: 0min-2%B, 4min-2%B, 45min-55%B, 50min-90%B, 51min-2%B, 60min-2%B. The flow rate was 0.5 mL/min, column temperature was 30°C, samples were injected without dilution at 50 µl, and detection was conducted at 260 and 488 nm. MPLA loading was quantified through a combination of fluorescent measurements of a fluorescent MPLA conjugate using a standard plate reader, and measurements of untagged MPLA using an Endosafe-MCS system (Charles River). Ovalbumin loading was quantified through fluorescent measurements of a fluorescent ovalbumin conjugate (invitrogen) using a standard plate reader. Data shown are means of loading studies conducted with fluorescent conjugates. Alternative approches were performed to ensure consistency of loading measurements.

3.2.5 RCC Uptake Studies

Uptake of RCC-loaded CpG was evaluated using a 5' fluorophore conjugated CpG (Integrated DNA Technologies). Primary DCs were treated with either free or RCC-associated fluorescent CpG for various lengths of time and then analyzed via either flow cytometry or confocal microscopy for uptake. For flow cytometry analysis of uptake, treated DCs were removed by scraping and stained for viability (Biolegend) and CD11c. Cells were analyzed on a BD LSRFortessa and the percentage of CpG+ cells among live CD11c+ cells was quantified. To evaluate uptake via confocal microscopy, cells were analyzed either live or fixed. For live cell imaging, DCs were seeded on glass bottom tissue culture plates (MatTek). Adjuvant-loaded cells were treated with Hoescht 33342 (Life Technologies) for 15 minutes followed by imaging on a Leica SP5 X MP Inverted Confocal Microscope equipped with a Ludin incubation chamber. For fixed cell imaging, DCs were seeded on glass coverslips. At the time of analysis, adjuvant-loaded DCs were fixed in 4% paraformaldehyde/PBS for 10 minutes at room temperature followed by permeabilization in 0.1% Triton X/PBS for 15 minutes. Cells were then stained with

Alexa Fluor 594-phalloidin (Life Technologies) and Hoescht 33342 (Life Technologies) and mounted on glass slides using ProLong Gold antifade reagent (Life Technologies). Cells were subsequently imaged on a Zeiss LSM 710 confocal microscope.

3.2.6 Generation of B16-mOVA cells

B16-mOVA cells were generated from B16-F10 wild type cells. Briefly, to generate B16-mOVA cells, a membrane-bound form of ovalbumin was cloned from pCl-neo-mOVA (Maria Castro lab, Addgene plasmid 25099) and inserted between the BamHI and SalI sites of pBABE-puro (Weinberg lab, Addgene plasmid 1764). The vector was sequenced to confirm the presence of the transgene and then used to produce VSV-G pseudotyped retrovirus using the Retro-X Universal Packaging System (Clontech). Parental B16-F10 cells were transduced with virus in the presence of 8 μg/ml polybrene (EMD Millipore) and selected for transgene expression by culturing in medium containing 1 μg/mL puromycin dihydrochloride (EMD Millipore) for 7 days. B16-mOVA cells were maintained in DMEM supplemented with 10% HI-FBS, 1% penicillin-streptomycin, and 1 μg/ml puromycin.

To validate OVA expression, generated B16-mOVA cells were co-cultured with B3Z reporter T cells. For B3Z co-culture studies, 5e4 B3Z cells were incubated with or without 5e4 wild type B16-F10 or B16-mOVA cells for 18 hours in the presence of 50 ng/ml recombinant interferon-gamma (Biolegend). β-galactosidase activity was assessed using a mammalian β-galactosidase assay kit (Thermo Scientific) according to the manufacturer's instructions.

3.2.7 Isolation of Primary DCs

Primary DCs were isolated from the bone marrow of 6-10 week old female C57BL/6J mice based on a previously described method[21]. Briefly, femurs were collected from mice and

flushed with PBS. DC precursors were seeded in petri dishes at 2e5 cells/ml in RPMI 1640 supplemented with 10% HI-FBS, 1% penicillin-streptomycin, 50 μM beta-mercaptoethanol, and 40 ng/ml GM-CSF (Peprotech). Media was refreshed on days 3 and 6 after initiating culture and DCs were used for experiments between days 7-10.

3.2.8 Derivation of Lysate

Cancer cell lysate was derived using a standard approach. Briefly, cancer cells were grown in flasks until near-confluency, then non-enzymatically removed by incubating cells with Ca-/Mg- PBS at 4°C for 5 minutes. After three washes with PBS, cells were resuspended at 5e6 cells/ml in PBS and subjected to 4 freeze-thaw cycles between liquid nitrogen and a 37°C water bath. After the final cycle, raw lysate suspensions were centrifuged at 400 rpm (35 rcf) for 10 minutes. The supernatant (lysate) was collected and stored at -20°C until use.

3.2.9 Transmission Electron Microscopy of RCCs

TEM was performed by depositing 3.5 μl of RCCs suspended at ~ 0.09 mg/ml on plasma-treated Formvar/carbon grids. Sample-coated grids were negatively stained by depositing 2% aqueous uranyl formate on the grids for 15 seconds and then air-dried prior to imaging on a Jeol JEM-1400 TEM operating at 80 kV. For immunoelectron microscopy, samples were deposited as described above followed by fixing in 4% paraformaldehyde/PBS for 10 minutes at room temperature. Fixed samples were subsequently blocked for 30 minutes in 2% BSA/PBS followed by probing with primary antibody diluted in 0.1% BSA/PBS, or with just 0.1% BSA/PBS for controls, for 1 hour. For intracellular CD47 staining, the EPR4150(2) clone (Abcam) was used. For extracellular CD47 staining, the MIAP301 clone (Biolegend) was used. After washing, retained primary antibody was probed using an appropriate 10 nm colloidal gold-conjugated

secondary antibody (Sigma-Aldrich) diluted in 0.1% BSA/PBS for 1 hour. Samples were then post-fixed in 2.5% glutaraldehyde/PBS for 10 minutes at room temperature and negatively stained and imaged as described above.

3.2.10 Western Blot Analysis of RCCs

For western blot analysis of RCCs, a BCA assay (Pierce Biotechnology) was first performed to quantify total protein content of samples or whole cell lysate. Samples were normalized based on total protein content, diluted in Laemmli buffer (Boston BioProducts), and loaded into 4-20% precast polyacrylamide gels (Bio-Rad) at 1.7 μg total protein per lane for TRP-2, β-actin, and histone H3 analysis, and 22.6 μg total protein per lane for lamin B1 analysis. After transferring, membranes were blocked for an hour in 5% skim milk/TBST and probed overnight at 4°C using the appropriate primary antibodies. Anti-TRP-2 was purchased from Origene. Anti-histone H3 and anti-lamin B1 were purchased from Novus Biologicals. Anti-β-actin was purchased from Sigma-Aldrich. The membranes were subsequently washed, re-blocked, and retained primary antibody was probed using an appropriate HRP-conjugated secondary antibody (Vector Labs). After washing the membranes thoroughly to remove any unbound secondary antibody, ECL reagent (GE Life Sciences) was used following the manufacturer's instructions and chemiluminescence was detected using autoradiography film.

3.2.11 DC Activation and Antigen Presentation Studies

For DC activation studies, adjuvant loaded sRCCs were prepared at total protein/adjuvant mass ratio of 1/0.05 for CpG, and 1/0.002 for MPLA. To evaluate the stimulatory functionality of RCC-loaded adjuvants, primary DCs were plated in non-tissue culture-treated plates, and 0.2 μM CpG or 0.02 μM MPLA, were added in free or RCC-associated form. The CpG stock used

for these studies was tested for endotoxin content and found to have <0.05 EU/mg endotoxin contamination. After a 12-15 hour stimulation, media samples were collected for IL-12 quantification via ELISA (Peprotech), and cells were removed by scraping and stained for viability, CD11c, MHC II, and the costimulatory molecules CD40 and CD86. DC activation was evaluated via flow cytometry based on the proportion of live CD11c+ cells that were positive for the activation markers.

Adjuvant loaded RCCs were prepared at total protein/CpG mass ratios of 1/0.05 for hybridoma T cell and OT-I CD8+ T cell co-culture studies. To evaluate the capacity of RCC-delivered antigen to be presented in MHC I and II, primary DCs were plated in non-tissue culture treated plates and treated with either free or RCC-associated antigens for 3 hours. Loaded DCs were subsequently co-cultured with either MF2.2D cells to investigate MHC II presentation, or primary CD8+ OT-I T cells to investigate MHC I cross-presentation, in a total culture volume of 0.2 ml. For co-culture experiments involving the use of the MF2.2D hybridoma line, co-culture was carried out for 12-15 hours after which media was collected for IL-2 quantification via ELISA (Peprotech). For CD8+ OT-I T cell co-culture, primary CD8+ T cells were isolated from OT-I mice as described above and stained with CFSE according to the manufacturer's instructions. CFSE-stained T cells were then co-cultured with treated DCs for 3 days. After the co-culture period, T cells were collected and stained for viability and CD8α and analyzed via flow cytometry. CFSE dilution of live CD8+ cells was evaluated.

3.2.12 Vaccination Studies

6-10 week old C57BL/6J mice were used for all vaccination studies. Mice were vaccinated subcutaneously in the flank, typically with 370 μg of RCCs per dose, or lysate derived from the same starting number of parent cells.

3.2.13 Ex Vivo Peptide Stimulation and Intracellular Cytokine Staining

For detection of functional peripheral blood OVA-specific CD8+ T cells, peripheral blood was collected at indicated time points, and erythrocytes were lysed with ACK buffer (Lonza). PBMCs were stimulated with 1 μM SIINFEKL peptide for 4 hours in the presence of GolgiPlug (BD), stained with a live/dead stain (eBioscience) and for surface CD8, fixed/permeabilized, and stained for IFNγ.

3.2.14 Detection of Serum Anti-OVA Antibodies

Sera was collected by centrifuging peripheral blood at 550 rcf for 5 minutes. Anti-OVA antibodies were detected by incubating diluted sera with OVA-coated plates overnight, and subsequently detecting relevant IgG subclasses using appropriate anti-mouse secondary antibodies.

3.2.15 IL-2 ELISPOT

Spleens were processed by mashing through a 70 μm nylon cell strainer and red blood cell lysing with ACK buffer. T cells were subsequently purified using a pan T cell negative selection MACS kit (Miltenyi Biotec). T cells were seeded at 500,000 cells per well in 96 well plates coated with anti-IL2 antibody (BD) and co-cultured for 18 hours with 50,000 irradiated (10,000 rad) B16-mOVA cells that had been treated overnight with 10 ng/ml IFNγ to increase MHC I presentation. Captured IL-2 was subsequently detected using an HRP-conjugated IL-2

antibody (BD). Automated spot quantification was performed using a CTL ImmunoSpot S4 analyzer.

3.2.16 Statistical Analysis

Statistical analysis was performed using GraphPad Prism. Unless otherwise stated, data were compared using the unpaired two-tailed t test and p-values less than 0.05 were considered to be statistically significant. Where applicable, data are reported as the mean ± SD.

3.3 Results

3.3.1 Derivation and Characterization of RCCs

Whole B16-F10 melanoma cells were disrupted via either mechanical extrusion (eRCCs) or sonication (sRCCs) to generate RCCs which were subsequently purified using density centrifugation. Both methods generated RCCs with nano-microscale size distributions (Figure 3.1A). Dynamic light scattering (DLS) measurements indicated that eRCCs had an average hydrodynamic diameter of ~ 400 nm whereas sRCCs had an average hydrodynamic diameter of ~ 500 nm associated with a broader, less monodisperse distribution and a higher PDI (Figure 3.1A). Both eRCCs and sRCCs had comparable zeta potentials of ~ -30 mV (Figure 3.1B), consistent with what has been reported previously for purified mammalian cell membranes[22, 23]. Examination of RCCs via TEM revealed structures within the size range predicted by DLS. Enhancement of contrast upon negative staining with uranyl formate suggests that both eRCCs and sRCCs represent enclosed structures (Figure 3.1C, D). Although partial membrane collapse

of the RCCs was observed following staining and dehydrating during TEM sample preparation, it is likely that the RCCs are spherical structures in the hydrated state.

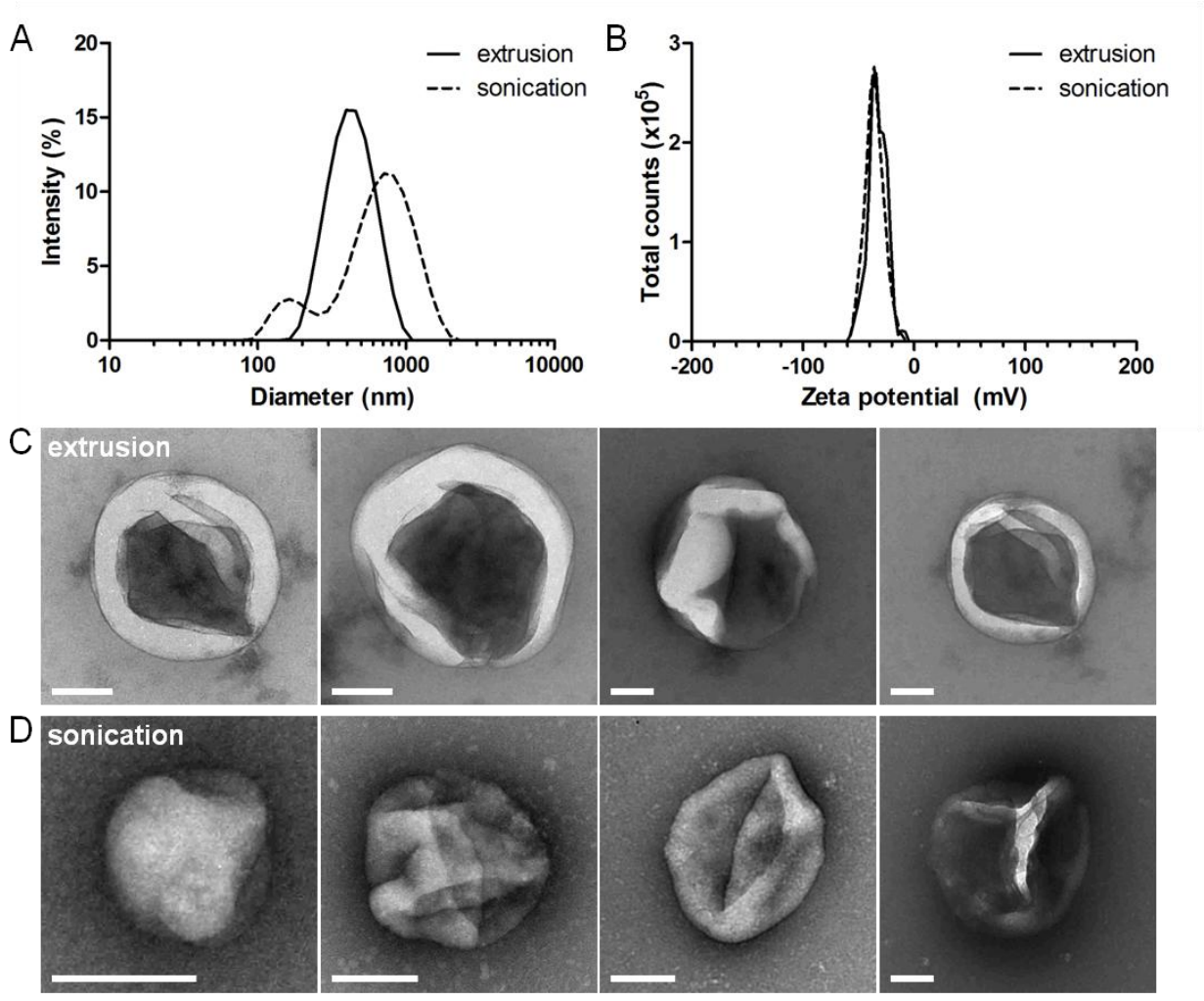

Figure 3.1. Derivation of RCCs. (A) Representative size intensity distributions of eRCCs and sRCCs as measured by DLS. (B) Representative zeta potential distributions of eRCCs and sRCCs as measured by DLS. Representative TEM images of eRCCs (C) and sRCCs (D). All scale bars = 100 nm.

In order to investigate the prospective antigen content of eRCCs and sRCCs, total and specific RCC protein retention was characterized. eRCCs were found to retain 10.8 ± 0.7% of total parent cell protein content whereas sRCCs were found to retain 22.7 ± 3.4% (Figure 3.2A).

Qualitative analysis of total protein content via coomassie staining showed that eRCCs exhibited the depletion of a number of prominent bands observed in the parent whole cell lysate whereas sRCCs maintained a protein distribution qualitatively more similar to the parent whole cell lysate (Figure 3.2B). When the same amount of total protein was loaded, western blotting for proteins localized to various cellular compartments indicated that while eRCCs showed a marked enrichment of membrane-associated proteins with a concomitant loss of proteins in other compartments, notably cytoplasmic and nuclear, protein retained by sRCCs was highly representative of all compartments of the parent cells based on the markers evaluated (Figure 3.2C). Given that many tumor antigens are localized to the cytoplasm and the nucleus[24], the ability to retain these fractions is likely to be functionally advantageous for a cancer vaccine. Because of this, as well as superior gross protein retention, sRCCs were used for all subsequent analyses.

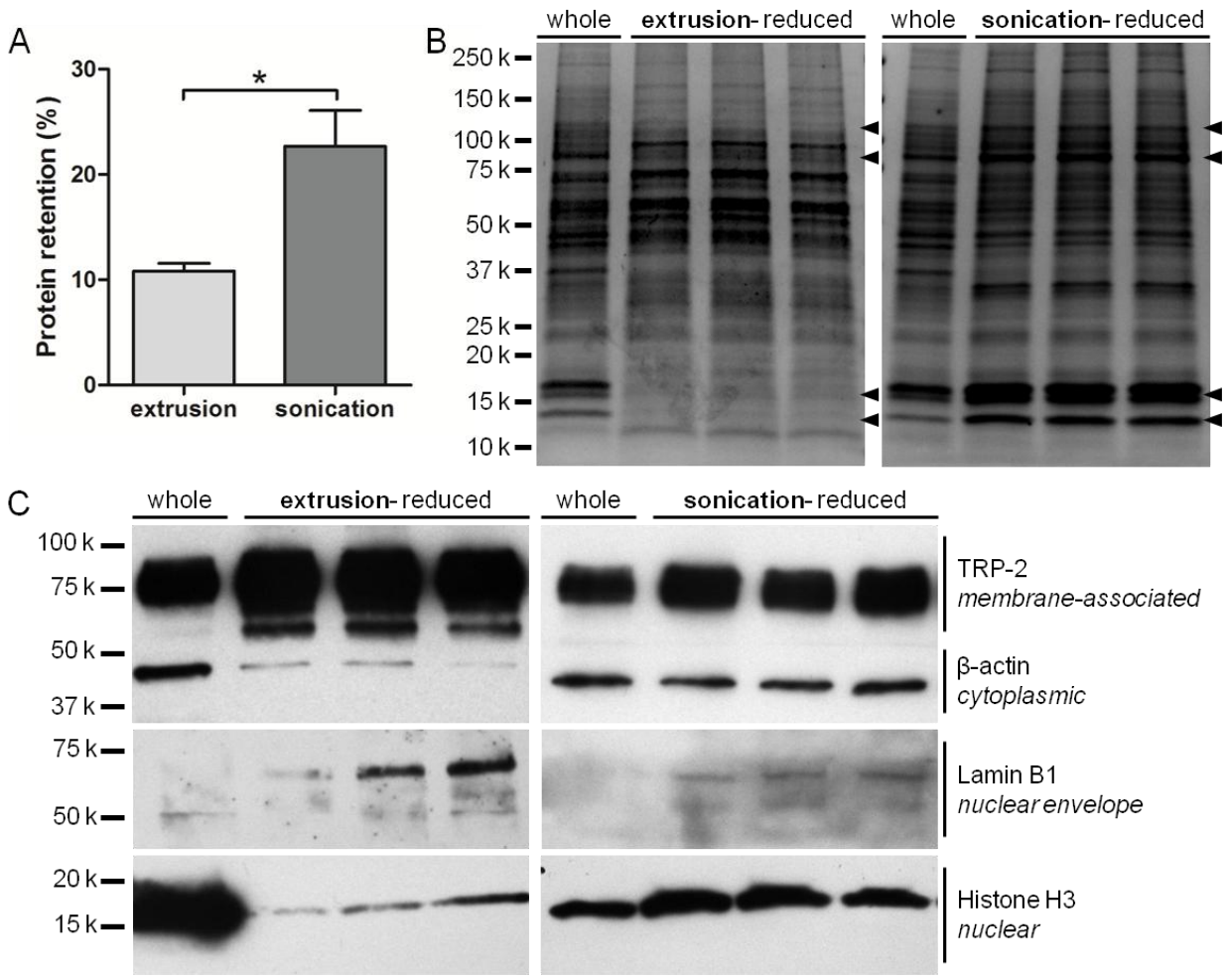

Figure 3.2. Protein retention of RCCs. (A) Percent protein retention of eRCCs and sRCCs relative to protein content of intact cells, analyzed via BCA assay. (B) Coomassie stain of three separate eRCC and sRCC samples as compared to the parent cells (whole) from which they were derived. Arrowheads indicate bands that were present in whole parent cells and largely depleted by eRCCs but maintained by sRCCs. (C) Western blot of three separate eRCC and sRCC samples as compared to the parent cells (whole) from which they were derived, probing for proteins localized to various cellular compartments: TRP-2 (membrane-associated), β-actin (cytoplasmic), lamin B1 (nuclear envelope), and histone H3 (nuclear). Data represent the mean ± SD, *$p<0.05$.

3.3.2 RCCs as Adjuvant Delivery Vehicles

To evaluate whether sRCCs could be loaded with adjuvant, a 5' fluorophore-conjugated CpG DNA was used as a model adjuvant, and loaded into sRCCs by mixing the parent cells with CpG and sonicating the CpG/cell suspension. CpG is a hydrophilic oligodeoxynucleotide-based adjuvant and a ligand for the endosomally-localized TLR9, an immune-activating pattern recognition receptor (PRR). CpG has been shown to be an effective adjuvant in cancer vaccine formulations[25-29]. When sRCCs were stained with a membrane dye and subjected to density centrifugation in a two-step (10%/50%) iodixanol gradient, significant enrichment of the dye was observed at the interface of the steps, representing the membrane-enclosed sRCC-rich fraction (Figure 3.3A). While free fluorescent CpG did not localize to a specific fraction upon density centrifugation, when CpG was mixed with the cell suspension and sRCCs were derived from the CpG/cell mixture, a fraction of the CpG was found to colocalize with the interfacial RCC band following density centrifugation (Figure 3.3A, B), suggesting CpG loading of the resultant sRCCs. Confocal microscopy of sRCCs also revealed colocalization of a membrane-specific dye and the fluorescent CpG (Figure 3.3C). To preclude the possibility that the fluorescent tag was facilitating loading, sRCCs were also loaded with untagged CpG and loading was quantified using HPLC and measuring absorbance at 260 nm. Loading of fluorescent CpG was similarly evaluated using HPLC and measuring absorbance at 260 nm as well as fluorescence at 488 nm. Comparison of tagged and untagged CpG did not reveal any differences in loading (Figure 3.4). Furthermore, no change in elution time was observed when HPLC was used to compare the fluorescent CpG stock and fluorescent CpG that had been sRCC-loaded and recovered following RCC lysing, suggesting that intact CpG is loaded into the RCCs (Figure 3.5). CpG loading of sRCCs was evaluated as a function of cell input, and 5e6 cells/ml was found to be the optimal cell concentration among those tested (Figure 3.6). This cell concentration was used for

subsequent experiments involving CpG-loaded sRCCs. Based on such analyses, it was found CpG could be loaded into sRCCs at 36.4% efficiency, the lipophilic adjuvant monophosphoryl lipid A (MPLA) could be loaded at 1.8% efficiency, and the model antigen ovalbumin (OVA) could be loaded at 7.0% efficiency (Figure 3.3D).

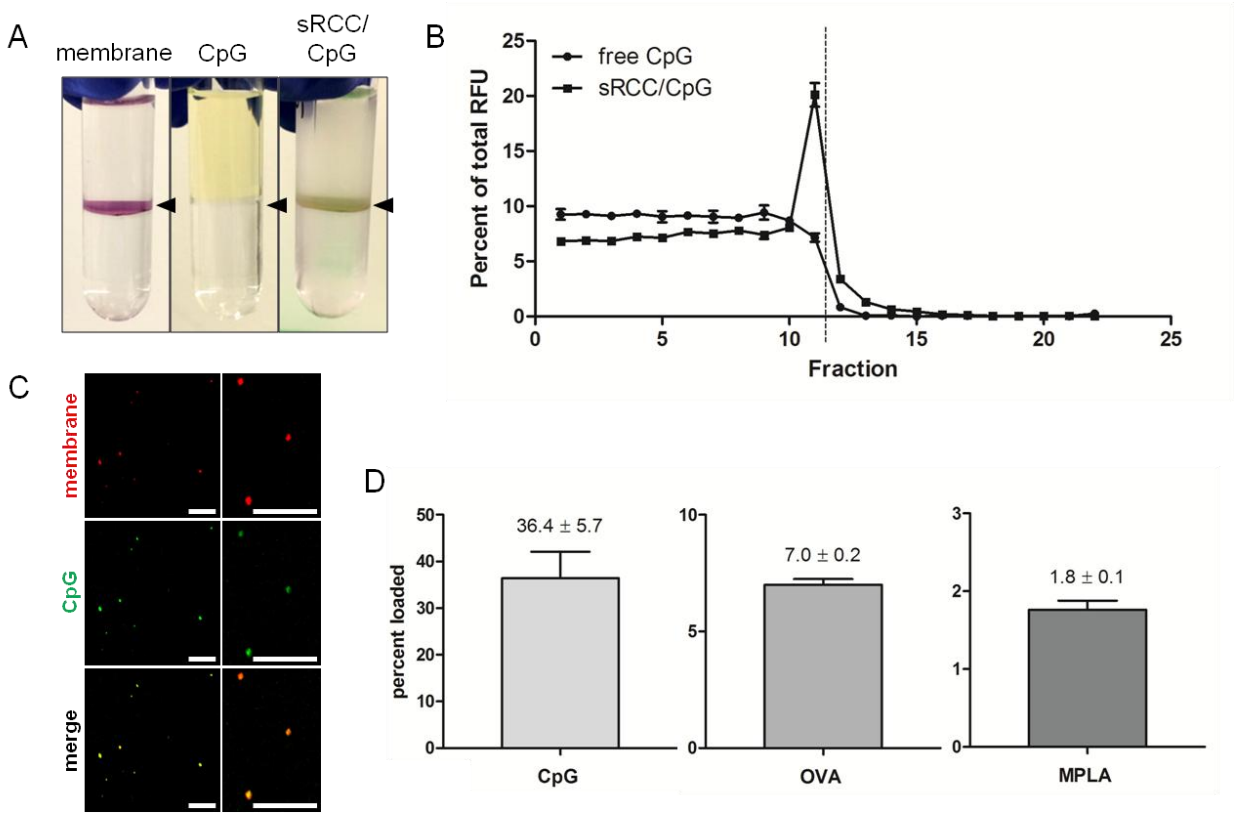

Figure 3.3. Loading of RCCs with diverse payloads. (A) Visualization of RCCs stained with membrane dye (left), free fluorescent CpG (middle), and RCCs loaded with fluorescent CpG (right) following density centrifugation. Black arrowheads point to location of interface. (B) Quantification of fluorescence as a function of fraction following density centrifugation of free fluorescent CpG or fluorescent CpG loaded into sRCCs. Dashed line represents location of interface. (C) Co-localization of a membrane-associated dye and fluorescent CpG following loading into sRCCs at low magnification (left) and high magnification (right). All scale bars = 10 μm. (D) Loading efficiency of CpG, OVA, and MPLA into sRCCs. Numbers represent mean loading efficiency ± SD.

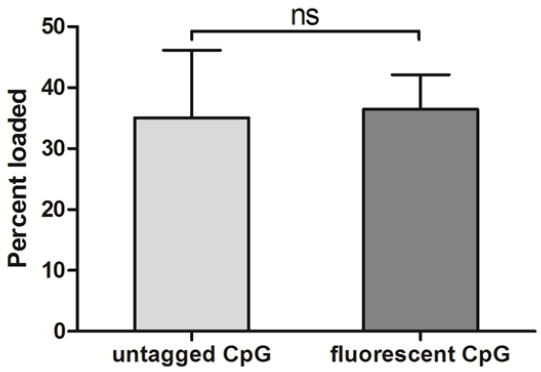

Figure 3.4. Quantification of sRCC-loaded untagged and fluorescent CpG measured using HPLC and detection at 260 nm. Data represent the mean ± SD.

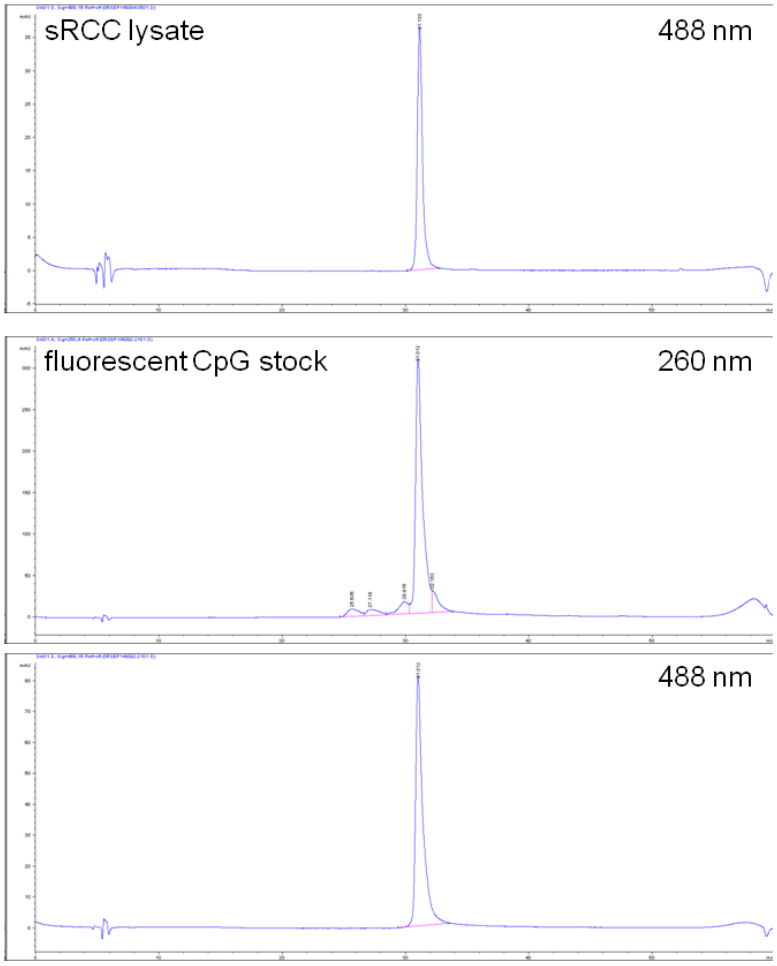

Figure 3.5. Chromatograms of fluorescent CpG stock and fluorescent CpG that was sRCC-loaded and subsequently retrieved. Samples were detected at 260 nm and 488 nm.

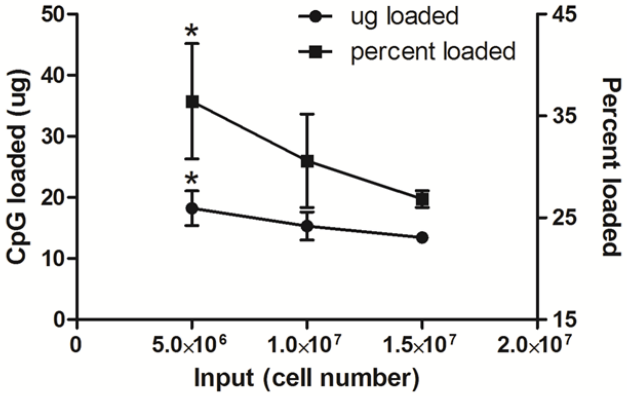

Figure 3.6. Quantification of sRCC-loaded CpG as a function of initial cell number. Data represent the mean ± SD, *$p<0.05$.

The ability of RCCs to facilitate the uptake of associated adjuvant by antigen presenting cells (APCs) was next evaluated using fluorescent CpG as a model adjuvant and primary bone marrow-derived dendritic cells (DCs) as a model APC. CpG associated with RCCs was taken up by DCs with faster kinetics and at a higher magnitude than a comparable amount of free CpG, with ~10% more DCs being CpG+ by 4 hours and beyond, and a greater than 4 and 5-fold higher MFI being observed among CpG+ cells at 4 and 8 hours, respectively (Figure 3.7A, B). These observations were confirmed with confocal microscopy wherein significantly more CpG signal was visible in DCs treated with RCC-associated versus free CpG at all timepoints evaluated (Figure 3.7C, 3.8A). Taking an orthogonal slice through a CpG+ DC, CpG fluorescence was apparent in the interior of the cell (Figure 3.7D) demonstrating true internalization of the CpG. This was further confirmed by visualizing slices through the z-axis of CpG+ DCs as CpG-associated fluorescence was observed throughout the cell volume (Figure 3.8B). CpG was found to be localized within the endolysosomal compartment of DCs after treatment for 4 hours (Figure 3.74E), which is likely to have functional implications as TLR9 is localized in the endosomal

compartment. Taken together, these data show faster uptake kinetics and a higher amount of CpG internalization with RCC-associated CpG compared to free CpG.

RCC sidedness, the orientation of the RCC membranes, could potentially have functional implications, and so was also analyzed. In particular, CD47 is a cell surface transmembrane protein that inhibits phagocytosis, and its upregulation is a common mechanism of immune evasion by tumor cells[30]. Immunoelectron microscopy of sRCCs was performed using antibodies that target either the extracellular or intracellular portion of CD47 (Figure 3.7F). sRCCs were stained by both antibodies suggesting that plasma membrane-derived structures among sRCCs were likely present in a mixture of right-side out and inside-out orientations. This contrasts with previous reports that plasma membrane vesicles derived via mechanical extrusion are primarily maintained in a right-side out orientation[19, 31], which could potentially hinder uptake by APCs if functional CD47 is retained.

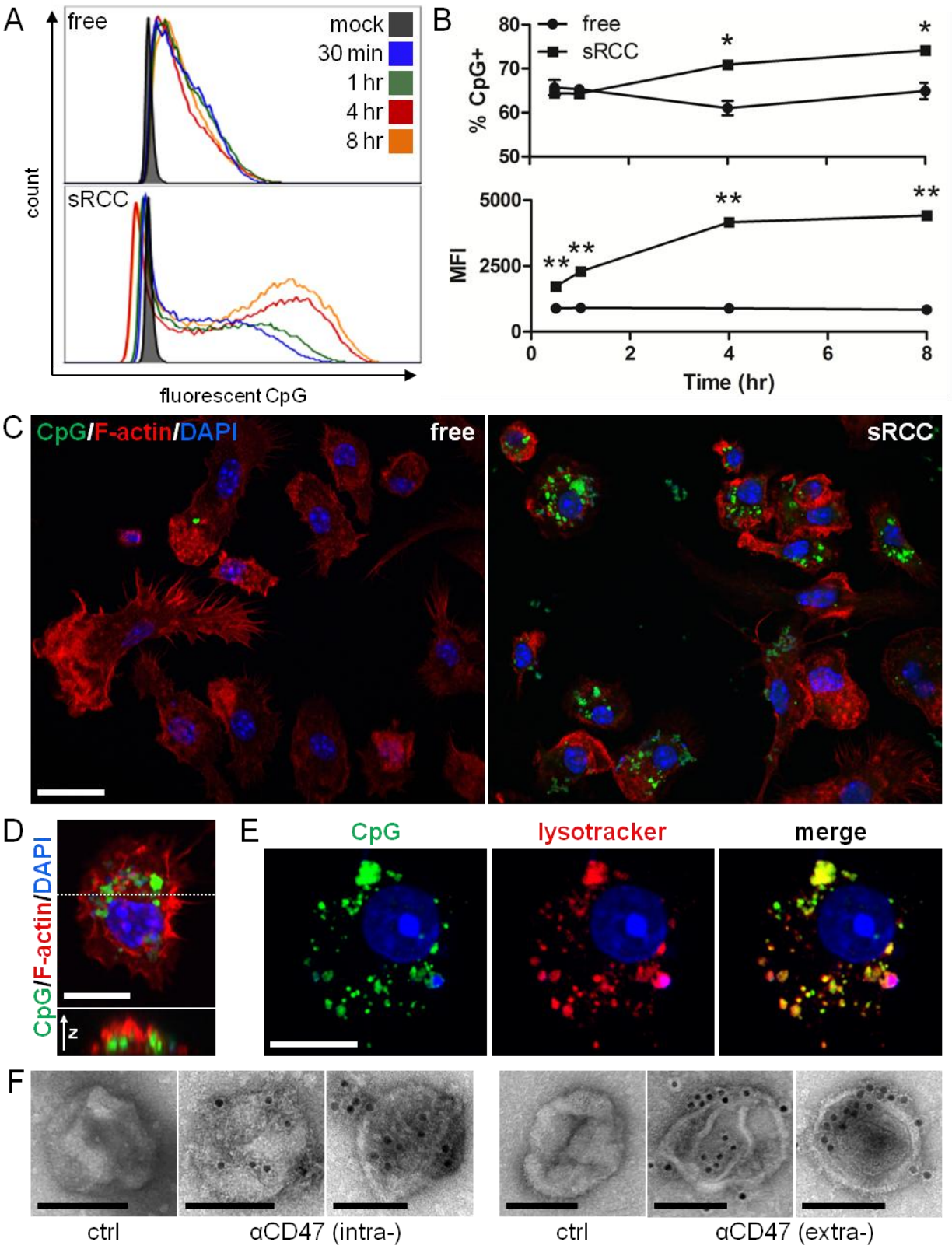
A
free
mock
30 min
1 hr
4 hr
8 hr
sRCC
count
fluorescent CpG
B
free
sRCC
% CpG+
MFI
Time (hr)
C
CpG/F-actin/DAPI
free
sRCC
D
CpG/F-actin/DAPI
z
E
CpG
lysotracker
merge
F
ctrl
αCD47 (intra-)
ctrl
αCD47 (extra-)

Figure 3.7. BMDC uptake of sRCC-associated CpG. (A) Flow cytometry analysis of BMDC uptake of free or sRCC-associated fluorescent CpG at various timepoints. (B) Quantification of data shown in (A) presented as percent of cells CpG+ (top), and MFI (geometric mean) of CpG+ population (bottom). Data represent the mean ± SD, *p<0.05, **p<0.001. (C) Confocal microscopy of BMDC uptake of free or sRCC-associated fluorescent CpG after 4 hour incubation. Scale bar = 20 μm. (D) High magnification image of a CpG+ BMDC (top), and an orthogonal slice through the cell (bottom) taken at the position indicated by the dashed line. Scale bar = 10 μm. (E) Confocal image demonstrating colocalization of fluorescent CpG and lysotracker signals after 4 hour incubation. Scale bar = 10 μm. (F) Immunoelectron microscopy of sRCC stained with a primary antibody specific for either the intracellular (left) or extracellular (right) domains of CD47 followed by an appropriate 10 nm gold colloid-conjugated secondary antibody. Primary antibody was omitted for controls. Two representative sRCC images are shown for each antibody stain. Scale bars = 100 nm.

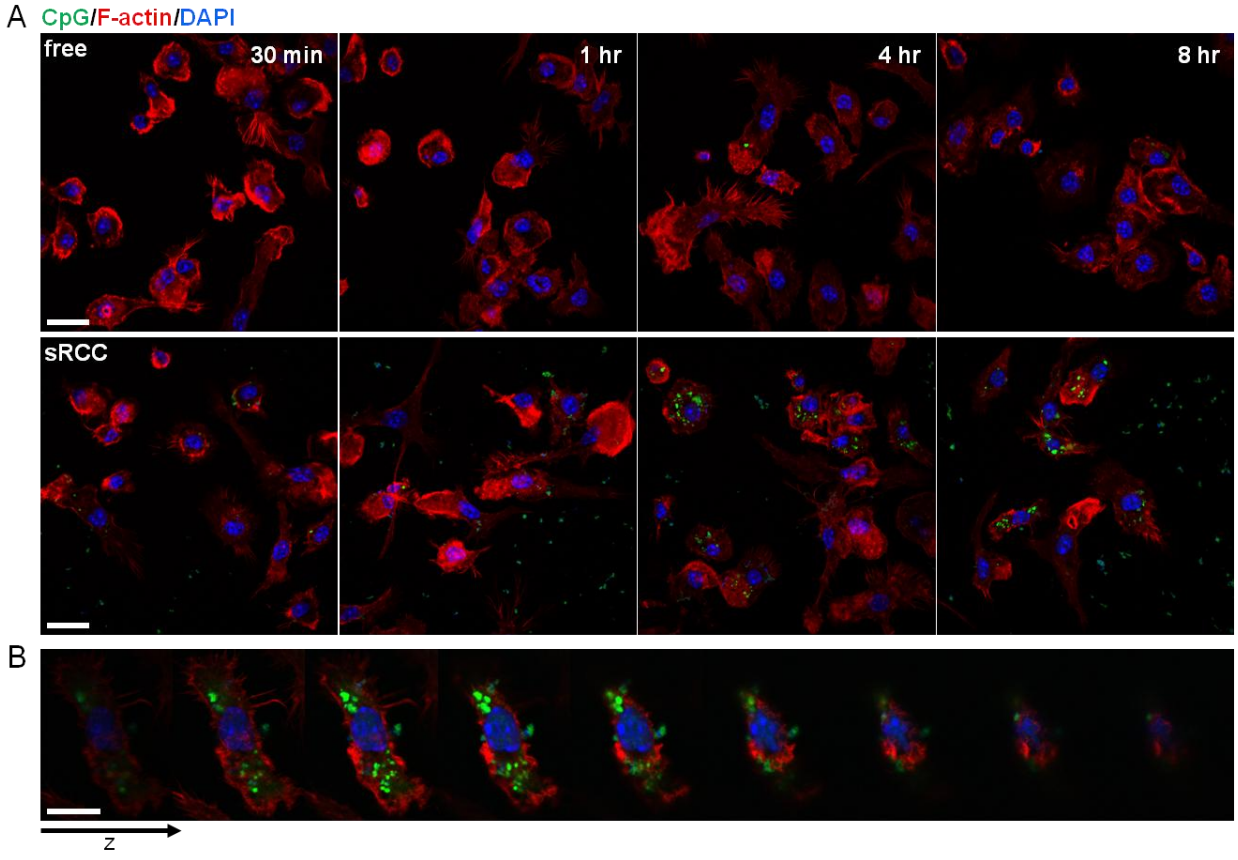

Figure 3.8. DC uptake of sRCC-associated CpG. (A) Representative confocal images of DC uptake of free or sRCC-associated fluorescent CpG at various timepoints as indicated. Scale bars

= 20 μm. (B) z-stack slices showing internalization of sRCC-associated fluorescent CpG following 8 hour incubation with DCs. Each slice is separated by 0.57 μm. Scale bar = 10 μm.

3.3.3 Immunologic Functionality of Adjuvant-Loaded RCCs *in vitro*

To evaluate the functionality of RCC-loaded adjuvants, DCs were treated with CpG and MPLA in either free or RCC-associated forms, and assayed for activation based on upregulation of surface activation markers and production of the proinflammatory cytokine IL-12. Treatment of DCs with blank sRCCs did not result in any increase in surface activation marker expression or IL-12 production compared to mock treatment. In contrast, treatment with sRCCs loaded with either CpG or MPLA significantly upregulated surface expression of MHC II and the costimulatory molecules CD86 and CD40 on DCs, to a similar or greater degree than the respective free adjuvant (Figure 3.9A). Notably, treatment of DCs with sRCC-associated adjuvants promoted significantly greater production of IL-12 than did the same amount of the respective free adjuvants, with a ~36% and ~80% increase observed with CpG and MPLA, respectively (Figure 3.9B). Treatment of DCs with CpG-loaded sRCCs also promoted a change in cell morphology characterized by increased spreading and aspect ratio relative to unactivated DCs (Figure 3.10). These morphology changes are consistent with what has been previously reported to take place upon in vitro DC activation[32].

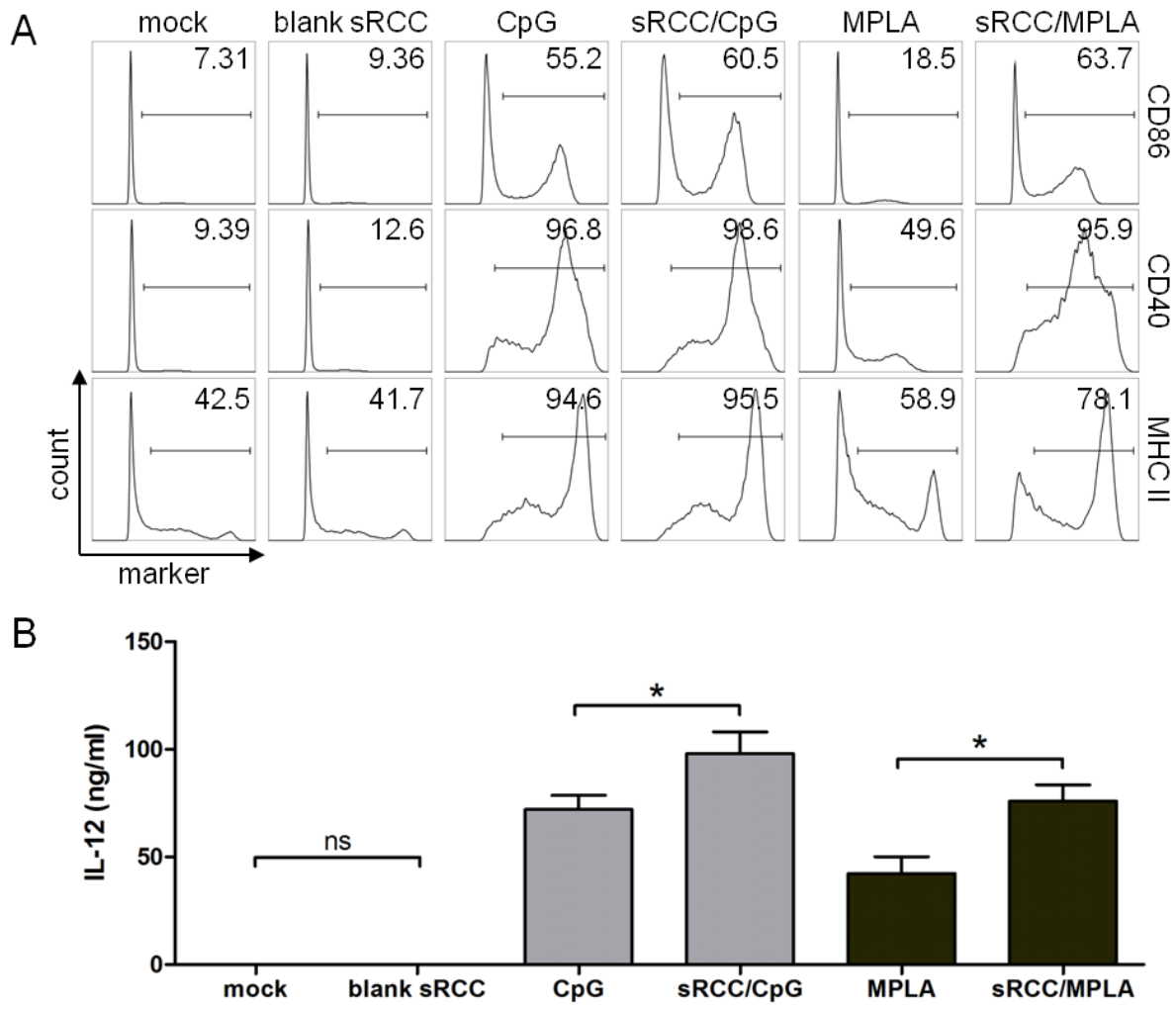

Figure 3.9. DC activation in response to adjuvant-loaded sRCCs. (A) Flow cytometry analysis of DC surface activation marker expression, and (B) quantification of IL-12 production via ELISA, following mock treatment or treatment with blank sRCCs, treatment with 0.2 μM CpG in free or sRCC-associated form, or treatment with 0.02 μM MPLA in free or sRCC-associated form, after 12-15 hour incubation. Numbers in (A) represent average percent positive cells based on gate shown. Values in (B) represent the mean ± SD, *$p<0.05$.

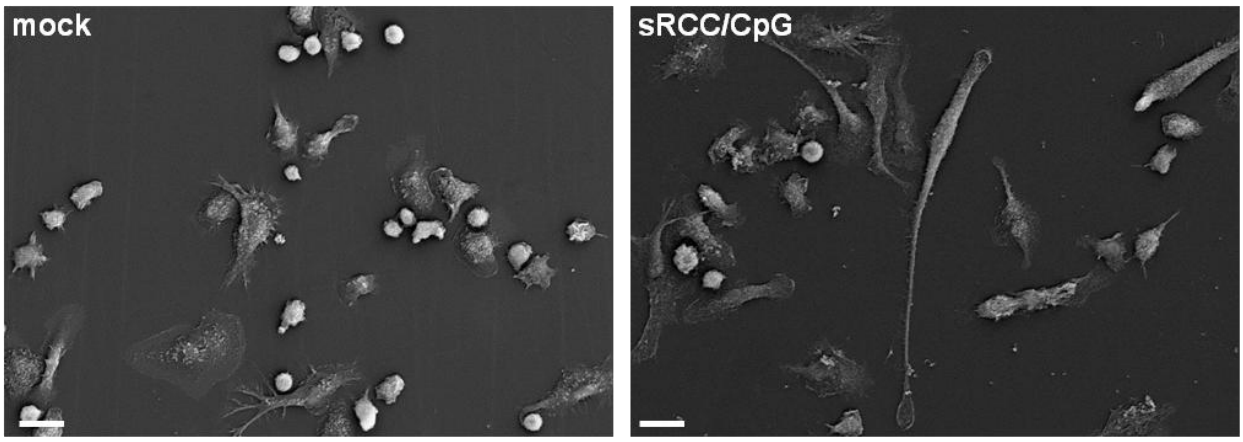

Figure 3.10. SEM of BMDCs treated with mock or CpG-loaded sRCCs for 4 hours. Scale bars = 20 μm.

Next, the ability of RCCs to facilitate antigen presentation by APCs was evaluated using the model antigen OVA. To evaluate presentation of RCC-associated antigens on MHC II, DCs were loaded with sRCCs derived from either wild-type B16-F10 cells (B16-WT), or B16-F10 cells transduced to express a membrane-bound form of OVA (B16-mOVA) (Figure 3.11), and co-cultured with MF2.2D hybridoma T cells. MF2.2D cells recognize an OVA-derived peptide presented on MHC II, and produce IL-2 in response to T cell receptor (TCR) stimulation. Whereas no increase in IL-2 production was observed over control conditions when DCs were treated with B16-WT sRCCs, a dose-dependent increase in IL-2 production was observed with B16-mOVA sRCC treatment over the concentration range tested (Figure 3.12A).

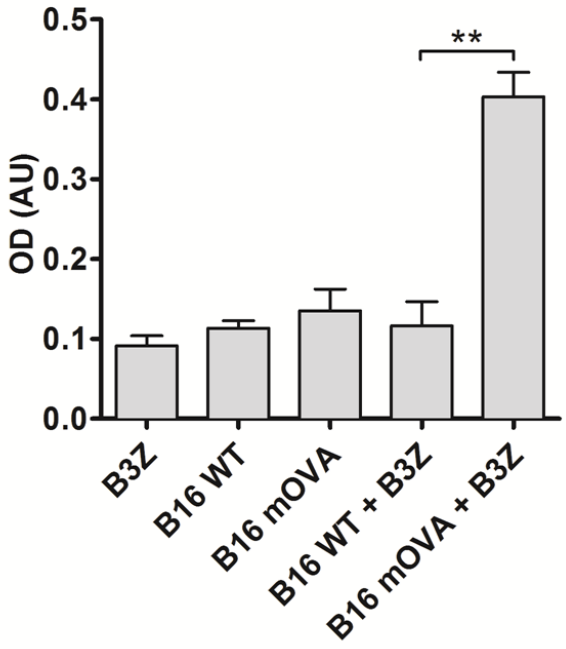

Figure 3.11. Quantification of OVA-dependent activation of B3Z hybridoma cell line based on β-galactosidase production. Data represent the mean ± SD, **p<0.001.

To evaluate MHC I-mediated cross-presentation of RCC-associated antigens, a process critical for robust anti-tumor immunity, DCs treated with various stimuli were co-cultured with CFSE-stained primary CD8+ T cells derived from OT-I mice, which express a transgenic T cell receptor specific for an OVA peptide presented on MHC I. T cell activation was evaluated by measuring CFSE dilution as a proxy for T cell proliferation. First, DCs were treated with either B16-WT sRCCs, B16-mOVA sRCCs, or cancer cell lysate from the same number of starting B16-mOVA parent cells. sRCC samples were either unloaded, or loaded with CpG, and lysate samples were either used as-prepared, or admixed with the same amount of soluble CpG. Whereas DCs treated with B16-WT sRCCs or B16-mOVA lysate, with or without CpG, facilitated minimal OT-I CD8+ T cell proliferation, DCs treated with B16-mOVA sRCCs loaded with CpG facilitated extremely robust OT-I CD8+ T cell proliferation (Figure 3.12B).

Because it is possible that the difference in antigen presentation efficiency between lysate and RCC could be due to differences in the level of the relevant protein retained by the two derivation procedures, the antigen presentation efficiency of soluble OVA protein was next compared to the same amount of OVA protein loaded into B16-WT sRCCs. Consistent with observations made with endogenously expressed OVA, it was observed that whereas DCs treated with soluble OVA admixed with CpG could facilitate moderate levels of OT-I CD8+ T cell proliferation, DCs treated with OVA-loaded and OVA/CpG-co-loaded B16-WT sRCCs facilitated significantly greater levels of OT-I CD8+ T cell proliferation relative to the respective soluble OVA conditions (Figure 3.12C). Taken together, these data demonstrate that antigens associated with adjuvant-loaded sRCCs are efficiently presented by DCs in vitro in a functional manner, and that the presentation of these sRCC-associated antigens is significantly more efficient than antigens delivered in a soluble format.

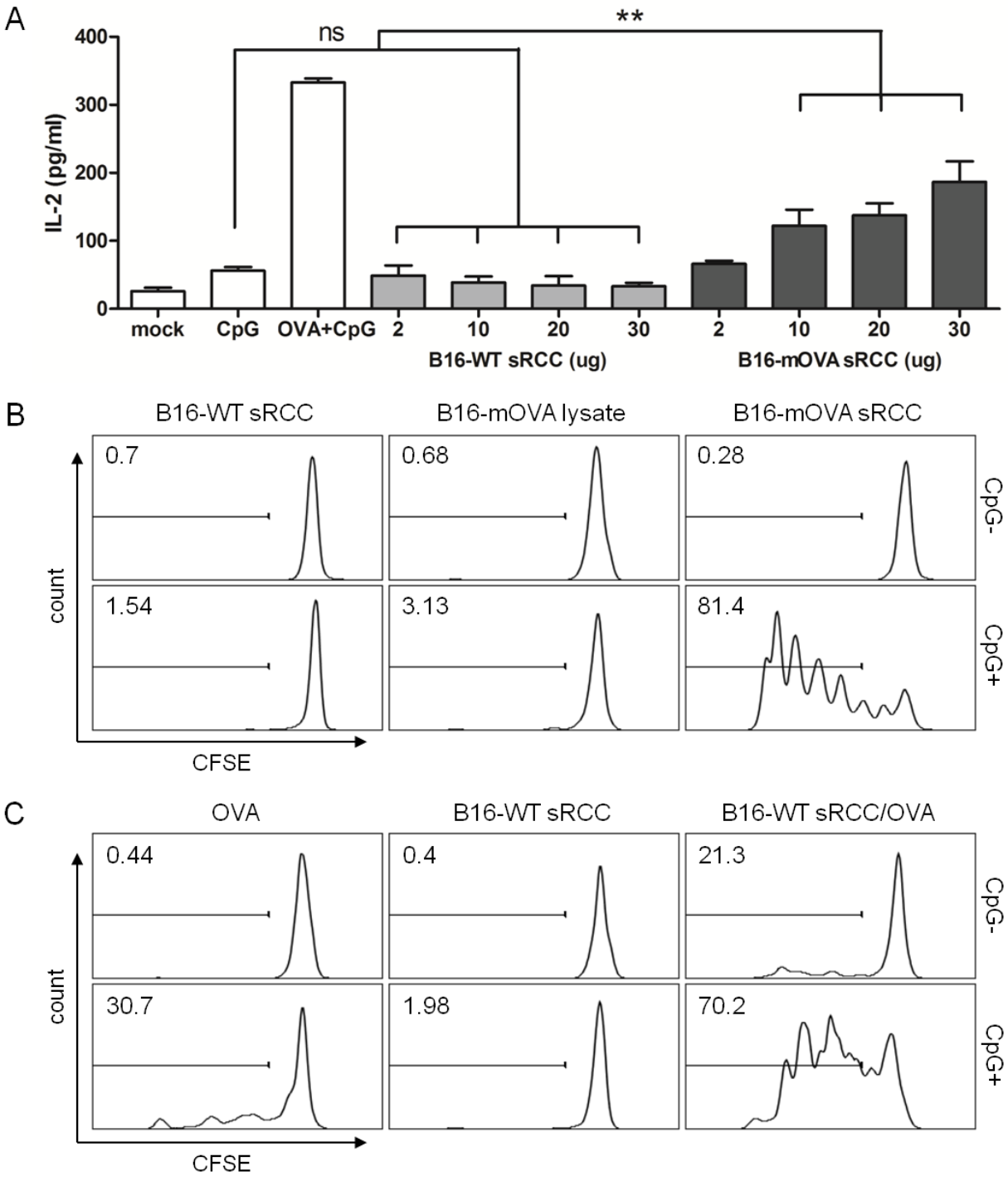

Figure 3.12. T cell response to sRCC-treated DCs. (A) Quantification of IL-2 production by MHC II-restricted MF2.2D hybridoma T cells in response to co-culture with DCs treated with B16-WT- or B16-mOVA-derived sRCCs. CpG samples were treated with 0.8 μM CpG, OVA samples were treated with 2.8 μM OVA, and OVA + CpG samples were treated with 2.8 μM OVA and 0.8 μM CpG. sRCC samples were treated with between 2-30 μg of sRCCs containing

between 0.1-1.5 μg (78.6 nM-1.2 μM) CpG based on a total protein/CpG mass ratio of 1/0.05. (B) Representative histograms in which sRCC conditions represent T cell response to BMDCs treated with 13.9 μg sRCCs (+/- 0.3 μg CpG; 0.2 μM). Lysate conditions represent T cell response to BMDCs treated with lysate derived from an equivalent number of whole cells, and admixed with an equivalent amount of CpG. (C) Representative histograms in which OVA conditions represent T cell response to BMDCs treated with 44.4 nM free OVA with or without 78.6 nM free CpG, an equivalent amount of OVA and CpG loaded into B16-WT sRCCs, or an equivalent amount of blank B16-WT sRCCs. All co-culture experiments were carried out in 0.2 ml volume. Gates and values in (B-C) indicate the mean percentage positive cells in respective sample. Data in (A) represent the mean ± SD, analyzed using one-way ANOVA, followed by Tukey post-test, *$p<0.05$.

3.3.4 Immunologic Functionality of Adjuvant-Loaded RCCs in vivo

The in vivo functionality of the RCCs was evaluated by performing vaccinations of naive mice and measuring antigen-specific cellular and humoral immune responses. First, vaccinations were performed either with B16-WT-derived lysate admixed with OVA protein and MPLA, or with B16-WT sRCCs co-loaded with the same amount of OVA and MPLA. Analysis of T cells in the peripheral blood 8 days post-vaccination showed significantly greater frequencies of functional IFNγ-producing CD8+ T cells in samples from mice treated with sRCCs as compared to mock-treated or lysate-treated mice, following ex vivo stimulation of peripheral blood mononuclear cells (PBMCs) with a relevant MHC I-restricted OVA peptide (Figure 3.13A). Consistent with this, sRCC vaccination also facilitated the induction of OVA-specific IgG1 and IgG2a antibody titers comparable to, or greater than lysate (Figure 3.13B).

Lastly, to evaluate the immune response to endogenous parent cell antigens elicited by sRCCs, naive mice were vaccinated with either B16-mOVA-derived lysate admixed with CpG and MPLA, or with B16-mOVA sRCCs co-loaded with the same amount of CpG and MPLA. Because immune responses can be induced against a diversity of different parent cell antigens,

the cellular immune response was evaluated by co-culturing T cells isolated from spleens of treated mice with irradiated B16-mOVA parent cells, and T cell stimulation evaluated via IL-2 production was measured using ELISPOT. sRCC vaccination facilitated the induction of functional B16-mOVA-specific T cells at frequencies comparable to, or greater than lysate (Figure 3.13C). Taken together, these data demonstrate that RCCs can facilitate the induction of antigen-specific cellular and humoral responses in vivo.

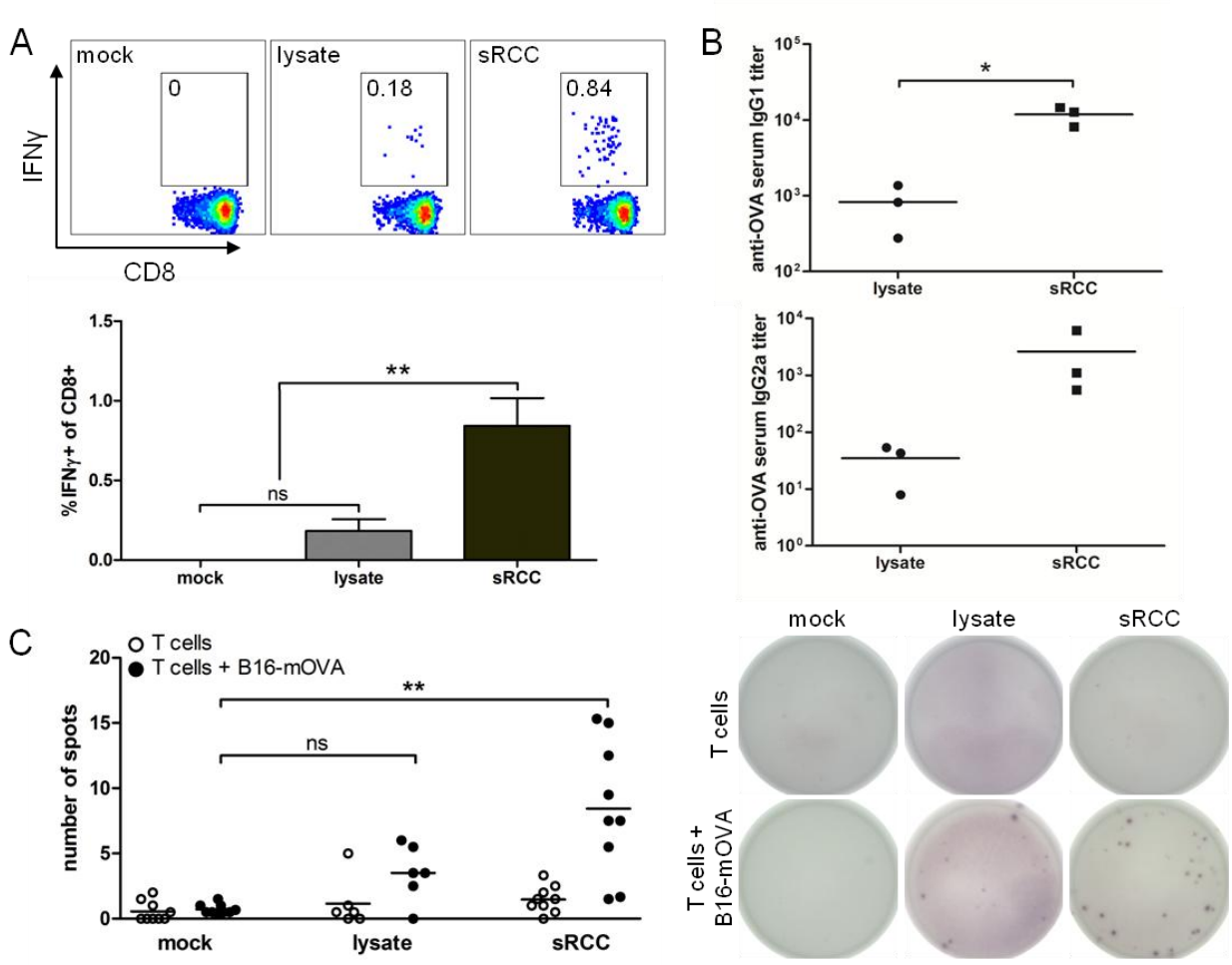

Figure 3.13. Cellular and humoral response to sRCC vaccinations in naive mice. (A)-(B) Cellular and humoral response to vaccination with sRCCs or cell lysate derived from B16-WT cells, and loaded or admixed, respectively, with exogenous OVA protein. (A) Representative flow cytometry plots with mean frequency of IFNγ-positive cells among live CD8+ cells in

peripheral blood (top), and quantification of data (bottom). Cells were stimulated in vitro with peptide. (B) anti-OVA IgG1 and IgG2a serum titers, on day 8 post-vaccination. Naive mice were vaccinated subcutaneously with either 370 μg B16-WT sRCCs loaded with 70 μg OVA and 90 ng MPLA, or cell lysate derived from the same number of B16-WT cells (5e6) and admixed with the same amount of OVA and MPLA. (C) Cellular response to vaccination with sRCCs or cell lysate derived from B16-mOVA cells. ELISPOT analysis of IL-2-producing T cells from spleens of mice following overnight co-culture with parent B16-mOVA cells on day 4 post-boost (day 22 post-vaccination). Naive mice were vaccinated subcutaneously on days 0 and 2 (prime), and days 16 and 18 (boost), with either 370 μg B16-mOVA sRCCs loaded with 18 μg CpG and 180 ng MPLA, or cell lysate derived from the same number of B16-mOVA cells (5e6) and admixed with the same amount of CpG and MPLA. Quantification of spots (left) and representative images of ELISPOT membranes (right). Values represent the mean ± SD, *$p<0.05$, **$p<0.001$. Data in (C) analyzed using one-way ANOVA, followed by Tukey post-test.

3.4 Discussion

In this work, we show that whole cancer cells can be processed to produce antigen-rich particles termed RCCs. Although these structures can be generated through various methods, a derivation method based on sonication led to the retention of greater than 20% of total protein content. Protein from different intracellular compartments were retained in a distribution similar to the parent cells, providing a broad antigen pool for anti-cancer immunization. In contrast, RCCs generated via extrusion using the method employed in this work retained significantly less total protein, with significant loss of non-membrane-associated protein. The difference in protein retention between the two methods likely stems from the different mechanisms of cell disruption that take place during extrusion versus sonication. Cell disruption during extrusion is expected to take place via mild mechanical shear, likely resulting in brief disruption of membrane-enclosed compartments as the cells are forced through the pores. In this work, cells were extruded through membranes with a minimal pore size of 1 μm, which is small enough to disrupt membrane-bound organelles, potentially resulting in the release of their contents. Indeed, while the majority of the

lipid content is recovered following density centrifugation, the significant loss of cystolic and nuclear proteins, but not membrane-associated (including nuclear envelope-associated) proteins suggests that this is the case. An additional factor contributing to protein loss could be fouling of the filter membrane during extrusion. In contrast, cell disruption during sonication takes place primarily via cavitation, involving the continuous mass nucleation, expansion, and implosion of microbubbles throughout the medium, which causes complete disintegration of membranes and the release of soluble protein content. A possible mechanism for the observed retention of soluble protein by the sonicated RCCs could involve the recapture of a fraction of the freed protein during the thermodynamically favored reformation of membrane-enclosed structures following membrane disintegration.

This work also demonstrated that sRCCs can be loaded with both hydrophilic (CpG) and lipophilic (MPLA) adjuvants, illustrating the versatility of this approach. This allows the flexibility to load adjuvants that differentially regulate the generated immune response, as well as diverse combinations of different adjuvants that activate nonredundant signaling pathways. The latter is particularly interesting as it could allow, for example, for the generation of RCCs loaded with multiple TLR or other PRR agonists in combinations that mimic natural pathogens. Indeed, it has been shown that the delivery of multiple PRR agonists enhances the resultant cytokine response by immune cells and that certain combinations show greater synergy than others[12, 33]. In the vaccination studies evaluating the immune response to endogenous parent cell antigens, combinatorial delivery of CpG and MPLA was employed, allowing for activation of both the MyD88- and TRIF-dependent pathways. Further studies exploring the synergy of various adjuvant combinations could allow for further optimization of this system.

It was observed that adjuvant was taken up more efficiently by DCs when it was associated with the sRCCs than when it was administered in free form. Treatment of DCs with adjuvant-loaded sRCCs enhanced the expression of surface activation markers and the production of the proinflammatory cytokine IL-12 compared to soluble adjuvant, and enhanced the efficiency of antigen presentation compared to soluble antigen sources such as lysate. The enhancement in payload uptake is likely due to the concentration of the adjuvant and antigen in a colloidal vehicle, which is consistent with previous findings[34]. Enhancement of DC activation by CpG, which signals via the endosomal TLR9, is likely also related to the enhanced uptake, and is also consistent with previous findings that association of CpG with a colloidal vehicle enhances its adjuvant activity[35]. Enhancement of DC activation by MPLA, which signals via the cell surface TLR4, is likely related to an enhancement of MPLA avidity on the surface of the sRCCs, which can facilitate TLR4 clustering and subsequent activation[36, 37]. Notably, it was observed that nonadjuvanted sRCCs did not activate DCs compared to mock treatment, demonstrating that the sRCCs themselves are not inherently immunostimulatory, for example, due to the retention of endogenous danger associated molecular patterns (DAMPs). Rather, loading the sRCCs with exogenous adjuvants is necessary to impart them with immunostimulatory capacity, and the ability to load these structures with adjuvant using this derivation method is critical to the utility of the generated structures for vaccination.

Collectively, the observations presented herein suggest that adjuvant-loaded sRCCs potentially represent an efficient and versatile cancer vaccine platform. Indeed, previous work employing material isolated from deconstructed cancer cells supports the idea that such material, when appropriately adjuvanted, can be employed as a cancer antigen source for vaccination both in vitro and in vivo[23, 38]. The generation of adjuvant-loaded sRCCs is a method for processing

cancer cells in which the antigen diversity of the parent cells is maintained, but the antigen content is reformulated to facilitate efficient antigen presentation. Notably, sRCC derivation does not involve the input of any exogenous material, and is therefore analogous to the preparation of tumor lysate, which is also a form of processed tumor material and is the current standard for primary cancer antigen mixtures. Importantly, lysate is commonly employed in diverse cancer vaccine systems in both the preclinical and clinical settings[25-27, 39-41], demonstrating that such tumor-derived material is generally considered a safe antigen source for vaccines. Tumor lysate as an antigen source is most commonly used in DC vaccines, vaccines that activate and load DCs with cancer antigen ex vivo for subsequent reinfusion. The in vitro observations reported in this study are compelling evidence that adjuvant-loaded RCCs may represent a superior alternative to tumor lysate in such vaccine approaches by facilitating enhanced uptake and cross-presentation of cancer antigens. Notably, the in vivo data also suggests that RCCs may be more effective than lysate in this context, although the relatively low frequency of antigen-specific T cells generated against endogenous cell antigens indicates that the RCCs will likely need to be optimized for direct in vivo applications. One suboptimal property of the RCCs for in vivo applications is their broad size distribution, which extends far beyond a feasible size range for passive drainage to the lymph nodes via the lymphatics[42, 43]. In order to optimize the RCCs for standalone vaccination, it may be necessary to improve the size distribution of the particles via further processing, for example, through post-sonication extrusion. Alternatively, improving the active trafficking of the RCCs to the lymph node by APCs could be achieved via surface modification with cues that enhance APC uptake[38], or by incorporating the RCCs into material scaffolds that bring large numbers of relevant APCs to the vaccination site[25-27, 29, 39].

3.5 Conclusion

In summary, whole cancer cells can be processed to produce subcellular vesicular particles within the nano- to microscale size range, that retain a broad distribution of proteins representative of the parent cells from which they are derived. When these structures, termed RCCs, are loaded with adjuvant, they facilitate enhanced DC activation and antigen presentation when compared to soluble adjuvant and antigen, respectively. Vaccination of mice with these structures also facilitates the induction of antigen specific cellular and humoral immune responses. Based on these observations, we propose that RCCs represent an attractive platform for cancer vaccination, in particular, as an alternative to tumor lysate in vaccine approaches that currently use lysate as an antigen source. RCCs could also have utility in various materials-based approaches that function to bring large numbers of APCs to the vaccination site, and may be potentially useful as a standalone particulate cancer vaccine system with optimization.

3.6 Acknowledgements

This work was supported by NIH Grant R01 EB015498 to D. Mooney. S. Koshy was supported by an HHMI ISRF. This work was performed in part at the Center for Nanoscale Systems (CNS) at Harvard University, a member of the National Nanotechnology Infrastructure Network (NNIN), which is supported by the National Science Foundation under NSF award no. ECS-0335765. The authors thank Dr. Steven Perrault, Dr. Alex Watters, Dr. Deniz Yuksel, Dr. Luo Gu, Dr. Omar Ali, Dr. Martin Thelin, Aileen Li, and Chris Johnson for scientific discussions, and Dr. Dennis Kasper for use of the CTL ImmunoSpot S4 analyzer. The authors

especially thank Dr. Kenneth Rock and the Dana-Farber Cancer Institute for providing the MF2.2D cell line, and Dr. Nilabh Shastri for providing the B3Z cell line.

3.7 References

1. Gerlinger, M. et al. Intratumor heterogeneity and branched evolution revealed by multiregion sequencing. *New England Journal of Medicine* **366**, 883-892 (2012).
2. Rabinovich, G.A., Gabrilovich, D. & Sotomayor, E.M. Immunosuppressive strategies that are mediated by tumor cells. *Annual review of immunology* **25**, 267 (2007).
3. Mittal, D., Gubin, M.M., Schreiber, R.D. & Smyth, M.J. New insights into cancer immunoediting and its three component phases—elimination, equilibrium and escape. *Current opinion in immunology* **27**, 16-25 (2014).
4. Schumacher, T.N. & Schreiber, R.D. Neoantigens in cancer immunotherapy. *Science* **348**, 69-74 (2015).
5. Rooney, M.S., Shukla, S.A., Wu, C.J., Getz, G. & Hacohen, N. Molecular and genetic properties of tumors associated with local immune cytolytic activity. *Cell* **160**, 48-61 (2015).
6. González, F.E. et al. Tumor cell lysates as immunogenic sources for cancer vaccine design. *Human vaccines & immunotherapeutics* **10**, 3261-3269 (2014).
7. Tighe, H. et al. Conjugation of protein to immunostimulatory DNA results in a rapid, long-lasting and potent induction of cell-mediated and humoral immunity. *European journal of immunology* **30**, 1939-1947 (2000).
8. Heit, A. et al. Protective CD8 T cell immunity triggered by CpG-protein conjugates competes with the efficacy of live vaccines. *The Journal of Immunology* **174**, 4373-4380 (2005).
9. Moon, J.J. et al. Interbilayer-crosslinked multilamellar vesicles as synthetic vaccines for potent humoral and cellular immune responses. *Nature materials* **10**, 243-251 (2011).
10. Scott, E.A. et al. Dendritic cell activation and T cell priming with adjuvant-and antigen-loaded oxidation-sensitive polymersomes. *Biomaterials* **33**, 6211-6219 (2012).
11. Wang, Q., Tan, M.T., Keegan, B.P., Barry, M.A. & Heffernan, M.J. Time course study of the antigen-specific immune response to a PLGA microparticle vaccine formulation. *Biomaterials* **35**, 8385-8393 (2014).

12. Black, M., Trent, A., Tirrell, M. & Olive, C. Advances in the design and delivery of peptide subunit vaccines with a focus on toll-like receptor agonists. (2010).

13. Blander, J.M. & Medzhitov, R. Toll-dependent selection of microbial antigens for presentation by dendritic cells. *Nature* **440**, 808-812 (2006).

14. Burgdorf, S., Schölz, C., Kautz, A., Tampé, R. & Kurts, C. Spatial and mechanistic separation of cross-presentation and endogenous antigen presentation. *Nature immunology* **9**, 558-566 (2008).

15. Rock, K.L. Presentation of exogenous antigens by macrophages: analysis of major histocompatibility complex class I and II presentation and regulation by cytokines. *European journal of immunology* **24**, 2421-2428 (1994).

16. Li, M. et al. Cell-associated ovalbumin is cross-presented much more efficiently than soluble ovalbumin in vivo. *The Journal of Immunology* **166**, 6099-6103 (2001).

17. Ruben, J.M. et al. Apoptotic blebs from leukemic cells as a preferred source of tumor-associated antigen for dendritic cell-based vaccines. *Cancer Immunology, Immunotherapy* **63**, 335-345 (2014).

18. Andre, F. et al. Tumor-derived exosomes: a new source of tumor rejection antigens. *Vaccine* **20**, A28-A31 (2002).

19. Jang, S.C. et al. Bioinspired exosome-mimetic nanovesicles for targeted delivery of chemotherapeutics to malignant tumors. *ACS nano* **7**, 7698-7710 (2013).

20. Wu, H. et al. Preparation, characterization, and surface immobilization of native vesicles obtained by mechanical extrusion of mammalian cells. *Integrative Biology* **4**, 685-692 (2012).

21. Boudreau, J., Koshy, S., Cummings, D. & Wan, Y. Culture of myeloid dendritic cells from bone marrow precursors. *JoVE (Journal of Visualized Experiments)*, e769-e769 (2008).

22. Parodi, A. et al. Synthetic nanoparticles functionalized with biomimetic leukocyte membranes possess cell-like functions. *Nature nanotechnology* **8**, 61-68 (2013).

23. Fang, R.H. et al. Cancer cell membrane-coated nanoparticles for anticancer vaccination and drug delivery. *Nano letters* **14**, 2181-2188 (2014).

24. Vigneron, N., Stroobant, V., Van den Eynde, B.J. & van der Bruggen, P. Database of T cell-defined human tumor antigens: the 2013 update. *Cancer Immunity Archive* **13**, 15 (2013).

25. Ali, O.A., Emerich, D., Dranoff, G. & Mooney, D.J. In situ regulation of DC subsets and T cells mediates tumor regression in mice. *Science translational medicine* **1**, 8ra19-18ra19 (2009).

26. Ali, O.A., Huebsch, N., Cao, L., Dranoff, G. & Mooney, D.J. Infection-mimicking materials to program dendritic cells in situ. *Nature materials* **8**, 151-158 (2009).

27. Ali, O.A., Tayalia, P., Shvartsman, D., Lewin, S. & Mooney, D.J. Inflammatory Cytokines Presented from Polymer Matrices Differentially Generate and Activate DCs In Situ. *Advanced functional materials* **23**, 4621-4628 (2013).

28. Gungor, B. et al. CpG ODN nanorings induce IFNα from plasmacytoid dendritic cells and demonstrate potent vaccine adjuvant activity. *Science translational medicine* **6**, 235ra261-235ra261 (2014).

29. Kim, J. et al. Injectable, spontaneously assembling, inorganic scaffolds modulate immune cells in vivo and increase vaccine efficacy. *Nature biotechnology* **33**, 64-72 (2015).

30. Weiskopf, K. et al. Engineered SIRPα variants as immunotherapeutic adjuvants to anticancer antibodies. *Science* **341**, 88-91 (2013).

31. Hu, C.-M.J. et al. 'Marker-of-self' functionalization of nanoscale particles through a top-down cellular membrane coating approach. *Nanoscale* **5**, 2664-2668 (2013).

32. Xing, F. et al. Comparison of immature and mature bone marrow-derived dendritic cells by atomic force microscopy. *Nanoscale research letters* **6**, 1-9 (2011).

33. Zhu, Q. et al. Toll-like receptor ligands synergize through distinct dendritic cell pathways to induce T cell responses: implications for vaccines. *Proceedings of the National Academy of Sciences* **105**, 16260-16265 (2008).

34. Brewer, J.M., Pollock, K.G., Tetley, L. & Russell, D.G. Vesicle size influences the trafficking, processing, and presentation of antigens in lipid vesicles. *The Journal of Immunology* **173**, 6143-6150 (2004).

35. De Titta, A. et al. Nanoparticle conjugation of CpG enhances adjuvancy for cellular immunity and memory recall at low dose. *Proceedings of the National Academy of Sciences* **110**, 19902-19907 (2013).

36. Triantafilou, M., Miyake, K., Golenbock, D.T. & Triantafilou, K. Mediators of innate immune recognition of bacteria concentrate in lipid rafts and facilitate lipopolysaccharide-induced cell activation. *Journal of cell science* **115**, 2603-2611 (2002).

37. Meraz, I.M. et al. Multivalent presentation of MPL by porous silicon microparticles favors T helper 1 polarization enhancing the anti-tumor efficacy of doxorubicin nanoliposomes. *PloS one* **9**, e94703 (2014).

38. van Broekhoven, C.L., Parish, C.R., Demangel, C., Britton, W.J. & Altin, J.G. Targeting Dendritic Cells with Antigen-Containing Liposomes A Highly Effective Procedure for Induction of Antitumor Immunity and for Tumor Immunotherapy. *Cancer research* **64**, 4357-4365 (2004).

39. Ali, O.A. et al. Identification of Immune Factors Regulating Antitumor Immunity Using Polymeric Vaccines with Multiple Adjuvants. *Cancer research* **74**, 1670-1681 (2014).

40. Prins, R.M. et al. Comparison of glioma-associated antigen peptide-loaded versus autologous tumor lysate-loaded dendritic cell vaccination in malignant glioma patients. *Journal of immunotherapy (Hagerstown, Md.: 1997)* **36**, 152 (2013).

41. Poschke, I. et al. A phase I clinical trial combining dendritic cell vaccination with adoptive T cell transfer in patients with stage IV melanoma. *Cancer Immunology, Immunotherapy* **63**, 1061-1071 (2014).

42. Reddy, S.T. et al. Exploiting lymphatic transport and complement activation in nanoparticle vaccines. *Nature biotechnology* **25**, 1159-1164 (2007).

43. Mueller, S.N., Tian, S. & DeSimone, J.M. Rapid and Persistent Delivery of Antigen by Lymph Node Targeting PRINT Nanoparticle Vaccine Carrier To Promote Humoral Immunity. *Molecular pharmaceutics* **12**, 1356-1365 (2015).

Chapter 4: Antigen-Presenting Cell-Mimetic Scaffolds for *ex vivo* T Cell Expansion

4.1 Introduction

In this chapter, we describe a composite material that can release soluble cues in a controlled manner, and present cues locally on the surface of a synthetic lipid bilayer at a predefined density. We formulate the material to present a set of T cell activating cues and evaluate its utility for *ex vivo* T cell expansion, an important step in adoptive cell transfer (ACT) therapies using T cells. ACT using T cells is a promising approach for the treatment of a variety of solid[1, 2] and hematologic[1-3] malignancies, and infectious diseases[2]. However, the rapid *ex vivo* expansion of functional T cells, a key step in the manufacture of diverse T cell products for ACT[1-3], remains one of the primary challenges in such approaches. In the body, T cell expansion takes place when T cells are activated by antigen-presenting cells (APCs) presenting an appropriate combination of cues. The minimum repertoire of cues that an APC must present in order to facilitate T cell activation consists of: (1) cell surface peptide-loaded major histocompatibility complex (pMHC) that the T cell can recognize via its T cell receptor (TCR), (2) cell surface costimulatory cue(s), and (3) soluble cytokines that promote T cell survival[4]. The quality of T cell activation, which determines T cell expansion rate and downstream T cell functionality, is critically dependent on the repertoire and density of cues presented by the APC[4-6].

Difficulties associated with large-scale sourcing, maintenance, and functional consistency limit the widespread use of primary APCs for *ex vivo* T cell expansion for ACT[7, 8]. As an alternative to primary APCs, engineered systems that mimic critical functional characteristics of APCs, referred to as "artificial APCs" (aAPCs), are commonly employed. A major class of

aAPCs are cellular aAPCs, cell lines that are transduced to express a cell surface TCR cue and costimulatory cues, potentially in combination with other functional cell surface molecules[9, 10]. A primary strength of cellular aAPC systems is the relative ease of modifying cells to express large combinations of cues[10]. In addition, cellular aAPCs surface-present T cell cues in the context of a plasma membrane, which has been shown to be important for full TCR activation[6]. However, the establishment of cellular aAPC cell lines is cumbersome and time-consuming, their maintenance in culture can lead to phenotypic drift, the relative densities at which they present the transduced T cell cues is difficult to precisely define, and the repertoire of expressed cues cannot be changed without reengineering the cell line. Synthetic material-based aAPCs are used as a simpler and more consistent alternative to cellular aAPC systems. Currently, commercial microbeads that are surface-functionalized with activating antibodies for CD3 (αCD3) and CD28 (αCD28) are the industry-standard synthetic aAPC system. These beads are cultured with T cells in media that is supplemented with the cytokine interleukin-2 (IL-2) to promote polyclonal T cell expansion. Although these commercial T cell expansion beads are convenient to use, their extreme simplicity limits their ability to recapitulate many important characteristics of natural APCs, consequently resulting in suboptimal T cell expansion rates[11, 12] and subfunctional or dysfunctional downstream T cells[13, 14]. In addition, they are not amenable to the higher order presentation of more complex combinations of cues.

Recently, many promising, more complex synthetic aAPC systems have been described that overcome various limitations of the commercial T cell expansion beads, leading to faster expansion rates and more functional T cell products[11, 12, 15-20]. However, many of these systems are not easily adapted to present large numbers of different T cell cues, and have limited control over the precise density at which cues are presented, fundamentally limiting how closely these

systems can emulate natural APCs with optimal T cell-activating functionality. Here, we describe a composite material for *ex vivo* T cell expansion that overcomes these limitations and additionally mimics numerous characteristics of natural APCs that have been shown to be functionally important. The system is based on biodegradable high aspect ratio mesoporous silica micro-rods (MSRs), which have previously been shown to facilitate the controlled release of diverse soluble payloads, and to spontaneously assemble into scaffolds that can be infiltrated by cells[21, 22]. In the present work, MSRs are coated with lipid to form supported lipid bilayers (SLBs) on the MSR surfaces (MSR-SLB), which are continuous and fluid, similar to cell membranes[23-25]. Lipid formulations containing predefined amounts of an adhesive lipid can be used to attach T cell cues to the bilayer surface at precise densities.

As a proof of concept, we prepared ternary MSR-SLB formulations that were loaded with (1) soluble IL-2, and surface presented (2) either αCD3 (polyclonal stimulus) or pMHC (antigen (Ag)-specific stimulus) as a TCR stimulus, and (3) αCD28 as a costimulatory cue. In culture, the composite material assembles into a scaffold, creating a synthetic microenvironment in which activating cues are presented to infiltrating T cells similarly to how they are presented by natural APCs. Specifically, (1) TCR-activating and costimulatory cues are presented on the surface of the material in the context of a fluid lipid bilayer that is permissive for T cell membrane reorganization, an important process mediating intracellular signaling during T cell activation[4, 6], and (2) IL-2 is released from the material in a controlled manner and delivered to material-associated T cells via a pseudo-paracrine process. Our results show that these structures, referred to as APC-mimetic scaffolds (APC-ms), when presenting αCD3, facilitated at least two-fold greater polyclonal expansion of primary mouse and human T cells than commercial T cell expansion beads after a two-week culture period. APC-ms presenting pMHC facilitated rapid

antigen (Ag)-specific expansion of functional primary mouse and human T cells, and enriched for rare populations of human T cells from either T cell isolates or PBMCs. Importantly, by tuning parameters of the material, the phenotype of the resultant T cell product could be tuned. This system is flexible and can be easily adapted to present complex combinations of soluble and surface-associated T cell cues. In particular, diverse repertoires of surface-associated T cell cues can be presented to T cells at precisely defined densities. Taken together, these observations demonstrate that this system could enable the rapid generation of highly functional T cells for ACT.

4.2 Materials and Methods

4.2.1 Cells and Reagents

The B16-F10 murine melanoma cell line (ATCC) was cultured in Dulbecco's modified Eagle's medium (DMEM) supplemented with 10% heat-inactivated fetal bovine serum (FBS) (HI-FBS) and 1% penicillin-streptomycin. The B3Z murine T cell hybridoma cell line, obtained from Dr. Nilabh Shastri, was cultured in RPMI 1640 supplemented with 10% HI-FBS, 2 mM L-glutamine, 1 mM sodium pyruvate, 50 μM beta-mercaptoethanol, and 1% penicillin-streptomycin. The T2 (174 x CEM.T2) human lymphoblast cell line, obtained from Dr. Gordon Freeman, was cultured in RPMI 1640 supplemented with 10% HI-FBS, 2 mM L-glutamine, 1 mM sodium pyruvate, 50 μM beta-mercaptoethanol, 0.1 mM non-essential amino acids, 1 mM sodium pyruvate, 10 mM HEPES, and 1% penicillin-streptomycin. Primary mouse and human T cells were cultured in RPMI 1640 supplemented with 10% HI-FBS, 2 mM L-glutamine, 1 mM sodium pyruvate, 50 μM beta-mercaptoethanol, 0.1 mM non-essential amino acids, 1 mM

sodium pyruvate, 10 mM HEPES, and 1% penicillin-streptomycin, supplemented with 30 U/ml recombinant mouse- or human-IL-2, respectively.

All chemical reagents for MSR synthesis were purchased from Sigma-Aldrich. All lipids were purchased from Avanti Polar Lipids. Specific lipids used in these studies are summarized in Appendix A, Table A1. FoxP3 antibodies were purchased from eBioscience. All other antibodies were purchased from Biolegend. Murine and human recombinant IL-2 were purchased from Biolegend. Biotinylated peptide-loaded MHC monomers and fluorophore-labeled tetramers were obtained from the National Institutes of Health Tetramer Core Facility. Mouse and human CD3/CD28 T cell expansion Dynabeads were purchased from ThermoFisher Scientific. The ovalbumin-derived peptide SIINFEKL was purchased from Anaspec. The EBV-derived peptides CLGGLLTMV and GLCTLVAML were purchased from Proimmune.

4.2.2 Animals

All procedures involving animals were done in compliance with National Institutes of Health and Institutional guidelines.

4.2.3 Synthesis of Mesoporous Silica Micro-Rods (MSRs)

MSRs were synthesized as previously reported[21, 22]. Briefly, 4 g of Pluronic P123 surfactant (average Mn ~5,800, Sigma-Aldrich) was dissolved in 150 g of 1.6 M HCl solution and stirred with 8.6 g of tetraethyl orthosilicate (TEOS, 98%, Sigma-Aldrich) at 40 °C for 20 h, followed by aging at 100 °C for 24 h. Subsequently, surfactant was removed from the as-prepared particles by extraction in 1% HCl/ethanol (v/v) at 70 °C for 20 hours. Particles were recovered by running the suspension through a 0.22 μm filter, washed with ethanol, and dried.

4.2.4 Primary mouse T Cell Isolation

Animals were purchased from The Jackson Laboratory. For polyclonal T cell expansion studies, C57BL/6J mice were used as cell donors. For antigen-specific T cell expansion studies, C57BL/6-Tg(TcraTcrb)1100Mjb/J (OT-I) mice were used as cell donors. All animals were female and used between 6 and 9 weeks old at the start of the experiment. To isolate T cells, splenocytes were prepared by mashing spleens through 70 μm nylon cell strainers, and red blood cells were lysed in ACK buffer. Subsequently, either CD3+ T cells were isolated for polyclonal T cell expansion studies using a pan T cell isolation MACS kit (Miltenyi Biotec), or CD8+ T cells were isolated for antigen-specific T cell expansion studies using a CD8a+ T cell isolation MACS kit (Miltenyi Biotec).

4.2.5 Primary Human T cell Isolation

Anonymized leukoreduction collars were obtained from the Brigham and Women's Hospital Specimen Bank. PBMCs were isolated from leukoreductions in a Ficoll gradient, followed by two washes to remove platelet contaminants. Subsequently, either CD3+ T cells were isolated for polyclonal T cell expansion studies using a pan T cell isolation MACS kit (Miltenyi Biotec), or CD8+ T cells were isolated for antigen-specific T cell expansion studies using a CD8+ T cell isolation MACS kit (Miltenyi Biotec).

4.2.6 Preparation of Antigen-Presenting Cell-Mimetic Scaffolds (APC-ms)

MSRs and liposomes were prepared prior to APC-ms assembly. To prepare liposomes, lipid films composed of predefined lipid formulations were first prepared by mixing lipid-

chloroform suspensions, evaporating the bulk chloroform under nitrogen, and removing residual chloroform overnight in a vacuum chamber. For all functional studies, 1-palmitoyl-2-oleoyl-sn-glycero-3-phosphocholine (POPC) was used as the primary lipid, and lipid formulations were doped with between 0.01-1 mol% of either the carboxyfluorescein-tagged lipid 1,2-dioleoyl-sn-glycero-3-phosphoethanolamine-N-(carboxyfluorescein), or the biotinylated lipid 1,2-di-(9Z-octadecenoyl)-sn-glycero-3-phosphoethanolamine-N-(cap biotinyl). For some characterization studies, the lipids 1,2-dioleoyl-sn-glycero-3-phosphocholine (DOPC) and 1,2-distearoyl-sn-glycero-3-phosphocholine (DSPC) were alternatively used as the primary lipid. Lipid films were resuspended in PBS at 2.5 mg/ml lipid, and rehydrated by vortexing every 10 minutes for an hour. Lipid suspensions were subsequently extruded through 100 nm polycarbonate filters using a Mini-Extruder (Avanti Polar Lipids) to obtain monodisperse liposome suspensions. Liposome suspensions were stored at 4 °C and used within a week. To prepare APC-ms formulations, MSRs (10 mg/ml) were incubated with recombinant IL-2 (0.04 mg/ml) in PBS for 1 hour at room temperature. To form MSR-SLBs, liposomes were added at lipid:MSR 1:4 (w/w), and incubated for 1 hour at room temperature with intermittent gentle pipetting. Next, the material was washed twice with PBS, and then blocked for 15 minutes by resuspending the material at 2.5 mg/ml (with respect to MSRs) in 0.25% bovine serum albumin (BSA) in PBS (w/v). Streptavidin, at an amount corresponding to 36% theoretical molar saturation of the amount of biotinylated lipid in the particular formulation (assuming 35% lipid retention for POPC), was subsequently added (25 μg streptavidin per 500 μg MSRs for 1% biotinylated-lipid formulations), and the suspension was mixed by pipetting every 5 minutes for 20 minutes. Next, biotinylated T cell activating cues (1:1 molar ratio TCR-activating cue:αCD28) were added at an amount corresponding to 80% molar saturation of the added streptavidin, and the suspension was

mixed by pipetting every 10 minutes for 1 hour. Finally, the material was washed twice with PBS, and resuspended in cell culture media for *in vitro* assays. APC-ms formulations were used immediately for T cell expansion experiments, or stored at 4 °C and used within a week for characterization studies.

4.2.7 Characterization of MSR-Supported Lipid Bilayer (MSR-SLB) Structure and Stability

Brightfield and fluorescence microscopy, used to evaluate MSR lipid coating, MSR-SLB dispersibility, and MSR-SLB degradation, was performed with an EVOS FL Cell Imaging System. Confocal microscopy was performed using a Zeiss LSM 710 confocal system. To evaluate lipid retention with MSRs, MSRs were coated with lipid formulations containing 1 mol% fluorophore-tagged lipid, and lipid retention was quantified using a plate reader. To calculate percent lipid retention over time, cultured material was recovered at specified timepoints by centrifuging at 700 rcf for 5 minutes, and fluorescence intensity was normalized to the fluorescence intensity prior to culture. To evaluate MSR-SLB fluidity, fluorescence recovery after photobleaching (FRAP) experiments were carried out on MSRs coated with lipid formulations containing 1 mol% fluorophore-tagged lipid using a Zeiss LSM 710 confocal system. Photobleaching was performed on the 488 nm laser line and images were taken every 10 seconds for at least 150 seconds. Fluorescence recovery was analyzed using ImageJ by normalizing the fluorescence intensity within the photobleached region to the fluorescence intensity in an unbleached region on a different rod, at each timepoint.

To quantify IL-2 loading and release, 500 μg of MSRs were loaded with 2 μg of IL-2, and then coated with lipid as described. After washing twice with PBS, IL-2-loaded MSR-SLBs

were resuspended in 500 µl release buffer (1% BSA in PBS (w/v)) and incubated at cell culture conditions. At indicated timepoints, samples were spun down (700 rcf for 5 minutes) and the supernatants were collected. Subsequently, samples were resuspended in fresh release buffer and returned to culture. IL-2 in supernatant samples was quantified via ELISA (Biolegend).

To quantify surface cue loading, MSR-SLB samples were prepared using lipid formulations containing 0.01, 0.1, or 1 mol% biotinylated lipid. Streptavidin, at an amount corresponding to 30% theoretical saturation of the retained biotinylated lipid (assuming 35% lipid retention for POPC), was added, followed by the addition of biotinylated IgG at an amount equal to either 40% or 80% saturation of the added streptavidin. As controls, samples containing the same amount of biotinylated IgG but no material were also prepared. All samples were spun at 700 rcf for 5 minutes to pellet the material, and the amount of IgG in the supernatant fractions were quantified via ELISA (eBioscience). The biotinylated IgG stock that was used for preparing the samples was also used to prepare standard curves. The amount of IgG loaded onto the material was calculated by subtracting the amount of IgG detected in control sample supernatants from the amount of IgG detected in respective material sample supernatants.

4.2.8 In vitro T Cell Expansion Studies

Polyclonal mouse and human T cell expansion experiments were carried out using primary CD3+ T cells. Antigen-specific mouse T cell expansion experiments were carried out using CD8+ T cells isolated from OT-I mice. Antigen-specific human T cell expansion experiments were carried out using either CD8+ T cells, or PBMCS, isolated from anonymized donor blood samples. Isolated primary mouse or human T cells, or human PBMCs, were mixed with activation stimulus, and cultured for up to two weeks. In all experiments, non-tissue culture-

treated culture vessels were used. For human antigen-specific T cell expansion studies, prior to establishment of cultures, donor samples were assayed for HLA-A2 MHC I expression via FACS, and prior EBV exposure via anti-EBV VCA ELISA (IBL International) of serum. Only HLA-A2+ EBV-experienced samples were used for expansion studies.

Mock-treated samples in human antigen-specific T cell expansion experiments were cultured in media supplemented with 30 U/ml recombinant IL-2. Mock-treated samples in all other T cell expansion experiments were cultured in non-supplemented media. For commercial Dynabead conditions, Dynabeads were used according to the manufacturer-optimized protocol included with the kit. Briefly, T cells were seeded at a density of $1x10^6$ T cells/ml with pre-washed Dynabeads at a bead-to-cell ratio of 1:1, in media supplemented with 30 U/ml recombinant IL-2. For Dynabead cultures, $1x10^5$ cells were seeded in the starting culture. Cells were counted every third day and fresh IL-2-supplemented media was added to bring the cell suspension to a density of $0.5\text{-}1x10^6$ cells/ml. In general, cells were maintained below a density of $2.5x10^6$ cells/ml throughout the culture period.

For mouse polyclonal studies, APC-ms were prepared that presented surface cues (αCD3 + αCD28) on between 0.2-1 mol% of the lipids at a 1:1 molar ratio, and added into the starting culture at 333 μg/ml. For human polyclonal studies, APC-ms were prepared that presented surface cues (αCD3 + αCD28) on either 0.1 mol% or 1 mol% of the lipids at a 1:1 molar ratio, and added into the starting culture at 33 μg/ml or 333 μg/ml. For mouse antigen-specific studies, APC-ms were prepared that presented surface cues (SIINFEKL/H-2K(b) + αCD28) on either 0.01 mol% or 0.1 mol% of the lipids at a 1:1 molar ratio, and added into the starting culture at 33 μg/ml or 333 μg/ml. For human antigen-specific studies, APC-ms were prepared that presented surface cues (CLGGLLTMV/HLA-A2 or GLCTLVAML/HLA-A2 + αCD28) on 1 mol% of the

lipids at a 1:1 molar ratio, and added into the starting culture at 333 μg/ml. APC-ms presenting cues on 1 mol% of lipids, added at 333 μg/ml, corresponds to ~55 nM of TCR stimulus and αCD28 in the starting culture. For APC-ms conditions, T cells were seeded with the specified amount of material at $5x10^4$ cells/ml in media that was not supplemented with IL-2. In all APC-ms conditions, $2.5x10^4$ cells were seeded in the starting culture. Media was added throughout the culture period to maintain cells below a density of $2.5x10^6$ cells/ml. Starting on day 7, when most material-loaded IL-2 has been released, fresh media that was added was supplemented with 30 U/ml recombinant IL-2. At specified timepoints, live cells were manually enumerated with a hemocytometer using Trypan blue exclusion, to avoid possible artifacts with automated counting systems as a result of material contaminants. After enumeration, cell phenotype was evaluated using flow cytometry. Gates were set for each timepoint and sample set independently based on fluorescence minus one (FMO) controls.

4.2.9 *In vitro* T Cell Functional Studies

For co-culture experiments in which T cell expression of IFNγ and TNFα was evaluated via intracellular cytokine staining, stimulator cells (mouse, B16-F10; human, T2) were first either unpulsed or pulsed with 1 μg/ml peptide (mouse, SIINFEKL; human, CLGGLLTMV or GLCTLVAML) for 30 minutes at 37 °C. Subsequently, $1x10^5$ expanded cells were cultured with $2x10^4$ stimulator cells for one hour before adding Brefeldin A (BD Biosciences) to inhibit cytokine secretion, and then for another four hours. Cells were then stained and analyzed using FACS.

In vitro killing assays were carried out by first incubating target cells (mouse, B16-F10; human, T2) in 20 μg/ml Calcein AM (Biotium) for 30 minutes at 37 °C. Target cells were

subsequently either unpulsed or pulsed with 1 μg/ml peptide (mouse, SIINFEKL; human, CLGGLLTMV or GLCTLVAML) for 30 minutes at 37 °C. $5x10^3$ target cells were then cultured with expanded effector cells at effector cell:target cell (E:T) ratios of 0, 1, 10, 25, or 50 for four hours. Cells were then pelleted and the fluorescence intensity of supernatant samples was quantified using a plate reader. IFNγ concentrations in supernatant samples were also quantified via ELISA (Biolegend).

4.3 Results

4.3.1 Assembly and Characterization of MSR-SLBs

The process for preparing APC-ms is summarized in Fig. 4.1a, and a detailed schematic of the structure of polyclonal (left) and Ag-specific (right) APC-ms formulations, and how they interact with T cells, is shown in Fig. 4.1b. MSRs were synthesized via a previously described reaction involving the condensation of a silica precursor in the presence of the surfactant, Pluronic P123, as a structure-directing agent[26, 27]. Specifically for this work, we prepared high aspect ratio MSRs with average dimensions of 88 μm length, 4.5 μm diameter, and 10.9 nm pores as previously described[21, 22] (Fig. 4.2a). MSRs were adsorbed with IL-2, and then coated with 140 nm liposomes (Fig. 4.2b), containing predefined amounts of a headgroup-biotinylated lipid, forming MSR-SLBs. Subsequently, biotinylated cues for TCR activation (αCD3 for polyclonal T cell expansion or pMHC Ag-specific T cell expansion), and costimulation (αCD28) were attached to MSR-SLB surfaces via a streptavidin anchor. In culture, scaffolds spontaneously assembled through the settling and random stacking of MSR-SLB rods (Appendix A, Movie A1), and T cells were able to infiltrate the interparticle space of the scaffolds

(Appendix A, Movie A2). Scaffolds present TCR-activating and costimulatory cues on the surface of the lipid bilayer coating, and release soluble IL-2 over time in a paracrine fashion to infiltrating T cells, similar to how these cues are presented to T cells by natural APCs. Scaffolds assembled from the ternary MSR-SLB formulations collectively presenting the three cues (αCD3/pMHC, αCD28, IL-2), are referred to as APC-ms.

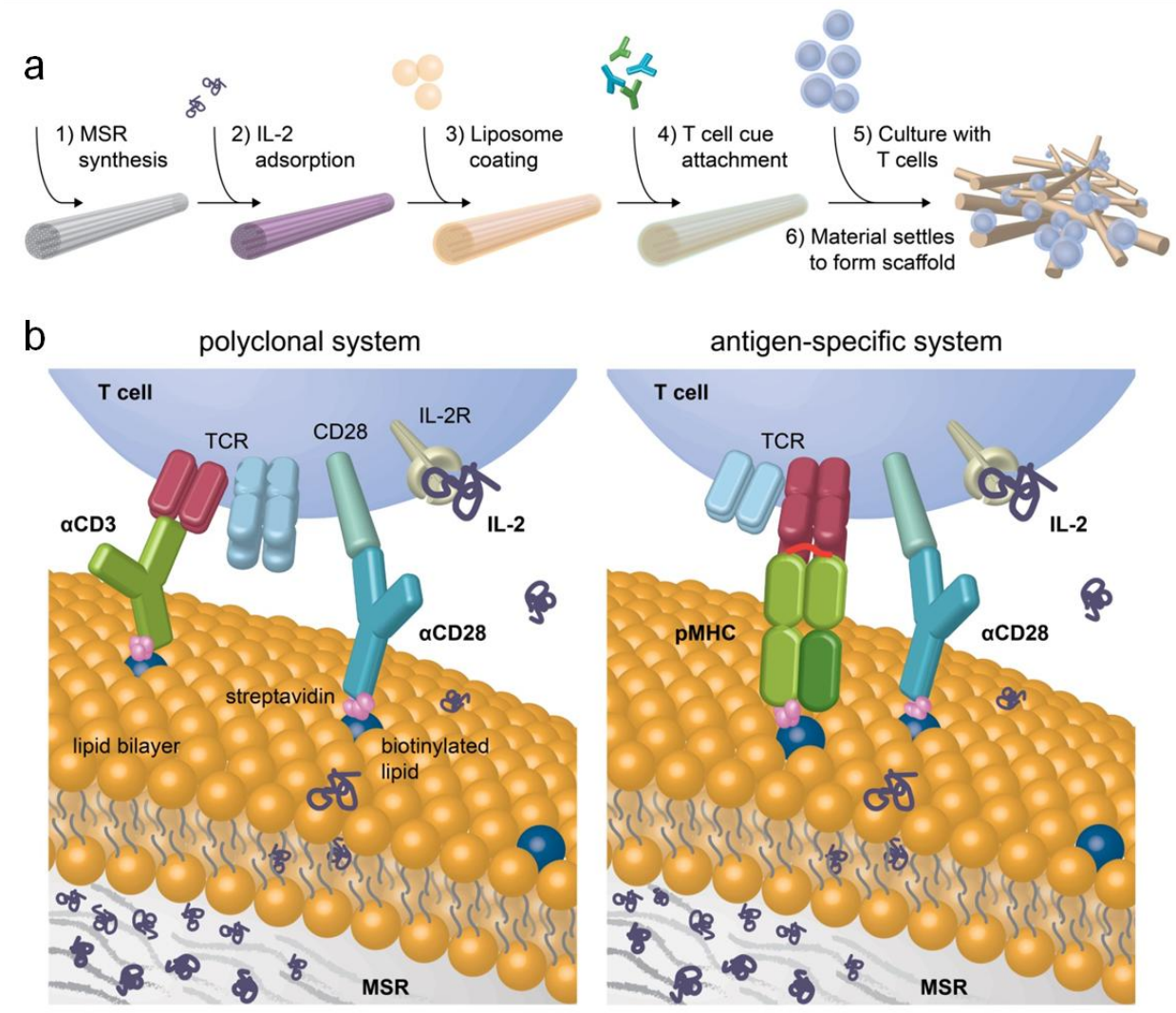

Figure 4.1. Design of antigen-presenting cell-mimetic scaffolds (APC-ms). (a) Process for preparing APC-ms. 1) Mesoporous silica micro-rods (MSRs) are synthesized. 2) MSRs are adsorbed with IL-2. 3) IL-2-adsorbed MSRs are treated with liposomes, leading to the formation of MSR-supported lipid bilayers (MSR-SLBs). 4) T cell activating cues are attached to the

surface of MSR-SLBs. 5) MSR-SLBs are cultured with T cells. 6) MSR-SLBs spontaneously settle and stack to form a scaffold that is infiltrated by T cells. MSR-SLB scaffolds loaded with IL-2 and surface-functionalized with T cell activating cues are referred to as APC-ms. (b) Structure and function of distinct APC-ms formulations. Adsorbed IL-2 is released from APC-ms over time, resulting in pseudo-paracrine delivery of IL-2 to APC-ms-interacting T cells. Incorporation of predefined amounts of a biotinylated phospholipid into liposome formulations enables the precise surface attachment of biotinylated T cell activating cues via streptavidin, mimicking the cell surface presentation of cues by natural APCs to T cells. For polyclonal T cell expansion, activating antibodies against CD3 (αCD3) and CD28 (αCD28) are attached (left). For antigen-specific T cell expansion, peptide-loaded MHC and αCD28 are attached (right).

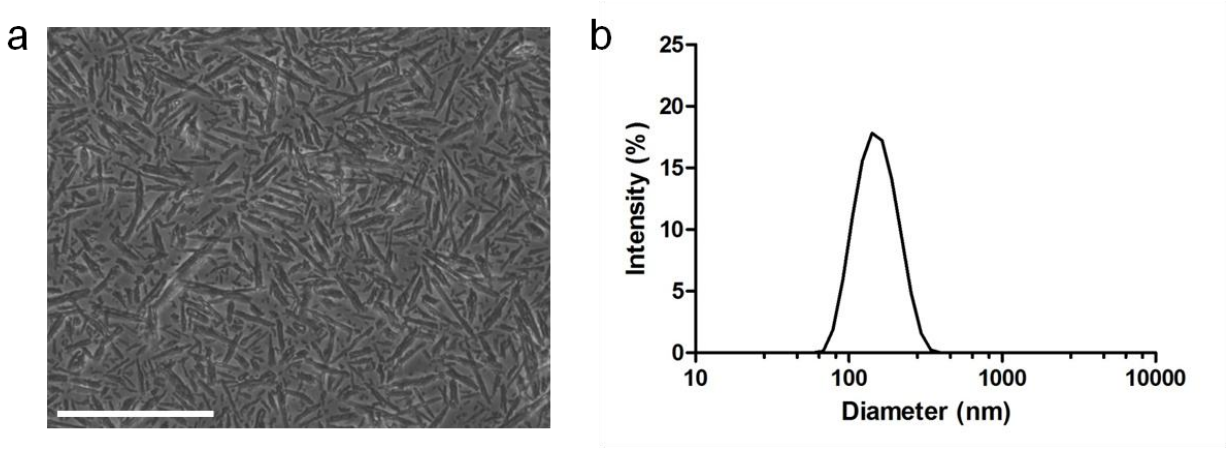

Figure 4.2. Physical characterization of components used to assembly MSR-SLBs. (a) Representative brightfield microscopy image of MSRs. Scale bar = 100 μm. (b) Size distribution of POPC liposomes as measured by DLS. Data in (b) represents mean size distribution of 3 samples.

In this work, MSRs were coated with the phospholipid 1-palmitoyl-2-oleoyl-sn-glycero-3-phosphocholine (POPC), which is commonly used as a model for mammalian cell membranes[24, 28]. POPC associated robustly with MSR surfaces, and whereas at a low lipid:MSR (1:20 w/w), lipid-mediated aggregation of MSRs was observed (Fig. 4.3), at a high lipid:MSR (1:4 w/w), MSRs could be coated with lipid and maintained in a dispersed single-particle state (Fig. 4.4a). At a lipid:MSR 1:4 (w/w), 34.1 ± 0.9% of the input POPC was retained with the

MSRs. Over a two week period at cell culture conditions, 74.2 ± 2.9% and 20.0 ± 1.5% of coated POPC was found to be retained with the MSRs in PBS and serum-containing media (cRPMI), respectively (Fig. 4.4b). Microscopy of POPC-coated MSRs maintained in cRPMI at cell culture conditions over time showed that the MSRs degraded over the culture period, consistent with previous observations[21], with fewer and smaller rods being observed at later time points (Fig. 4.4c). To demonstrate that the coating of MSRs with lipid was not specific to POPC but could be generalized to other phospholipids, MSRs were also successfully coated with 1,2-dioleoyl-sn-glycero-3-phosphocholine (DOPC) and 1,2-distearoyl-sn-glycero-3-phosphocholine (DSPC), and lipid retention and stability was similarly analyzed as for POPC. In general, a trend was observed in which more saturated phospholipids tended to be more highly retained with MSRs initially (Fig. 4.5a), likely due to tighter packing in the lipid bilayers, but no significant differences were observed in the stability of the various lipid coatings (Supplementary Fig. 4.5b-d). To evaluate whether MSR lipid coatings are continuous, fluid SLB structures, fluorescence recovery after photobleaching (FRAP) studies were carried out using MSRs coated with lipid formulations containing 1 mol% of a fluorophore-tagged lipid. Recovery of fluorescence at photobleached regions of lipid-coated MSRs and coincident normalization of fluorescence across bleached rods was observed, demonstrating that the treatment of MSRs with lipid in this way results in the formation of continuous, fluid MSR-SLBs (Fig. 4.4d).

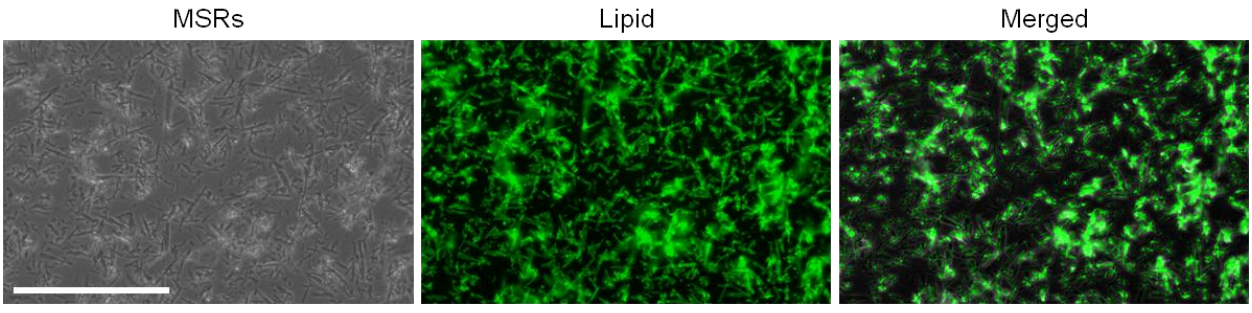

Figure 4.3. Aggregation of MSRs at low lipid:MSR. Representative microscopy images of lipid-coated MSRs (lipid:MSR 1:20 w/w) showing brightfield image of MSRs (left), fluorophore-tagged phospholipid (1 mol% of total lipid; middle), and co-localization of MSRs and lipid (right). Scale bar = 200 μm.

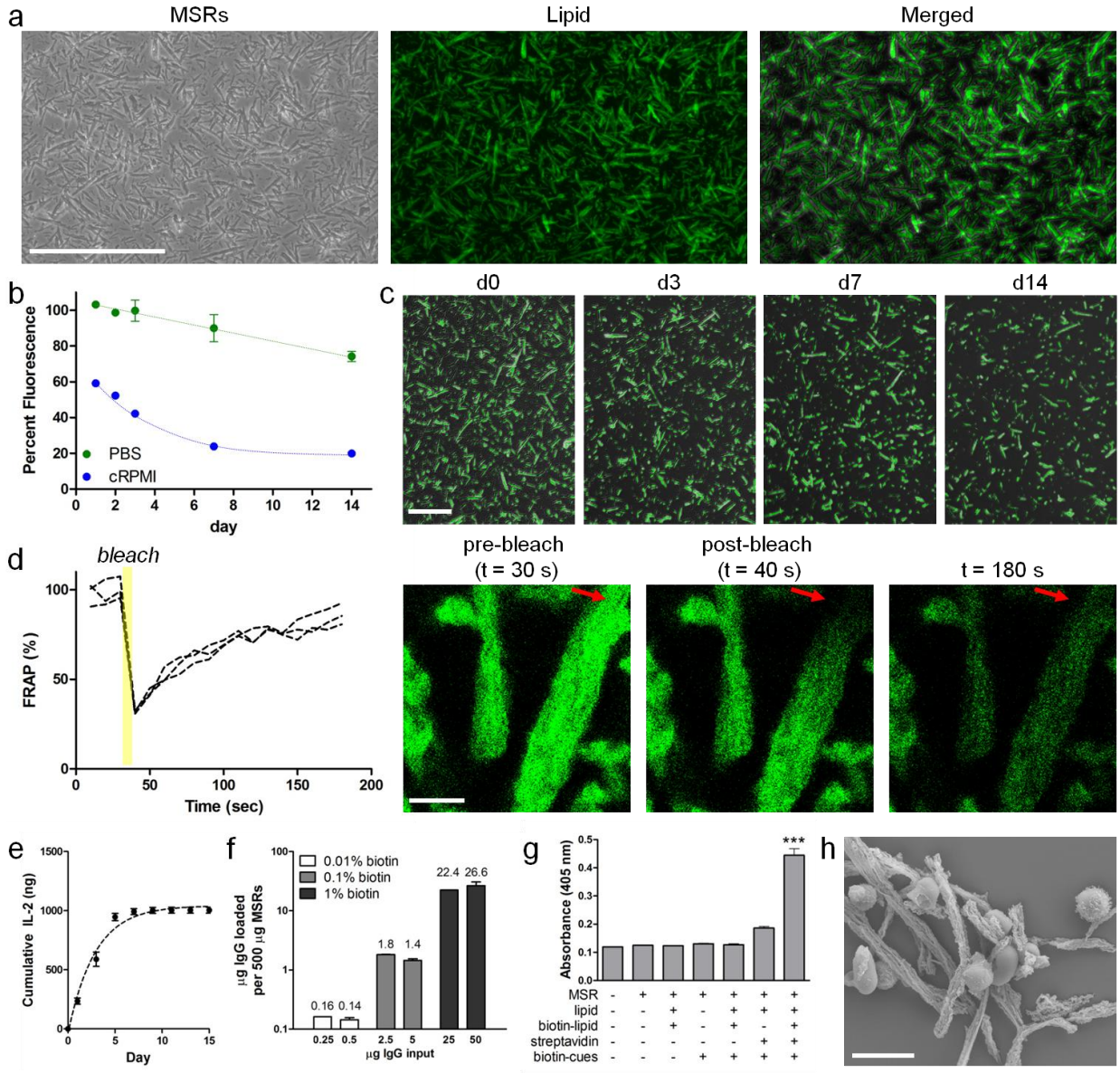

Figure 4.4. Assembly and characterization of MSR-SLBs. (a) Representative microscopy images of lipid-coated MSRs (lipid:MSR 1:4 w/w) showing brightfield image of MSRs (left), fluorophore-tagged phospholipid (1 mol% of total lipid; middle), and co-localization of MSRs and lipid (right). Scale bar = 200 μm. (b) Retention of lipid coating (containing 1 mol% fluorophore-tagged lipid) on MSRs over time in either PBS or RPMI media containing 10%

serum (cRPMI), maintained at cell culture conditions. (c) Representative overlaid fluorescence microscopy images of lipid-coated MSRs (MSRs, brightfield; lipid (1 mol% fluorophore-tagged lipid), green), maintained in cRPMI under standard cell culture conditions, over time. Scale bar = 100 μm. (d) FRAP studies showing recovery of fluorescence over time in photobleached region of MSRs coated with a lipid formulation containing 1 mol% fluorophore-tagged lipid. Quantification of FRAP for three independent MSR-SLB samples (left). Confocal fluorescence microscopy images at various timepoints from representative FRAP experiment (right). Red arrows indicate photobleached region. Scale bar = 4 μm. (e) Quantification of IL-2 released from MSR-SLBs (500 μg of MSRs) in vitro over time (data points) with one phase exponential fit (dashed line; $R^2 = 0.98$). (f) Quantification of attachment of various inputs of biotinylated IgG onto MSRs coated with lipid formulations containing 0.01 mol%, 0.1 mol%, or 1 mol% biotinylated lipid. Values above bars indicate μg of IgG attached for respective condition. (g) Quantification of β-galactosidase activity as a measure of B3Z T cell reporter line activation in response to culture with complete APC-ms, or material formulations missing one or more components. (h) SEM image showing close association of primary human T cells with APC-ms. Scale bar = 10 μm. Data in (b), (e-g) represent mean ± s.d. of at least three experimental replicates. ***$p < 0.001$, analyzed using one-way ANOVA, followed by Tukey HSD post-hoc test.

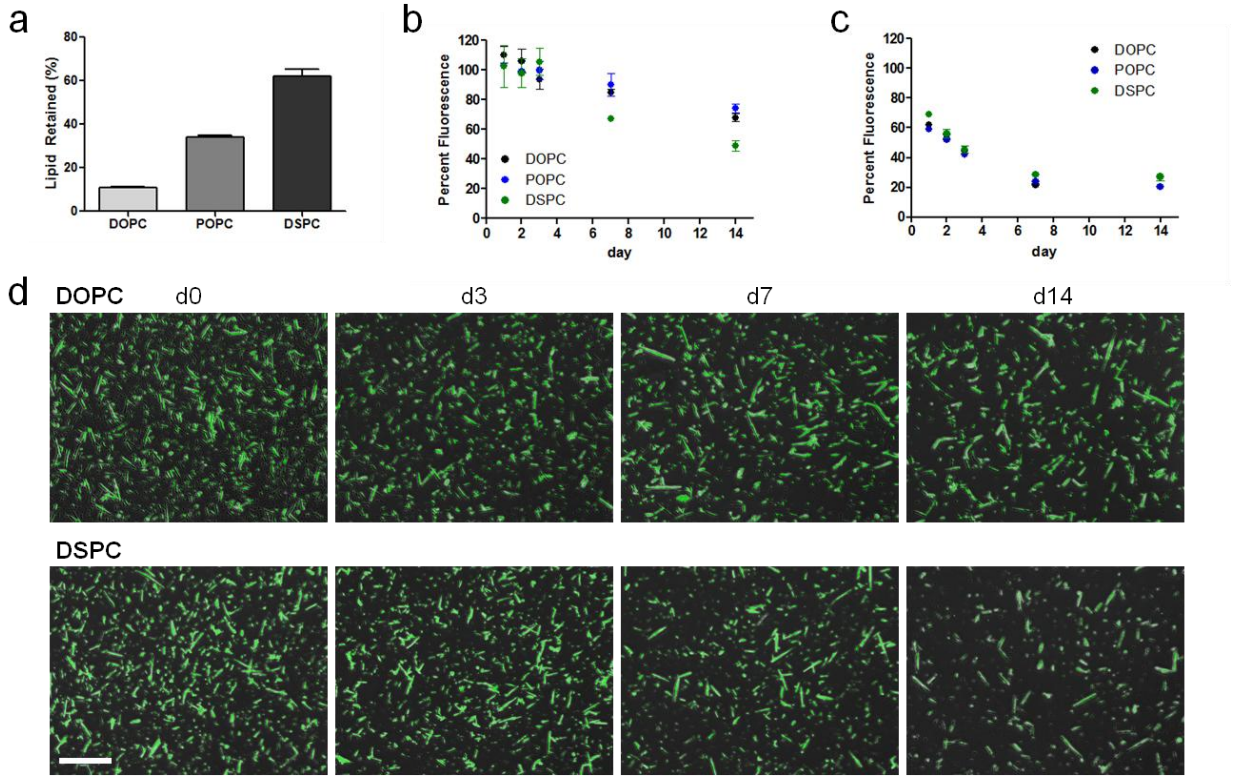

Figure 4.5. Characterization of MSR-SLBs prepared using different phospholipids. (a) Quantification of lipid retained with MSRs when MSRs are coated with various phospholipids. (b) Retention of different lipid coatings (containing 1 mol% fluorophore-tagged lipid) on MSRs over time in PBS. (c) Retention of different lipid coatings (containing 1 mol% fluorophore-tagged lipid) on MSRs over time in RPMI media containing 10% serum (cRPMI). (d) Representative overlaid fluorescence microscopy images of different lipid-coated MSRs (MSRs, brightfield; lipid (1 mol% fluorophore-tagged lipid), green), maintained in cRPMI under standard cell culture conditions, over time. Scale bar = 100 μm. Data in (a-c) represent mean ± s.d. of at least three experimental replicates.

We next characterized the loading and release of soluble cues, and the loading of surface cues, onto MSR-SLBs. First, the loading and release of soluble IL-2 was quantified. Because of their mesoporous structure, MSRs have a very high surface area available for surface adsorption of molecular payloads[21]. We found that when 500 μg of MSRs were loaded with 2 μg of IL-2 (0.04 mg/ml IL-2), 50.2 ± 1.2% of the input IL-2 was retained with the MSRs. The loaded IL-2 was subsequently observed to be released in a controlled manner over 9 days. The trend could be well approximated using a one phase exponential function ($R^2 = 0.98$), demonstrating that the release of IL-2 roughly followed first-order kinetics (Fig. 4.4e). We next quantified the attachment of cues onto the surface of the bilayer. We hypothesized that the density of surface cues could be precisely defined by the amount of the adhesive lipid species incorporated into the lipid formulation. Lipid formulations were prepared containing 0.01 mol%, 0.1 mol%, or 1 mol% biotinylated lipid, and used to prepare MSR-SLBs. The MSR-SLB formulations were treated with an amount of streptavidin equivalent to 36% of the respective amount of biotinylated lipid groups by mol. This amount of streptavidin was chosen because theoretically half of the biotinylated lipids in the SLB would be facing the MSR surface and would be inaccessible, and to avoid over-saturating the available biotinylated lipid, which would leave soluble streptavidin that could sequester the biotinylated cues. Subsequently, biotinylated IgG was added as a surface

cue proxy, and the loading of biotinylated IgG onto the various MSR-SLB formulations was quantified. At the maximal amount of IgG that could be attached, the difference in the total amount of IgG loaded onto the various MSR-SLB formulations approximately differed by a factor of 10, consistent with the difference in the percentage of biotinylated lipid incorporated into the lipid formulations (Fig. 4.4f). This demonstrates that that the density of surface cues on MSR-SLBs can be precisely controlled by defining the percentage of adhesive lipid in the coating lipid formulation. In all subsequent experiments, MSR-SLBs are saturated with surface cues as described, and relative surface cue density is described by the mol% of biotinylated lipid. TCR-activating cues and αCD28 are attached at a 1:1 molar ratio.

To further confirm that surface cues are attached to the bilayer specifically via the biotinylated lipid and streptavidin, and to demonstrate that activating cues that are attached and presented in this way remain functional, either the complete APC-ms formulation, presenting αCD3 and αCD28, or MSR-SLB formulations missing one or more components, were cultured with B3Z cells, a reporter T cell line that produces β-galactosidase upon activation. Quantification of β-galactosidase activity showed that maximal activation of the B3Z cells required the complete APC-ms formulation (Fig. 4.4g). This demonstrates that T cell activating cues attached in this way remain functional, and suggests that the biotinylated activating cues are primarily attached to the bilayer surface specifically via the biotinylated lipids and streptavidin. Lastly, to confirm that the presentation of activating cues on the scaffold surface promotes T cell interactions with the material, primary T cells were cultured either with MSR-SLBs without surface T cell activating cues, or complete APC-ms. Whereas T cells largely ignored MSR-SLBs without surface T cell activating cues, they associated robustly with APC-ms, facilitating the formation of extensive cell-material clusters (Fig. 4.6, Fig. 4.4h).

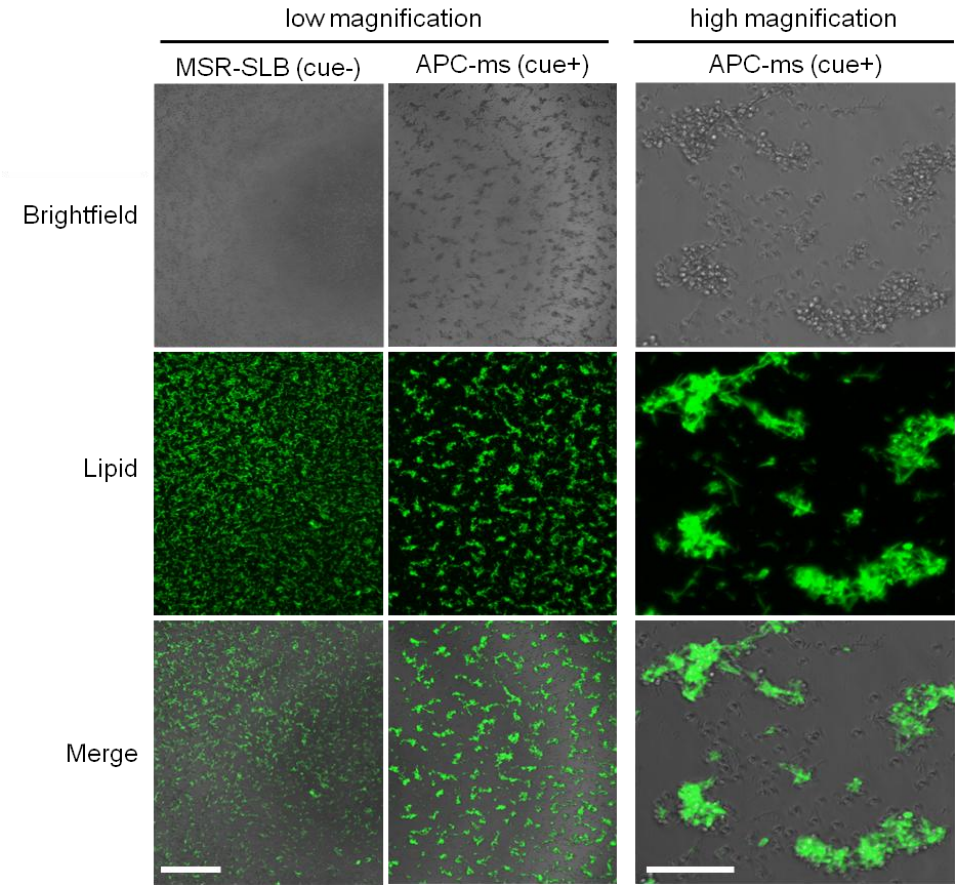

Figure 4.6. Association of T cells with APC-ms. Representative microscopy images of MSR-SLBs either not presenting any surface cues (cue-), or surface-presenting αCD3 and αCD28 (cue+), at low (left) and high (right) magnification, cultured with primary mouse T cells for one day. Cells and material are visible in brightfield images (top) and MSR-SLB lipid coatings are visible in the green channel (1 mol% fluorophore-tagged lipid; middle). Merged images are shown on the bottom. Low magnification scale bar = 500 μm, high magnification scale bar = 100 μm.

4.3.2 Polyclonal Expansion of Primary Mouse and Human T Cells

First, ternary APC-ms formulations surface presenting αCD3 and αCD28, and loaded with soluble IL-2, were compared to industry-standard commercial CD3/CD28 T cell expansion beads (Dynabeads) for polyclonal T cell expansion. We first evaluated APC-ms formulations for

the polyclonal expansion of primary mouse T cells. To establish a functional range of activating cue input with our material, primary mouse T cells were cultured for three days with APC-ms presenting αCD3 and αCD28 on between 0.2-1 mol% biotinylated lipid, and assayed for activation via Alamar Blue reduction and IFNγ production. Within this range, it was observed that APC-ms presenting αCD3 and αCD28 on 1 mol% biotinylated lipid was most functional (Fig. 4.7), and this formulation was used in subsequent mouse polyclonal expansion experiments. Next, primary mouse T cells were cultured for 13 days with either Dynabeads, according to the manufacturer-optimized protocol, or with APC-ms. T cell culture with APC-ms led to the formation of large cell-material clusters. The size and frequency of such clusters was observed to be greater in APC-ms cultures than in Dynabead cultures (Fig. 4.8a). Strikingly, culture with APC-ms promoted more rapid T cell expansion than culture with Dynabeads, MSR-SLB without surface activating cues, the cues in free form, or mock treatment, with a more than two-fold greater expansion observed with APC-ms after 13 days of culture than with Dynabeads (Fig. 4.8b). Interestingly, whereas Dynabeads promoted moderate CD8-biased skewing of the T cell population over the culture period, the particular APC-ms formulation used in these studies promoted extreme CD8-biased skewing, with greater than 95% of total T cells being CD8+ T cells by day 7, which was maintained until the end of the culture period (Fig. 4.8c). Effector CD8+ T cells expanded using APC-ms upregulated the cytotoxic mediator Granzyme B (Fig. 4.9a) more rapidly and to a greater extent over the culture period than did CD8+ T cells expanded with Dynabeads. In both Dynabead- and APC-ms-expanded T cell products, no expansion of CD4+ FoxP3+ cells was observed (Fig. 4.9b). Importantly, at the end of the 13 day culture period, despite the rapid expansion rate observed, the majority of APC-ms expanded T cells remained negative for the exhaustion marker PD-1 (Fig. 4.9c).

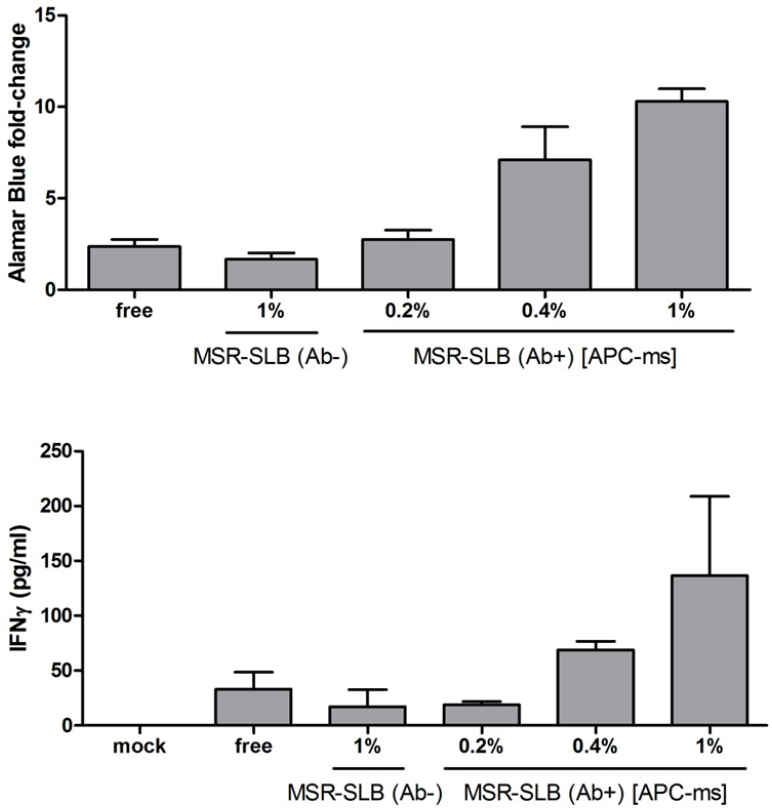

Figure 4.7. Short-term culture of primary mouse T cells with APC-ms formulations. Quantification of Alamar Blue reduction (top) and IFNγ production as measured by ELISA (bottom), by primary mouse T cells after three days of culture following either mock treatment, culture with free cues (110 nM αCD3, 110 nM αCD28, 1.3 μg/ml IL-2), or culture with APC-ms formulations presenting αCD3and αCD28 saturating between 0.2-1 mol% biotinylated lipid, input at 33 μg/ml of MSRs to initial culture. Data represent mean ± s.d. of three experimental replicates and are representative of at least two independent experiments.

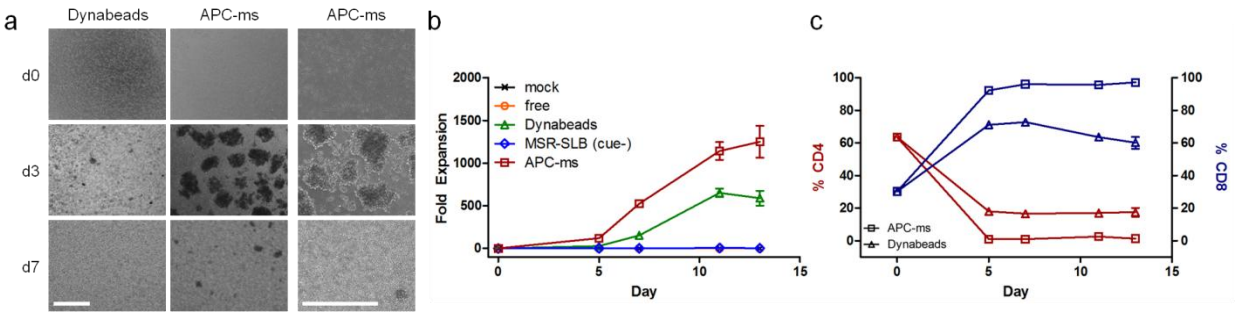

Figure 4.8. Polyclonal expansion of primary mouse T cells. (a) Representative brightfield microscopy images of primary mouse T cells cultured with Dynabeads or APC-ms, at various timepoints, at low magnification (left) or high magnification with APC-ms (right). Scale bars = 500 μm. (b) Expansion of primary mouse T cells that were either untreated (mock), or cultured with free cues (110 nM αCD3, 110 nM αCD28, 1.3 μg/ml IL-2), commercial CD3/CD28 mouse T cell expansion beads and exogenous IL-2 (Dynabeads), IL-2-loaded MSR-SLBs without T cell cues presented on the bilayer surface (MSR-SLB (cue-)), or APC-ms (loaded with αCD3, αCD28, IL-2). Curves for mock and free are indistinguishable from the MSR-SLB (cue-) curve. (c) Frequencies of CD4+ and CD8+ cells among live single cells over time in APC-ms or Dynabead cultures, measured using FACS. Data in (b-c) represent mean ± s.d. of three experimental replicates and are representative of at least two independent experiments.

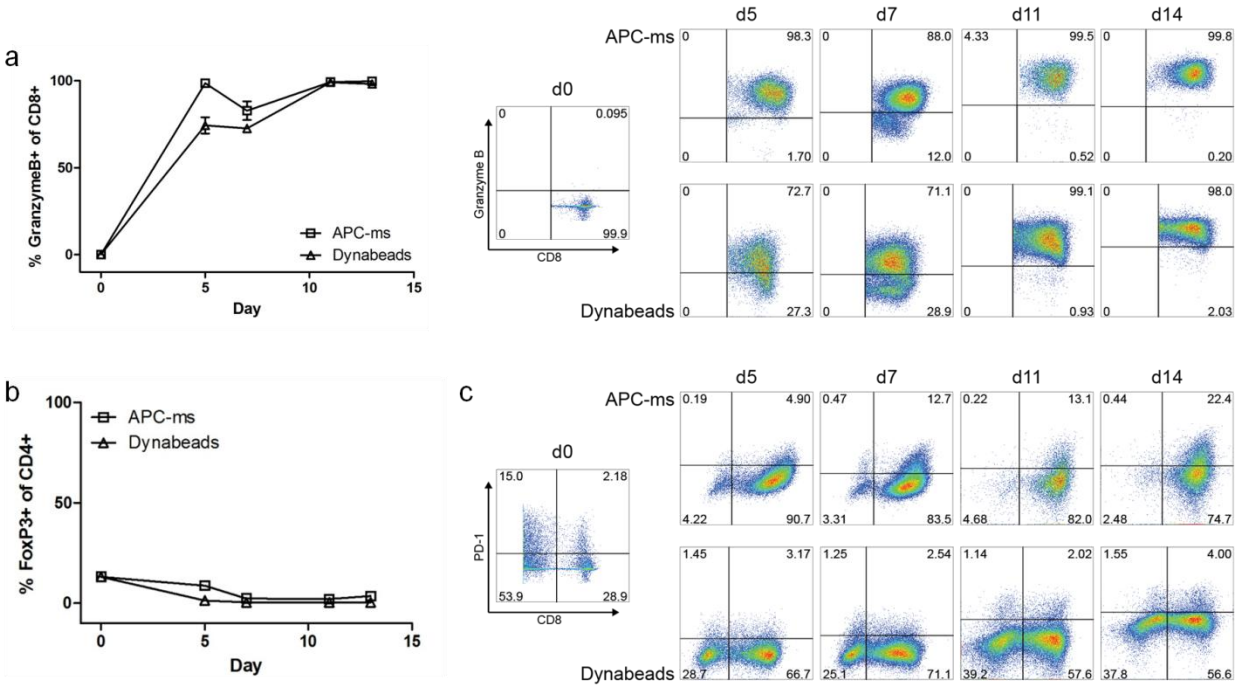

Figure 4.9. Extended phenotypic characterization of polyclonally expanded primary mouse T cells. (a) FACS quantification of Granzyme B positive cells among live single CD8+ cells, in samples expanded either with Dynabeads or with APC-ms (left), and representative FACS plots (right). (b) FACS quantification of FoxP3 positive cells among live single CD4+ cells, in samples expanded either with Dynabeads or with APC-ms. (c) Representative FACS plots showing PD-1 expression on live single cells, as a function of CD8 expression. Flow data are gated on Fluorescence Minus One (FMO) controls for each sample, at each timepoint. Data represent mean ± s.d. of three experimental replicates and are representative of at least two independent experiments.

Given that APC-ms facilitated the robust polyclonal expansion of primary mouse T cells, we next evaluated whether APC-ms could be used for efficient polyclonal primary human T cell expansion. Primary human T cells were cultured for two weeks with either Dynabeads, according to the manufacturer-optimized protocol, or with various APC-ms formulations. Similar to the polyclonal mouse studies, primary human T cell culture with APC-ms led to the formation of large cell-material clusters, with the size and frequency of such clusters being greater in APC-ms cultures than in Dynabead cultures. The stability and persistence of these clusters was observed to be dependent on both surface cue density and initial material input (Fig. 4.10a). Culture with all of the APC-ms formulations tested promoted more rapid T cell expansion than culture with Dynabeads, with between two to ten-fold greater total expansion observed with the various APC-ms formulations than with Dynabeads after 14 days of culture (Fig. 4.10b). Interestingly APC-ms conditions containing higher amounts of T cell stimulus, either due to higher surface cue density or higher initial material input, promoted extreme CD4-biased skewing after 14 days of culture. In contrast, APC-ms condition "D", which contained a lower overall amount of T cell stimulus relative to the other APC-ms conditions, promoted much more balanced CD4+ and CD8+ expansion, similar to the Dynabeads (Fig. 4.10c). Among the APC-ms formulations tested, a positive correlation was observed between total amount of T cell stimulus and the frequency of cells that co-expressed the exhaustion markers PD-1 and LAG-3, after 14 days of culture. Strikingly, despite nearly 10-fold greater expansion over a two-week culture period, similar low frequencies of PD-1 and LAG-3 co-expressing cells (<5%) was observed among cells expanded with Dynabeads and cells expanded with APC-ms formulation "D". Interestingly, a higher frequency of cells co-expressing PD-1 and LAG-3 was observed among cells expanded with Dynabeads at day 7 of culture than among cells expanded with APC-

ms formulation "D" (Fig. 4.10d). We also evaluated expression of the lymphoid homing molecules CCR7 and CD62L, which indicate a more naive T cell phenotype and have been shown to be important for function after *in vivo* transfer[29]. No significant differences were observed between Dynabead- or APC-ms-expanded cell products in the frequency of cells that co-expressed these markers (Fig. 4.10e). Taken together, these results show that APC-ms formulations presenting αCD3 and αCD28 can facilitate faster expansion of primary mouse and human T cells than industry-standard commercial Dynabeads presenting the same cues. In addition, the phenotype of the T cell product can be tuned by tuning the APC-ms formulation.

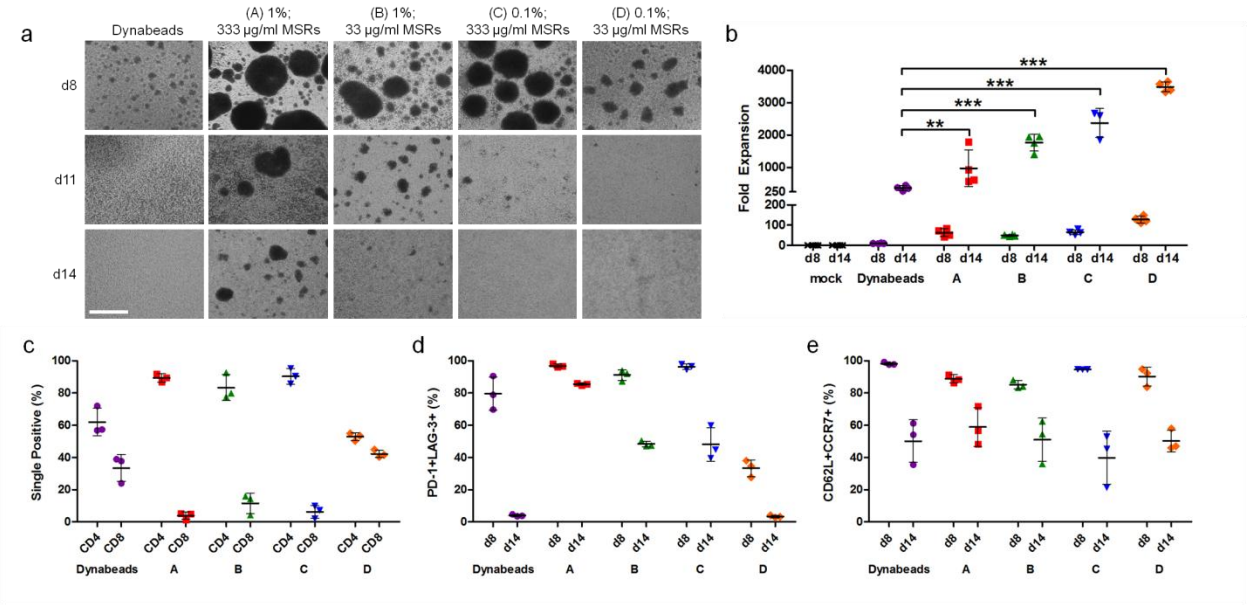

Figure 4.10. Polyclonal expansion of primary human T cells. (a) Representative brightfield microscopy images of primary human T cells cultured with Dynabeads or APC-ms formulations, at various timepoints. Scale bars = 500 μm. (A) APC-ms presenting αCD3and αCD28 saturating 1 mol% biotinylated lipid, input at 333 μg/ml of MSRs to initial culture, (B) APC-ms presenting αCD3and αCD28 saturating 1 mol% biotinylated lipid, input at 33 μg/ml of MSRs to initial culture, (C) APC-ms presenting αCD3and αCD28 saturating 0.1 mol% biotinylated lipid, input at 333 μg/ml of MSRs to initial culture, and (D) APC-ms presenting αCD3and αCD28 saturating 0.1 mol% biotinylated lipid, input at 33 μg/ml of MSRs to initial culture. (b) Expansion of primary human T cells that were either untreated (mock), or cultured with commercial CD3/CD28 human T cell expansion beads and exogenous IL-2 (Dynabeads), or with various

APC-ms formulations. (c) FACS quantification of CD4 and CD8 single positive cells among live single CD3+ cells, in samples expanded for 14 days either with Dynabeads or with various APC-ms formulations. (d) FACS quantification of cells co-expressing PD-1 and LAG-3 among live single cells, in samples expanded either with Dynabeads or with various APC-ms formulations. (e) FACS quantification of live single cells co-expressing CD62L and CCR7, in samples expanded either with Dynabeads or with APC-ms. Data in (b) represent mean ± s.d. of at least three different donor samples from two independent experiments. Data in (c-e) represent mean ± s.d. of three different donor samples and are representative of at least two independent experiments. $^{**}p < 0.01$, $^{***}p < 0.001$, (e) analyzed using two-way ANOVA, followed by Tukey HSD post-hoc test.

4.3.3 Antigen-Specific Expansion of Primary Mouse T cells

In light of the robust polyclonal expansion observed with APC-ms, we next evaluated whether the system could be adapted for Ag-specific expansion. To this end, APC-ms formulations were prepared that surface presented a specific pMHC and αCD28, and released IL-2. To evaluate the use of APC-ms for the Ag-specific expansion of primary mouse T cells, CD8+ T cells isolated from OT-I mice, which express a TCR specific for the SIINFEKL peptide in the H-2K(b) MHC I, were used as a model. Whereas minimal cell-material interactions were observed when OT-I CD8+ T cells were cultured with an APC-ms formulation presenting an irrelevant peptide (SVYDFFVWL), robust interactions resulting in the formation of extensive cell-material clusters was observed when the cells were cultured with an APC-ms formulation presenting SIINFEKL (Fig. 4.11a). Culture of OT-I CD8+ T cells with various APC-ms formulations presenting SIINFEKL/H-2K(b) promoted robust expansion, even with surface cues presented on as low as 0.01 mol% of the lipids (Fig. 4.11b). The functionality of the T cell products was evaluated in co-culture experiments with B16-F10 melanoma cells that were either unpulsed, or pulsed with SIINFEKL peptide. We observed that specifically in response to SIINFEKL presentation, the

expanded T cells secreted IFNγ (Fig. 4.11c), upregulated the co-expression of IFNγ and TNFα (Fig. 4.11d), and killed target cells *in vitro* (Fig. 4.11e).

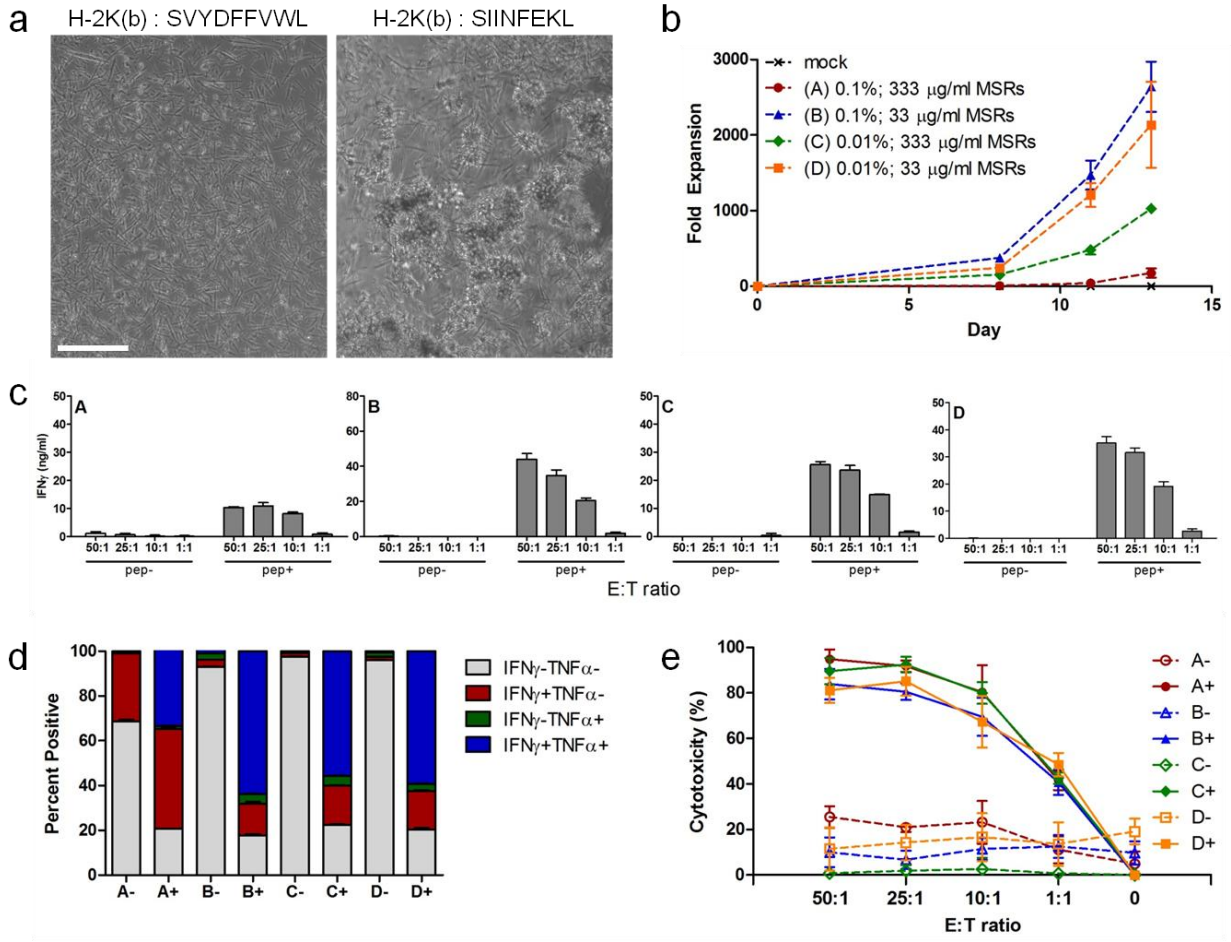

Figure 4.11. Antigen-specific expansion of primary mouse T cells. (a) Representative brightfield microscopy images of primary CD8+ OT-I T cells cultured for two days with APC-ms presenting an irrelevant peptide (SVYDFFVWL; left) or the relevant peptide (SIINFEKL; right) in H-2K(b). Scale bar = 100 μm. (b) Expansion of primary CD8+ OT-I T cells that were either untreated (mock), or cultured with various APC-ms formulations. (A) APC-ms presenting SIINFEKL/H-2K(b) and αCD28 saturating 1 mol% biotinylated lipid, input at 333 μg/ml of MSRs to initial culture, (B) APC-ms presenting SIINFEKL/H-2K(b) and αCD28 saturating 1 mol% biotinylated lipid, input at 33 μg/ml of MSRs to initial culture, (C) APC-ms presenting SIINFEKL/H-2K(b) and αCD28 saturating 0.1 mol% biotinylated lipid, input at 333 μg/ml of MSRs to initial culture, and (D) APC-ms presenting SIINFEKL/H-2K(b) and αCD28 saturating 0.1 mol% biotinylated lipid, input at 33 μg/ml of MSRs to initial culture. (c) Quantification of IFNγ secretion by CD8+ OT-I T cells expanded for 13 days with various APC-ms formulations

in response to co-culture at various effector:target cell ratios with B16-F10 cells that were either mock pulsed (pep-), or pulsed with SIINFEKL peptide (pep+). (d) FACS quantification of IFNγ and TNFα expression by live single CD8+ OT-I T cells expanded for 13 days with various APC-ms formulations and then co-cultured with B16-F10 cells that were either mock pulsed (-), or pulsed with SIINFEKL peptide (+). (e) Quantification of in vitro killing of mock-pulsed (-) or SIINFEKL-pulsed (+) B16-F10 target cells by CD8+ OT-I T cells that were expanded for 13 days with various APC-ms formulations, and then co-cultured at various effector:target cell ratios. Data in (b-e) represent mean ± s.d. of three experimental replicates and are representative of at least two independent experiments.

4.3.4 Antigen-Specific Expansion of Primary Human T Cells

In certain situations, it is desirable to specifically expand and enrich rare populations of T cells[30, 31]. Since we observed that APC-ms formulations robustly promoted the Ag-specific expansion of pure populations of mouse CD8+ T cells, we next wanted to evaluate whether the system could be used for the Ag-specific expansion and enrichment of rare populations of primary human T cells. Specifically, we used the Epstein-Barr virus (EBV) as a model system, and adapted the material to expand rare pre-existing populations of circulating EBV-specific T cells from human blood. APC-ms formulations were prepared that presented one of two peptides (abbreviated either CLG or GLC), from different EBV-derived proteins, in the HLA-A2 MHC I. Human blood samples were screened for HLA-A2 expression via FACS, and prior EBV exposure via EBV viral capsid antigen IgG ELISA (Appendix A, Fig. A1). CD8+ T cells from HLA-A2+ samples with prior EBV exposure were either mock treated with soluble IL-2 (30 U/ml) or cultured with APC-ms presenting either the CLG or GLC peptide in HLA-A2. The frequency of CD8+ T cells specific for each EBV peptide was analyzed over a two week culture period using tetramer staining. A summary of the results for two different donor samples is presented in Table 4.1. In a representative sample, whereas very minimal expansion of total cells

was observed (Fig. 4.12a), we observed robust Ag-specific enrichment and expansion of the two T cell subsets. Specifically, the frequency of CLG-specific CD8+ T cells increased from 0.04% of CD8+ T cells at day 0, to 3.3 ± 0.9% of CD8+ T cells at day 14 when cultured with CLG-presenting APC-ms (Fig. 4.13a). Similarly, the frequency of GLC-specific CD8+ T cells increased from 0.66% of CD8+ T cells at day 0, to 48 ± 9% at day 14 when cultured with GLC-presenting APC-ms (Fig. 4.13b). The absolute number of CLG-specific CD8+ T cells was observed to increase from ~$4x10^2$ in the initial culture at day 0, to ~$7x10^4$ at day 14 when cultured with CLG-presenting APC-ms, corresponding to a 170 ± 67-fold expansion (Fig. 4.13c). The number of GLC-specific CD8+ T cells was observed to increase from ~$7x10^3$ in the initial culture at day 0, to ~$2x10^6$ at day 14 when cultured with GLC-presenting APC-ms, corresponding to a 300 ± 95-fold expansion (Fig. 4.13d). The functionality of the T cell products was evaluated in co-culture experiments with T2 cells, an HLA-A2+ cell line that is deficient in the transporter associated with antigen processing (TAP) protein, resulting in no presentation of self peptides in MHC I. Prior to co-culture, T2 cells were either unpulsed, or pulsed with the CLG or GLC peptide, resulting in peptide-mediated stabilization of cell surface HLA-A2 molecules, and specific presentation of the pulsed peptide by the T2 cells. Following co-culture, T cell functionality was assayed by measuring the secretion of IFNγ (Fig. 4.12b), the frequency of cells co-expressing IFNγ and TNFα (Fig. 4.12c, Fig. 4.13e), and the *in vitro* killing of peptide-loaded target cells (Fig. 4.13f). We observed that CD8+ T cell populations expanded with CLG-presenting APC-ms responded strongly to CLG-presenting T2 cells, and that CD8+ T cell populations expanded with GLC-presenting APC-ms responded strongly to GLC-presenting T2 cells. Notably, the frequency of cells that co-expressed IFNγ and TNFα following co-culture with T2 cells presenting either CLG or GLC was similar to the frequency of CD8+ T cells found

to be specific for the respective peptide via tetramer staining, demonstrating that the majority of the expanded peptide-specific cells are functional.

Quantification of peptide target-specific cells										
sample	stimulus	peptide target	frequency (%)			number of cells			fold-expansion	
			d0	d7	d14	d0	d7	d14	d7	d14
A	mock	CLG	0.04	0.10 ± 0.03	--	420	790 ± 179	--	1.88 ± 0.43	--
	APC-ms/CLG			1.62 ± 0.39	3.25 ± 0.93		12702 ± 4399	70773 ± 28163	30.24 ± 10.5	168.51 ± 67.06
	APC-ms/GLC			0.42 ± 0.10	0.18 ± 0.05		3523 ± 175	7421 ± 1000	8.39 ± 0.42	17.67 ± 2.38
A	mock	GLC	0.66	0.74 ± 0.01	--	6600	5831 ± 511	--	0.88 ± 0.08	--
	APC-ms/CLG			0.86 ± 0.08	1.26 ± 0.07		6668 ± 1663	27776 ± 8095	1.01 ± 0.25	4.21 ± 1.23
	APC-ms/GLC			3.62 ± 0.57	47.9 ± 9.17		31512 ± 9097	2022049 ± 62747	4.77 ± 1.38	306.37 ± 95.1
B	mock	CLG	0.15	0.09 ± 0.02	--	1500	1029 ± 274	--	0.69 ± 0.18	--
	APC-ms/CLG			1.25 ± 0.07	3.51 ± 1.87		22193 ±3290	125077 ± 56734	14.80 ± 2.19	83.38 ± 37.82
	APC-ms/GLC			0.38 ± 0.08	0.26 ± 0.01		6687 ± 2242	9519 ± 1130	4.46 ± 1.49	6.35 ± 0.75
B	mock	GLC	2.89	1.57 ± 0.04	--	28900	16884 ± 1670	--	0.58 ± 0.06	--
	APC-ms/CLG			1.19 ± 0.13	0.10 ± 0.06		21117 ± 3240	36475 ± 5670	0.73 ± 0.11	1.26 ± 0.20
	APC-ms/GLC			0.77 ± 0.05	3.97 ± 0.88		13574 ± 3256	146050 ± 40963	0.47 ± 0.11	5.05 ± 1.42

Table 4.1 Summary of antigen-specific expansion of CD8+ T cell expansion from T cell isolates.

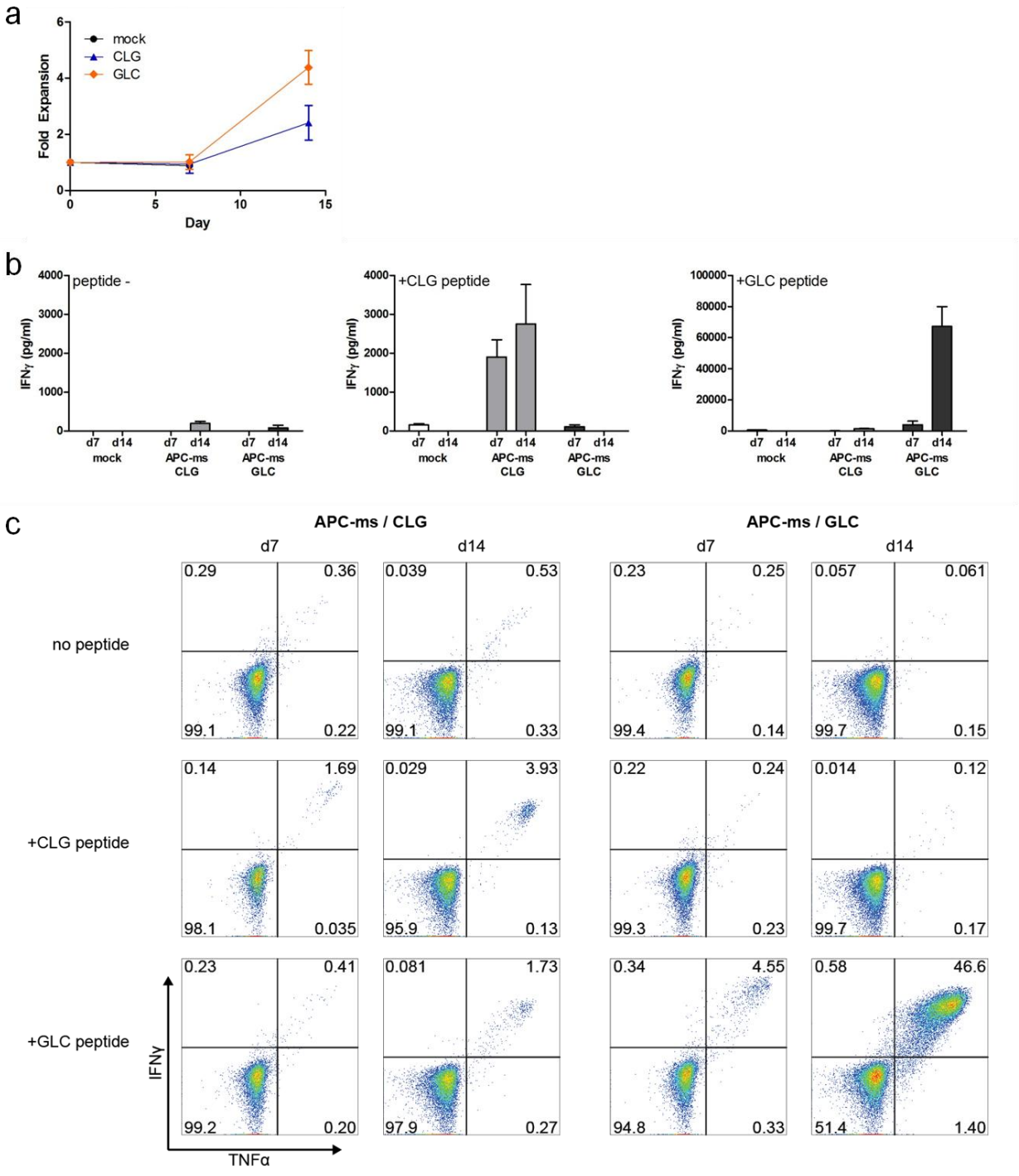

Figure 4.12. Extended characterization of primary human T cells expanded with antigen-specific APC-ms formulations. (a) Total expansion of primary human CD8+ T cell isolates that were mock treated (30 U/ml IL-2), or cultured with APC-ms (loaded with pMHC, αCD28, IL-2) either presenting the CLG or GLC peptide in HLA-A2. Data for mock-treated cells only available for days 0 and 7. (b) Quantification of IFNγ secretion of CD8+ T cell isolates that were

mock treated (30 U/ml IL-2), or cultured with APC-ms presenting either the CLG peptide (APC-ms CLG) or GLC peptide (APC-ms GLC), following co-culture with T2 cells that were either unpulsed (peptide-), pulsed with CLG peptide (+CLG peptide), or pulsed with GLC peptide (+GLC peptide). Data for mock-treated cells only available for day 7. (c) Representative FACS plots showing IFNγ and TNFα expression, of CD8+ T cell isolates that were cultured with APC-ms presenting either the CLG peptide (APC-ms / CLG) or GLC peptide (APC-ms / GLC), following co-culture with T2 cells that were either unpulsed (no peptide; top), pulsed with CLG peptide (+CLG peptide; middle), or pulsed with GLC peptide (+GLC peptide; bottom). Data in (a-b) represent mean ± s.d. of three experimental replicates and are representative of two experiments with two different donor samples.

All prior experiments up to this point were performed on T cell isolates. However, from a cell manufacturing perspective, it would be significantly more efficient if T cells could be expanded directly from complex mixtures of cells, such as PBMCs. To explore this possibility in a challenging scenario, we lastly evaluated whether APC-ms could be used to expand and enrich rare populations of human CD8+ T cells directly from PBMCs. PBMC samples from HLA-A2+ donors with prior EBV exposure were cultured with a GLC-presenting APC-ms formulation. A summary of the results for two different donor samples is presented in Table 4.2. In a representative sample, whereas we observed minimal changes in the frequency of GLC-specific CD8+ T cells in mock-treated samples, we observed a marked increase in the frequency of these cells in samples treated with GLC-presenting APC-ms from 0.66% at day 0, to 15 ± 1% at day 7 (Fig. 4.13g). In the initially seeded PBMC population, this is equivalent to ~$5x10^2$ GLC-specific CD8+ T cells at day 0, and ~$3x10^4$ at day 7, which corresponds to a 60 ± 9-fold expansion after only 7 days in culture (Fig. 4.13h). Notably, this corresponds to a more than 4-fold greater enrichment, and 12-fold greater absolute fold-expansion of GLC-specific cells, than when cells were expanded from T cell isolates over the same culture period. Finally, T cell functionality was evaluated by co-culturing the expanded cell products with T2 cells that were either unpulsed, or

pulsed with the CLG or GLC peptide. Through quantification of the frequency of cells co-expressing TNFα and IFNγ (Fig. 4.13i), and IFNγ secretion (Fig. 4.13j), we observed that cell populations that were expanded with GLC-presenting APC-ms responded robustly only to co-culture with GLC-pulsed T2 cells. Taken together, these data demonstrate that APC-ms can be used to promote robust Ag-specific expansion of rare populations of primary human CD8+ T cells from either T cell isolates or PBMCs.

Quantification of peptide target-specific cells							
sample	stimulus	peptide target	frequency (%)		number of cells		fold-expansion
			d0	d7	d0	d7	d7
A	mock	GLC	0.66	0.71 ± 0.15	455	801 ± 214	1.76 ± 0.47
	APC-ms/GLC			15.17 ± 1.26		27376 ± 3920	60.11 ± 8.61
B	mock	GLC	2.89	0.73 ± 0.11	2977	2393 ± 432	0.80 ± 0.15
	APC-ms/GLC			9.36 ± 2.81		33002 ±6422	11.09 ± 2.16

Table 4.2 Summary of antigen-specific expansion of CD8+ T cell expansion from PBMCs.

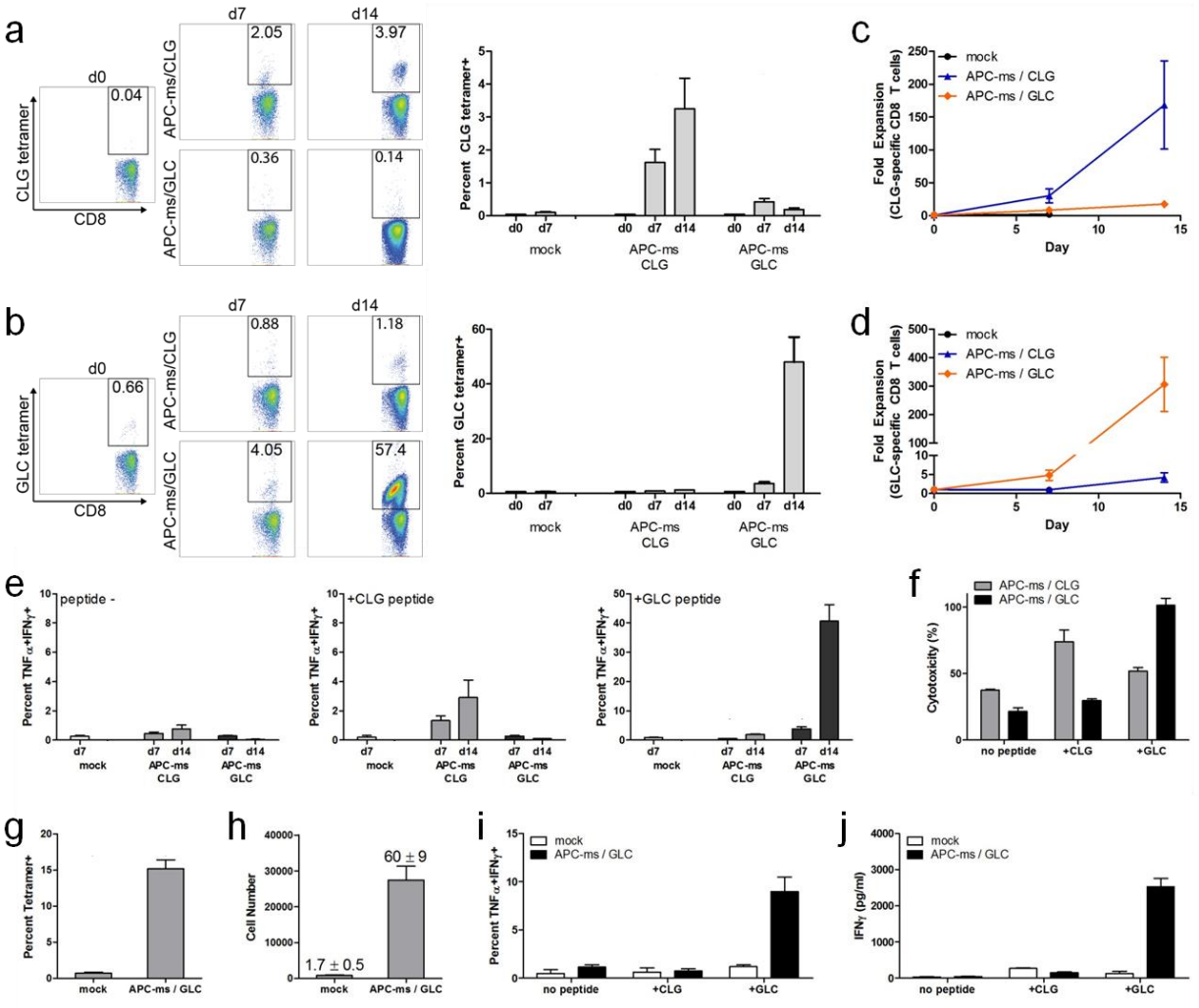

Figure 4.13. Antigen-specific expansion of primary human T cells. (a-f) Antigen-specific expansion of primary human T cells from CD8+ T cell isolates. (a-b) Tetramer analysis of live CD8+ single cells specific for the EBV-derived peptides CLGGLLTMV (CLG; a) and GLCTLVAML (GLC; b). Representative FACS plots with numbers in gates denoting the percent of live single CD8+ cells that are positive for the respective tetramer (left), and quantification of FACS data at various timepoints (right), of primary HLA-A2+ human CD8+ T cells that were mock treated (30 U/ml IL-2), or cultured with APC-ms (loaded with pMHC, αCD28, IL-2) presenting either the CLG or GLC peptide in HLA-A2. Data for mock-treated cells only available for days 0 and 7. (c-d) Expansion of primary human CD8+ T cells specific for CLG (c) or GLC (d) that were either mock treated, or cultured with APC-ms presenting either the CLG or GLC peptide in HLA-A2. Data for mock-treated cells only available for days 0 and 7. (e) Frequencies of TNFα+IFNγ+ cells among live single CD8+ T cells that were mock treated, or cultured with APC-ms presenting either the CLG or GLC peptide in HLA-A2, following co-culture with T2 cells that were either unpulsed (peptide-; left), pulsed with CLG peptide (+CLG

peptide; middle), or pulsed with GLC peptide (+GLC peptide; right). Data for mock-treated cells only available for day 7. (f) Quantification of in vitro killing of T2 target cells that were mock-pulsed (no peptide), or pulsed with either the CLG peptide (+CLG) or GLC peptide (+GLC), by primary human CD8+ T cells expanded for 14 days with APC-ms presenting either the CLG or GLC peptide in HLA-A2. (g-j) Antigen-specific expansion of primary human T cells from PBMCs. (g) Frequency of GLC-specific cells among live single CD8+ T cells, within PBMCs cultured for 7 days in 30 U/ml IL-2 (mock), or with APC-ms presenting the GLC peptide in HLA-A2. (h) Number of GLC-specific CD8+ T cells within PBMCs cultured for 7 days in 30 U/ml IL-2 (mock), or with APC-ms presenting the GLC peptide in HLA-A2. Numbers above bars denote fold expansion (mean ± s.d.). (i-j) Frequency of TNFα+IFNγ+ cells among live single CD8+ T cells (i), and IFNγ secretion (j), from PBMCs that were cultured for 7 days in 30 U/ml IL-2 (mock), or with APC-ms presenting the GLC peptide in HLA-A2, following co-culture with T2 cells that were either unpulsed (no peptide), pulsed with CLG peptide (+CLG), or pulsed with GLC peptide (+GLC). All data represent mean ± s.d. of three experimental replicates and are representative of two experiments with two different donor samples.

4.4 Discussion

We developed a material that can be used for the rapid *ex vivo* polyclonal and Ag-specific expansion of functional mouse and human T cells. The material is comprised of fluid lipid bilayers supported on porous silica micro-rod cores. Soluble T cell cytokines can be adsorbed to the porous silica core and released over time in a controlled manner, while endogenously cell surface-localized T cell activating cues can be attached to, and presented on the lipid bilayer surface, mimicking how these cues are naturally presented to T cells by real APCs. In culture, the composite material spontaneously assembles into a scaffold that can be infiltrated by T cells, and acts as a synthetic microenvironment supporting robust T cell activation and expansion. Here, we refer to ternary formulations of the material that surface-present a TCR-activating cue (αCD3; polyclonal stimulus, or pMHC; Ag-specific stimulus) in combination with a costimulatory cue (αCD28), and that release soluble IL-2, as APC-mimetic scaffolds (APC-ms). Using APC-ms formulations that surface-present αCD3, at least two-fold greater polyclonal

expansion of primary mouse and human T cells was observed over a two week culture period than with industry-standard commercial T cell expansion beads presenting the same surface cues, and used according to the manufacturer-optimized protocol. Using APC-ms formulations that surface-present pMHC, robust Ag-specific expansion of functional primary mouse T cells, and Ag-specific enrichment and expansion of rare populations of primary human T cells, was observed. APC-ms formulations were additionally shown to be highly functional when used with both T cell isolates, or more complex cell mixtures, such as PBMCs.

In the polyclonal mouse T cell expansion studies, the particular APC-ms formulation we used promoted extreme CD8-biased skewing of the T cell population relative to Dynabeads. In the human polyclonal studies, APC-ms conditions containing higher amounts of T cell stimulus promoted extreme CD4-biased skewing, whereas the APC-ms condition containing a relatively lower overall amount of T cell stimulus promoted more balanced CD4+ and CD8+ T cell expansion. Importantly, if the mechanism(s) that contribute(s) to defining the CD4:CD8 ratio can be understood, it could be possible to tune the parameters of the material in order to define the CD4:CD8 ratio of the output T cell product, which affects the function of the product. Indeed, it has recently been shown that CAR T cell products prepared in a defined 1:1 CD4:CD8 ratio outperformed undefined products[32]. Although it is unclear what the exact mechanism underlying the CD4/CD8 bias is, the local concentration of IL-2 sensed by the T cells early on in culture, which can differentially regulate processes in CD4 and CD8 T cells[33], may play a role. In these studies, T cells in Dynabead cultures, which contain exogenously supplemented IL-2 in the bulk media, will be exposed to a different local IL-2 concentration than T cells in APC-ms cultures, in which IL-2 is released by the material[16]. Differences in the initial input of APC-ms material will also lead to differences in the local IL-2 concentration. An alternative, or potentially,

complementary process that may also contribute to the differential skewing observed in Dynabead versus APC-ms cultures, could be related to differences in how the αCD3 stimulus is perceived by the T cell. Whereas with Dynabeads, αCD3 is attached to the stiff surface of a solid microbead that is smaller than the T cell itself, on APC-ms, αCD3 is attached to a fluid lipid bilayer coating a particle that is significantly larger than the T cell. CD4 and CD8 T cells may respond differently to a TCR stimulus that is preclustered on a small solid bead than to a stimulus that is presented in a fluid structure permissive for reorganization[4, 6]. In addition, previous work supports a model in which native pMHC binds the TCR in an orthogonal orientation, and TCR signaling requires an extracellular torque that is generated from lateral movement of the TCR relative to the TCR-activating cue, for example due to movement of a T cell relative to an APC[34]. There will be differences in the torque sensed by T cells when they are interacting with small beads that they can readily displace, as versus significantly larger particles, and it is possible that this could result in differential activation of T cells.

A powerful aspect of this system is its degradability. In this work we observed that the composite material degrades over the culture period, and the degradation profile of the material is likely to be primarily defined by the degradation profile of the MSR core. Future work will go towards a more rigorous characterization of MSR degradation under cell culture conditions, and exploration of ways in which the MSR synthesis protocol can be modified to tune the degradation kinetics of the material. Of note, the MSRs used in this work are composed of amorphous silica, which is known to be biodegradable[35], and is generally recognized as safe by the US Food and Drug Administration. From a manufacturing perspective, the degradability of the material may allow for the elimination of a purification step in which the material must be removed from the cell product, making the process more time- and cost-efficient. In addition, in

clinical ACT protocols that employ Dynabeads for T cell expansion, residual Dynabead contamination in the cell product, even after several purifications, is frequently observed[36]. In contrast, if the activating material spontaneously degrades during culture, concerns related to cell product contamination with residual functional material, which could lead to inflammatory toxicities following transfer, could be avoided. In addition to these practical benefits, the degradability of the material also affords the potential to tune the temporal profile of activating cue presentation, by tuning the kinetics of material degradation. This is important as the duration of activating cue presentation to T cells has been shown to affect their downstream phenotype and functionality, in particular, with chronic or repeated stimulation of T cells resulting in exhaustion or dysfunction[37, 38]. The degradation profile of APC-ms can be potentially tuned by changing the degradation kinetics of the MSRs[35], or by changing the lipid formulation used to prepare the SLB[39]. Overall, this system could enable precise control over not only the spatial, but also the temporal profile of T cell activating cue presentation.

Fundamentally, the composite MSR-SLB system is a flexible drug delivery device that can be adapted to release soluble cues in a controlled manner, and present surface-immobilized cues locally in the context of a fluid lipid bilayer. By defining the amount of adhesive lipid in the lipid formulation and the relative amounts of activating cues added, the surface-immobilized cues can be attached at a specific density, and complex mixtures of cues can be presented at a specific relative ratio. Importantly, in this work, with only two different surface cues per APC-ms formulation, we observed robust T cell activation with the cues attached to between 0.01-1 mol% biotinylated lipid. Based on this observation, it is possible to increase the number of different surface cues significantly without compromising the density of other cues, or reaching saturation on the bilayer surface. In this proof of concept work, we limited the parameter space

and described only simple ternary APC-ms formulations that released a single soluble cue (IL-2), and surface-presented a single TCR-activating cue (αCD3 or pMHC) in combination with a single costimulatory cue (αCD28) maintained at a 1:1 molar ratio. Maintaining this set of cues, we explored the effect of changing the density of surface cues and the initial input of material and observed that these parameters affected not only the expansion rate, but also the phenotype of the resultant T cells, which relates to their function. Given the flexibility of APC-ms to be adapted to present complex repertoires of cues with a high degree of spatiotemporal precision, this system represents a powerful tool that could enable the establishment of better optimized T cell products for ACT. As an example, many studies using cellular aAPCs have demonstrated that different cell surface costimulatory and adhesion molecules often have dramatic, nonredundant effects on the phenotype and function of the resultant T cell product[10]. These studies can be used as a foundation to inform the design of more complex APC-ms formulations presenting a larger variety of cues. The APC-ms platform, which, unlike the establishment of cell lines, is amenable to rapid iteration, could in turn be used to further optimize the repertoire of presented cues as well as the spatiotemporal pattern at which these cues are presented.

We envision that future iterations of this system will enable more precise tuning of T cell activating cue presentation. In particular, changing the aspect ratio, pore size, or surface properties of the MSRs could enable tuning of the structure of the scaffold microenvironment, and the degradation profile of the material. Using more complex lipid mixtures could allow for the preparation of bilayers that more closely mimic natural APC plasma membranes, and could enable tuning of SLB stability[39], which would affect the temporal profile of surface cue presentation, or SLB fluidity[40], which would affect the amount of force T cells would need to generate to reorganize the membrane. The spatial precision with which surface cues are

presented could be further improved by using lipid formulations composed of species with limited miscibility, resulting in lipid partitioning and microdomain formation[41-43]. Alternatively, it could be possible to directly translate native APC membranes onto MSR surfaces, as has been shown to be feasible for membranes from various cell types with diverse materials[44-46]. Lastly, in this work, we attached surface cues via biotin-streptavidin interactions. However, we could easily adapt the system for surface cue attachment via covalent modification[47-49], or through alternative forms of affinity pairing such as poly-histidine-tagged proteins onto chelator lipids[24], Fc-fusion proteins onto lipid-immobilized Fc capture Abs. Alternatively native transmembrane proteins could be directly inserted into the lipid bilayer[50]. Overall, this system represents a versatile platform technology that, when appropriately optimized, could enable the generation of highly functional T cell products for diverse ACT applications.

4.5 Acknowledgements

David Zhang and Sandeep Koshy helped perform some of the experiments in this work. This work was supported by the National Institutes of Health (NIH) (1R01EB015498) and the Wyss Institute for Biologically Inspired Engineering at Harvard University. This work was performed in part at the Center for Nanoscale Systems (CNS), a member of the National Nanotechnology Coordinated Infrastructure Network (NNCI), which is supported by the National Science Foundation under NSF award no. 1541959. CNS is part of Harvard University. We thank the National Institutes of Health (NIH) Tetramer Core Facility for the SIINFEKL/H-2K(b) biotinylated monomer, Alexa Fluor 647-labeled SIINFEKL/H-2K(b) tetramer, CLGGLLTMV/HLA-A*02:01 biotinylated monomer, Alexa Fluor 647-labeled

CLGGLLTMV/HLA-A*02:01 tetramer, GLCTLVAML/HLA-A*02:01 biotinylated monomer, and Alexa Fluor 647-labeled GLCTLVAML/HLA-A*02:01 tetramer, Dr. Nilabh Shastri for the B3Z cell line, and Dr. Gordon Freeman for the T2 cell line. We also thank Dr. Caterina Stamoulis from Boston Children's Hospital and the Harvard Catalyst for her help with statistical analysis; Harvard Catalyst is supported, in part, by the NIH (UL1 TR001102). Lastly, we thank Dr. Jerome Ritz, Dr. Marcela Maus, and Weiwei Aileen Li for valuable scientific discussions.

4.6 References

1. Rosenberg, S.A. & Restifo, N.P. Adoptive cell transfer as personalized immunotherapy for human cancer. *Science* **348**, 62-68 (2015).
2. June, C.H., Riddell, S.R. & Schumacher, T.N. Adoptive cellular therapy: A race to the finish line. *Science translational medicine* **7**, 280ps287-280ps287 (2015).
3. Fesnak, A.D., June, C.H. & Levine, B.L. Engineered T cells: the promise and challenges of cancer immunotherapy. *Nature Reviews Cancer* **16**, 566-581 (2016).
4. Huppa, J.B. & Davis, M.M. T-cell-antigen recognition and the immunological synapse. *Nature Reviews Immunology* **3**, 973-983 (2003).
5. Schamel, W.W., Risueño, R.M., Minguet, S., Ortíz, A.R. & Alarcón, B. A conformation- and avidity-based proofreading mechanism for the TCR–CD3 complex. *Trends in immunology* **27**, 176-182 (2006).
6. Minguet, S., Swamy, M., Alarcón, B., Luescher, I.F. & Schamel, W.W. Full activation of the T cell receptor requires both clustering and conformational changes at CD3. *Immunity* **26**, 43-54 (2007).
7. Eggermont, L.J., Paulis, L.E., Tel, J. & Figdor, C.G. Towards efficient cancer immunotherapy: advances in developing artificial antigen-presenting cells. *Trends in biotechnology* **32**, 456-465 (2014).
8. Cheung, A.S. & Mooney, D.J. Engineered materials for cancer immunotherapy. *Nano today* **10**, 511-531 (2015).
9. Zeng, W., Su, M., Anderson, K.S. & Sasada, T. Artificial antigen-presenting cells expressing CD80, CD70, and 4-1BB ligand efficiently expand functional T cells specific to tumor-associated antigens. *Immunobiology* **219**, 583-592 (2014).

10. Hasan, A., Selvakumar, A. & O'Reilly, R. Artificial Antigen Presenting Cells: An Off the Shelf Approach for Generation of Desirable T-Cell Populations for Broad Application of Adoptive Immunotherapy. *Advancements in Genetic Engineering* **2015** (2015).

11. Zappasodi, R. et al. The effect of artificial antigen-presenting cells with preclustered anti-CD28/-CD3/-LFA-1 monoclonal antibodies on the induction of ex vivo expansion of functional human antitumor T cells. *haematologica* **93**, 1523-1534 (2008).

12. Fadel, T.R. et al. A carbon nanotube–polymer composite for T-cell therapy. *Nature nanotechnology* **9**, 639-647 (2014).

13. Li, Y. & Kurlander, R.J. Comparison of anti-CD3 and anti-CD28-coated beads with soluble anti-CD3 for expanding human T cells: differing impact on CD8 T cell phenotype and responsiveness to restimulation. *Journal of translational medicine* **8**, 1 (2010).

14. Jin, C. et al. Allogeneic lymphocyte-licensed DCs expand T cells with improved antitumor activity and resistance to oxidative stress and immunosuppressive factors. *Molecular Therapy—Methods & Clinical Development* **1** (2014).

15. Maus, M.V. et al. Ex vivo expansion of polyclonal and antigen-specific cytotoxic T lymphocytes by artificial APCs expressing ligands for the T-cell receptor, CD28 and 4-1BB. *Nature biotechnology* **20**, 143-148 (2002).

16. Steenblock, E.R. & Fahmy, T.M. A comprehensive platform for ex vivo T-cell expansion based on biodegradable polymeric artificial antigen-presenting cells. *Molecular Therapy* **16**, 765-772 (2008).

17. Mandal, S. et al. Polymer-Based Synthetic Dendritic Cells for Tailoring Robust and Multifunctional T Cell Responses. *ACS chemical biology* **10**, 485-492 (2014).

18. Sunshine, J.C., Perica, K., Schneck, J.P. & Green, J.J. Particle shape dependence of CD8+ T cell activation by artificial antigen presenting cells. *Biomaterials* **35**, 269-277 (2014).

19. Perica, K. et al. Enrichment and expansion with nanoscale artificial antigen presenting cells for adoptive immunotherapy. *ACS nano* **9**, 6861-6871 (2015).

20. Fadel, T.R. et al. Enhanced cellular activation with single walled carbon nanotube bundles presenting antibody stimuli. *Nano letters* **8**, 2070-2076 (2008).

21. Kim, J. et al. Injectable, spontaneously assembling, inorganic scaffolds modulate immune cells in vivo and increase vaccine efficacy. *Nature biotechnology* **33**, 64-72 (2015).

22. Li, W.A. et al. The effect of surface modification of mesoporous silica micro-rod scaffold on immune cell activation and infiltration. *Biomaterials* **83**, 249-256 (2016).

23. Thid, D. et al. Supported phospholipid bilayers as a platform for neural progenitor cell culture. *Journal of Biomedical Materials Research Part A* **84**, 940-953 (2008).

24. Torres, A.J., Contento, R.L., Gordo, S., Wucherpfennig, K.W. & Love, J.C. Functional single-cell analysis of T-cell activation by supported lipid bilayer-tethered ligands on arrays of nanowells. *Lab on a Chip* **13**, 90-99 (2013).

25. Worsfold, O., Voelcker, N.H. & Nishiya, T. Biosensing using lipid bilayers suspended on porous silicon. *Langmuir* **22**, 7078-7083 (2006).

26. Zhao, D., Huo, Q., Feng, J., Chmelka, B.F. & Stucky, G.D. Nonionic triblock and star diblock copolymer and oligomeric surfactant syntheses of highly ordered, hydrothermally stable, mesoporous silica structures. *Journal of the American Chemical Society* **120**, 6024-6036 (1998).

27. Schmidt-Winkel, P., Yang, P., Margolese, D.I., Chmelka, B.F. & Stucky, G.D. Fluoride-induced hierarchical ordering of mesoporous silica in aqueous acid-syntheses. *Advanced Materials* **11**, 303-307 (1999).

28. Jerabek, H.r., Pabst, G., Rappolt, M. & Stockner, T. Membrane-mediated effect on ion channels induced by the anesthetic drug ketamine. *Journal of the American Chemical Society* **132**, 7990-7997 (2010).

29. Gattinoni, L. et al. Acquisition of full effector function in vitro paradoxically impairs the in vivo antitumor efficacy of adoptively transferred CD8+ T cells. *The Journal of clinical investigation* **115**, 1616-1626 (2005).

30. Mazzarella, T. et al. Ex vivo enrichment of circulating anti-tumor T cells from both cutaneous and ocular melanoma patients: clinical implications for adoptive cell transfer therapy. *Cancer Immunology, Immunotherapy* **61**, 1169-1182 (2012).

31. Chapuis, A.G. et al. Transferred WT1-reactive CD8+ T cells can mediate antileukemic activity and persist in post-transplant patients. *Science translational medicine* **5**, 174ra127-174ra127 (2013).

32. Turtle, C.J. et al. CD19 CAR–T cells of defined CD4+: CD8+ composition in adult B cell ALL patients. *The Journal of clinical investigation* **126** (2016).

33. Janas, M.L., Groves, P., Kienzle, N. & Kelso, A. IL-2 regulates perforin and granzyme gene expression in CD8+ T cells independently of its effects on survival and proliferation. *The Journal of Immunology* **175**, 8003-8010 (2005).

34. Kim, S.T. et al. The αβ T cell receptor is an anisotropic mechanosensor. *Journal of Biological Chemistry* **284**, 31028-31037 (2009).

35. Cauda, V., Schlossbauer, A. & Bein, T. Bio-degradation study of colloidal mesoporous silica nanoparticles: effect of surface functionalization with organo-silanes and poly (ethylene glycol). *Microporous and Mesoporous Materials* **132**, 60-71 (2010).

36. Hollyman, D. et al. Manufacturing validation of biologically functional T cells targeted to CD19 antigen for autologous adoptive cell therapy. *Journal of immunotherapy (Hagerstown, Md.: 1997)* **32**, 169 (2009).

37. Jelley-Gibbs, D.M. et al. Repeated stimulation of CD4 effector T cells can limit their protective function. *The Journal of experimental medicine* **201**, 1101-1112 (2005).

38. Bignon, A. et al. DUSP4-mediated accelerated T-cell senescence in idiopathic CD4 lymphopenia. *Blood* **125**, 2507-2518 (2015).

39. Puu, G. & Gustafson, I. Planar lipid bilayers on solid supports from liposomes–factors of importance for kinetics and stability. *Biochimica et Biophysica Acta (BBA)-Biomembranes* **1327**, 149-161 (1997).

40. Anderson, N.A., Richter, L.J., Stephenson, J.C. & Briggman, K.A. Characterization and control of lipid layer fluidity in hybrid bilayer membranes. *Journal of the American Chemical Society* **129**, 2094-2100 (2007).

41. Collins, M.D. & Keller, S.L. Tuning lipid mixtures to induce or suppress domain formation across leaflets of unsupported asymmetric bilayers. *Proceedings of the National Academy of Sciences* **105**, 124-128 (2008).

42. Reich, C. et al. Asymmetric structural features in single supported lipid bilayers containing cholesterol and G M1 resolved with synchrotron X-ray reflectivity. *Biophysical journal* **95**, 657-668 (2008).

43. Longo, G.S., Schick, M. & Szleifer, I. Stability and liquid-liquid phase separation in mixed saturated lipid bilayers. *Biophysical journal* **96**, 3977-3986 (2009).

44. Parodi, A. et al. Synthetic nanoparticles functionalized with biomimetic leukocyte membranes possess cell-like functions. *Nature nanotechnology* **8**, 61-68 (2013).

45. Hu, C.-M.J. et al. Erythrocyte membrane-camouflaged polymeric nanoparticles as a biomimetic delivery platform. *Proceedings of the National Academy of Sciences* **108**, 10980-10985 (2011).

46. Fang, R.H. et al. Cancer cell membrane-coated nanoparticles for anticancer vaccination and drug delivery. *Nano letters* **14**, 2181-2188 (2014).

47. Kwong, B., Liu, H. & Irvine, D.J. Induction of potent anti-tumor responses while eliminating systemic side effects via liposome-anchored combinatorial immunotherapy. *Biomaterials* **32**, 5134-5147 (2011).

48. Koo, H. et al. Bioorthogonal Copper-Free Click Chemistry In Vivo for Tumor-Targeted Delivery of Nanoparticles. *Angewandte Chemie International Edition* **51**, 11836-11840 (2012).

49. Desai, R.M., Koshy, S.T., Hilderbrand, S.A., Mooney, D.J. & Joshi, N.S. Versatile click alginate hydrogels crosslinked via tetrazine–norbornene chemistry. *Biomaterials* **50**, 30-37 (2015).

50. Granéli, A., Rydström, J., Kasemo, B. & Höök, F. Formation of supported lipid bilayer membranes on SiO2 from proteoliposomes containing transmembrane proteins. *Langmuir* **19**, 842-850 (2003).

Chapter 5: Conclusions, Implications, and Future Directions

5.1 Conclusions

In this thesis, we developed two biomaterial systems for cancer immunotherapy applications. In Chapter 3, we developed a method for processing cancer cells that co-localizes native cancer antigens with adjuvants within nano- to microscale particles. These particles mimic natural pathogens in size and in their physical co-localization of prospective antigens and danger signals. Biochemical characterization of the particles revealed that they retained protein content from various intracellular compartments, suggesting that the retained protein could serve as a diverse source of prospective native cancer antigens for cancer vaccination. The particles could also be loaded with various adjuvants having diverse physicochemical properties. These particles were found to be more efficient at facilitating DC activation and antigen presentation *in vitro* than soluble mixtures of antigen and adjuvant, and promoted a greater antigen-specific T cell response than soluble mixtures of cancer cell lysate and adjuvant when used for vaccination in mice. Together, these observations demonstrate the utility of these particles for cancer vaccination and suggest that they may represent a more effective substitute for soluble mixtures of antigens and adjuvants in non-targeted cancer vaccines.

In Chapter 4, we developed a modular biomaterial that can release soluble cues in a controlled manner, and also surface-present cues locally on a synthetic lipid bilayer. This material facilitates the presentation of soluble and endogenously cell surface-localized T cell cues in a manner that mimics how these cues are naturally presented by APCs. Specifically, we demonstrated that functional T cell cues could be efficiently attached to the surface of the lipid bilayer at a density defined by the lipid formulation, and that T cell cytokines could be released

to interacting T cells in a paracrine manner. When the material was formulated to present polyclonal T cell activating cues, it expanded T cells faster than industry-standard commercial T cell expansion beads. Despite the increased expansion rate, the T cells retained a functional phenotype. When this material was formulated to present specific antigens, it promoted robust antigen-specific expansion of functional T cell subpopulations from complex T cell isolates or PBMCs. This composite material represents a flexible system that can be adapted to present diverse repertoires of cues to T cells, and that can be used for the rapid expansion of functional T cells.

5.2 Implications

This work demonstrates the importance of the spatiotemporal context in which cues are presented to the immune system. Further, it supports the idea that designing systems to present cues in patterns that mimic natural contexts can lead to more robust responses from the immune system. Overall, many current cancer immunotherapy approaches present cues to the immune system with limited to no spatiotemporal control. Addressing this lack of control, such as through the use of biomaterial systems like those described in this thesis, could allow for the development of therapies with greater efficacy and lower toxicity.

In Chapter 3, we developed a method for preparing particles that were co-loaded with mixtures of native cancer antigens and adjuvants. These particles were found to elicit a more robust antigen-specific T cell response in mice than soluble mixtures of antigens and adjuvants. The reasons underlying this enhanced effectiveness are likely two-fold: (1) packaging of the cues in pathogen-sized particles leading to enhanced uptake by APCs, and (2) physical co-localization

of the cues. Importantly, unlike most previous material systems that achieve these two properties, the approach described here is able to generate particles that are loaded with complex mixtures of undefined prospective cancer antigens, which is challenging for most synthetic particulate systems. In addition, we describe a generalizable approach for processing cancer cells, analogous to lysate derivation, which is not limited to particular cell types, and does not involve the additional synthesis of an exogenous base material. These observations suggest that these particles could potentially be used as a single-compartment substitute for soluble mixtures of tumor lysate and adjuvant to improve non-targeted cancer vaccines.

In Chapter 4, we described the development of a biomaterial that can present cues to T cells in a spatiotemporal context that mimics how these cues are naturally presented by APCs. In these studies, a minimal set of cues was loaded onto the material, comprised of a single TCR cue (αCD3 or pMHC), a single costimulatory cue (αCD28), and IL-2. This same set of cues is used in polyclonal T cell expansion approaches commonly employed in the clinic such as the rapid expansion protocol for tumor infiltrating lymphocyte (TIL) expansion[1], or commercial T cell expansion Dynabeads[2]. We observed that our material promoted faster polyclonal T cell expansion than industry-standard commercial T cell expansion beads, and that the expanded T cell product retained a functional phenotype. Together, these observations suggest that this system could be used as a substitute for current expansion approaches that utilize this same set of activating cues, for more efficient T cell expansion. We also observed that our material promoted robust antigen-specific expansion of rare T cell subpopulations from complex T cell isolates or PBMCs. This material could therefore also be used for the selective expansion of rare T cell populations such as circulating cancer-specific T cells[3, 4], or TILs with specific antigen specificity[5]. Importantly, we also observed that by manipulating parameters of the system, we

could tune the phenotype of the output cell products. Additionally, this modular system is amenable to the presentation of large, diverse repertoires of cues, and different material formulations can be easily and rapidly prepared. Together, this suggests that this system could be used to generate and test T cell products with diverse phenotypes for ACT, and that these studies could be iterated rapidly because of the ease with which different formulations of the material can be prepared. This could potentially enable the identification and production of significantly more optimized T cell products for ACT.

5.3 Future Directions

This thesis describes proof of concept studies that establish the utility of two material systems for cancer immunotherapy. Optimization of these systems will likely lead to more robust responses from the immune system.

The work presented in Chapter 3 describes a method for processing cancer cells to generate native cancer antigen and adjuvant co-loaded particles. Although we demonstrate that in the particle population, proteins from several distinct cellular compartments are retained in a relative distribution similar to the parent cells, we have an incomplete understanding of the exact repertoire of proteins retained in the particles. In addition, it is unclear whether particles in the overall population are associated with similar protein repertoires, or whether specific particle subpopulations are associated with proteins derived from particular cell compartments. We also find that with the current derivation method, we obtain a polydisperse distribution of particle sizes. If particle subpopulations associated with protein repertories from specific cell compartments exist, it would also be important to understand whether these various particle

subpopulations are associated with specific particle sizes or surface properties. If so, sorting particles, for example based on size or surface charge, could enable the enrichment of proteins from particular cell compartments for selective vaccination.

It could also be valuable to modify the particle derivation procedure in order to obtain a more monodisperse particle size distribution. Achieving a more monodisperse particle population would likely enable more uniform uptake of the particles by APCs, which would ensure that the generated T cell response would not be inherently biased towards specific subsets of proteins. Modifying the size of the particles would be particularly valuable if the size distribution could be maintained in a range that has shown to be optimal for lymph node drainage following subcutaneous or intradermal injection[6, 7]. In such case, the utility of the system as a standalone vaccine would likely be greatly enhanced. In general, gaining a better understanding of these particle properties would provide a clearer picture of the composition of the antigen mixture. From a practical perspective, it could also enable better control over the antigen targets that are being vaccinated against, and allow the system to be improved to generate more robust and controlled immune responses.

The material described in Chapter 4 is a flexible composite system that can facilitate the controlled release of soluble cues and present cues locally on the surface of a synthetic lipid bilayers. In the proof of concept work described in this thesis, we demonstrate that when the material is formulated to present a minimal set of cues for T cell activation, it outperforms a standard commercial T cell expansion system in which the same set of cues is presented. The greatest strengths of this material are its flexibility and tunability. The material is amenable to the presentation of very large repertoires of T cell cues, and the density of surface cues can be precisely defined. Future work on this system should involve diversification of cues, in

particular, (1) the addition of different or additional soluble cues, which can differentially direct T cell biasing or phenotype[8, 9], (2) the attachment of different combinations of co-stimulatory cues, many of which have non-redundant functions[10-13], and (3) the attachment of adhesion ligands, which also play a role in T cell activation[10, 13]. When used for antigen-specific T cell expansion, it would also be possible to have the material present a combination of different antigens and simultaneously expand multiple T cell subpopulations. Diversifying the system in these ways and others will likely enable the production of significantly more functional T cell products.

In the work described in this thesis, cues were attached to the surface of the material via biotin-streptavidin interactions. Although this approach was found to facilitate efficient attachment, the need for streptavidin as an intermediate adds an additional step to the preparation process. In addition, we observed that the streptavidin and material concentrations needed to be maintained below a certain threshold, or else extensive streptavidin-mediated aggregation of the material took place. To obviate the need for such an intermediate, alternate methods can be used to attach cues to the bilayer surface. For example, cues can be covalently attached to lipids[14, 15], or via alternate forms of affinity pairing, such as poly-histidine tagged proteins with chelator lipids[16].

In addition to the repertoire of cues presented by the material, the material itself is also highly amenable to tuning, and modification of material properties can affect the spatiotemporal context in which cues are presented. For example, MSR particle size, pore structure, and surface chemistry can be varied through modifications to the synthesis protocol. Changing these properties would likely affect the loading and release kinetics of soluble payloads. Modifications to the MSR synthesis protocol could also affect the degradation kinetics of the material. This

would affect the temporal pattern with which activating cues are presented by the material, which has been shown to be an important determinant of downstream T cell phenotype and function[17, 18]. Diversifying the lipid formulation, for example, by including lipids with limited miscibility, could facilitate spontaneous lipid partitioning and microdomain formation, which could allow for the pre-clustering of cues[19-21]. In addition, the lipid formulation could be modified to prepare synthetic bilayers that more closely mimic natural APC plasma membranes, for example, with respect to composition or fluidity[22], which could enable the preparation of material formulations that even more closely mimic APCs. Overall, this composite material system can be modified in many different ways that affect how T cells sense the presented cues and subsequently respond. Future work on this system should expand the explored parameter space in order to generate material formulations that promote faster expansion of more functional T cells.

5.4 References

1. Dudley, M.E., Wunderlich, J.R., Shelton, T.E., Even, J. & Rosenberg, S.A. Generation of tumor-infiltrating lymphocyte cultures for use in adoptive transfer therapy for melanoma patients. *Journal of immunotherapy (Hagerstown, Md.: 1997)* **26**, 332 (2003).
2. Rasmussen, A.-M. et al. Ex vivo expansion protocol for human tumor specific T cells for adoptive T cell therapy. *Journal of immunological methods* **355**, 52-60 (2010).
3. Mazzarella, T. et al. Ex vivo enrichment of circulating anti-tumor T cells from both cutaneous and ocular melanoma patients: clinical implications for adoptive cell transfer therapy. *Cancer Immunology, Immunotherapy* **61**, 1169-1182 (2012).
4. Chapuis, A.G. et al. Transferred WT1-reactive CD8+ T cells can mediate antileukemic activity and persist in post-transplant patients. *Science translational medicine* **5**, 174ra127-174ra127 (2013).
5. Rosenberg, S.A. & Restifo, N.P. Adoptive cell transfer as personalized immunotherapy for human cancer. *Science* **348**, 62-68 (2015).

6. Manolova, V. et al. Nanoparticles target distinct dendritic cell populations according to their size. *European journal of immunology* **38**, 1404-1413 (2008).

7. Reddy, S.T. et al. Exploiting lymphatic transport and complement activation in nanoparticle vaccines. *Nature biotechnology* **25**, 1159-1164 (2007).

8. Waldmann, T.A. The biology of interleukin-2 and interleukin-15: implications for cancer therapy and vaccine design. *Nature Reviews Immunology* **6**, 595-601 (2006).

9. Caserta, S., Alessi, P., Basso, V. & Mondino, A. IL-7 is superior to IL-2 for ex vivo expansion of tumour-specific CD4+ T cells. *European journal of immunology* **40**, 470-479 (2010).

10. Hasan, A., Selvakumar, A. & O'Reilly, R. Artificial Antigen Presenting Cells: An Off the Shelf Approach for Generation of Desirable T-Cell Populations for Broad Application of Adoptive Immunotherapy. *Advancements in Genetic Engineering* **2015** (2015).

11. Zeng, W., Su, M., Anderson, K.S. & Sasada, T. Artificial antigen-presenting cells expressing CD80, CD70, and 4-1BB ligand efficiently expand functional T cells specific to tumor-associated antigens. *Immunobiology* **219**, 583-592 (2014).

12. Hendriks, J. et al. CD27 is required for generation and long-term maintenance of T cell immunity. *Nature immunology* **1**, 433-440 (2000).

13. Maus, M.V. et al. Ex vivo expansion of polyclonal and antigen-specific cytotoxic T lymphocytes by artificial APCs expressing ligands for the T-cell receptor, CD28 and 4-1BB. *Nature biotechnology* **20**, 143-148 (2002).

14. Kwong, B., Liu, H. & Irvine, D.J. Induction of potent anti-tumor responses while eliminating systemic side effects via liposome-anchored combinatorial immunotherapy. *Biomaterials* **32**, 5134-5147 (2011).

15. Granéli, A., Rydström, J., Kasemo, B. & Höök, F. Formation of supported lipid bilayer membranes on SiO2 from proteoliposomes containing transmembrane proteins. *Langmuir* **19**, 842-850 (2003).

16. Koo, H. et al. Bioorthogonal Copper-Free Click Chemistry In Vivo for Tumor-Targeted Delivery of Nanoparticles. *Angewandte Chemie International Edition* **51**, 11836-11840 (2012).

17. Jelley-Gibbs, D.M. et al. Repeated stimulation of CD4 effector T cells can limit their protective function. *The Journal of experimental medicine* **201**, 1101-1112 (2005).

18. Bignon, A. et al. DUSP4-mediated accelerated T-cell senescence in idiopathic CD4 lymphopenia. *Blood* **125**, 2507-2518 (2015).

19. Collins, M.D. & Keller, S.L. Tuning lipid mixtures to induce or suppress domain formation across leaflets of unsupported asymmetric bilayers. *Proceedings of the National Academy of Sciences* **105**, 124-128 (2008).

20. Reich, C. et al. Asymmetric structural features in single supported lipid bilayers containing cholesterol and G M1 resolved with synchrotron X-ray reflectivity. *Biophysical journal* **95**, 657-668 (2008).

21. Longo, G.S., Schick, M. & Szleifer, I. Stability and liquid-liquid phase separation in mixed saturated lipid bilayers. *Biophysical journal* **96**, 3977-3986 (2009).

22. Anderson, N.A., Richter, L.J., Stephenson, J.C. & Briggman, K.A. Characterization and control of lipid layer fluidity in hybrid bilayer membranes. *Journal of the American Chemical Society* **129**, 2094-2100 (2007).

Appendix A: Chapter 4 Supplemental Materials

Lipid	alternate name	alternate name	Avanti Cat#	Tm (°C)
1,2-dioleoyl-*sn*-glycero-3-phosphocholine	18:1 (Δ9-Cis) PC	DOPC	850375C	-17
1-palmitoyl-2-oleoyl-sn-glycero-3-phosphocholine	16:0-18:1 PC	POPC	850457C	-2
1,2-distearoyl-*sn*-glycero-3-phosphocholine	18:0 PC	DSPC	850365C	55
1,2-di-(9Z-octadecenoyl)-*sn*-glycero-3-phosphoethanolamine-N-(cap biotinyl)	PE-cap-biotin		870273C	
1,2-dioleoyl-*sn*-glycero-3-phosphoethanolamine-N-(carboxyfluorescein)	18:1 PE CF		810332C	

Table A1. Lipids used in Chapter 4.

Supplemental Movies

Movie A1. Representative z-stack of lipid-coated MSRs (1 mol% fluorophore-tagged lipid, green).

Movie A2. Representative z-stack of lipid-coated MSRs with live primary mouse T cells (1 mol% fluorophore-tagged lipid, green; T cells, red).

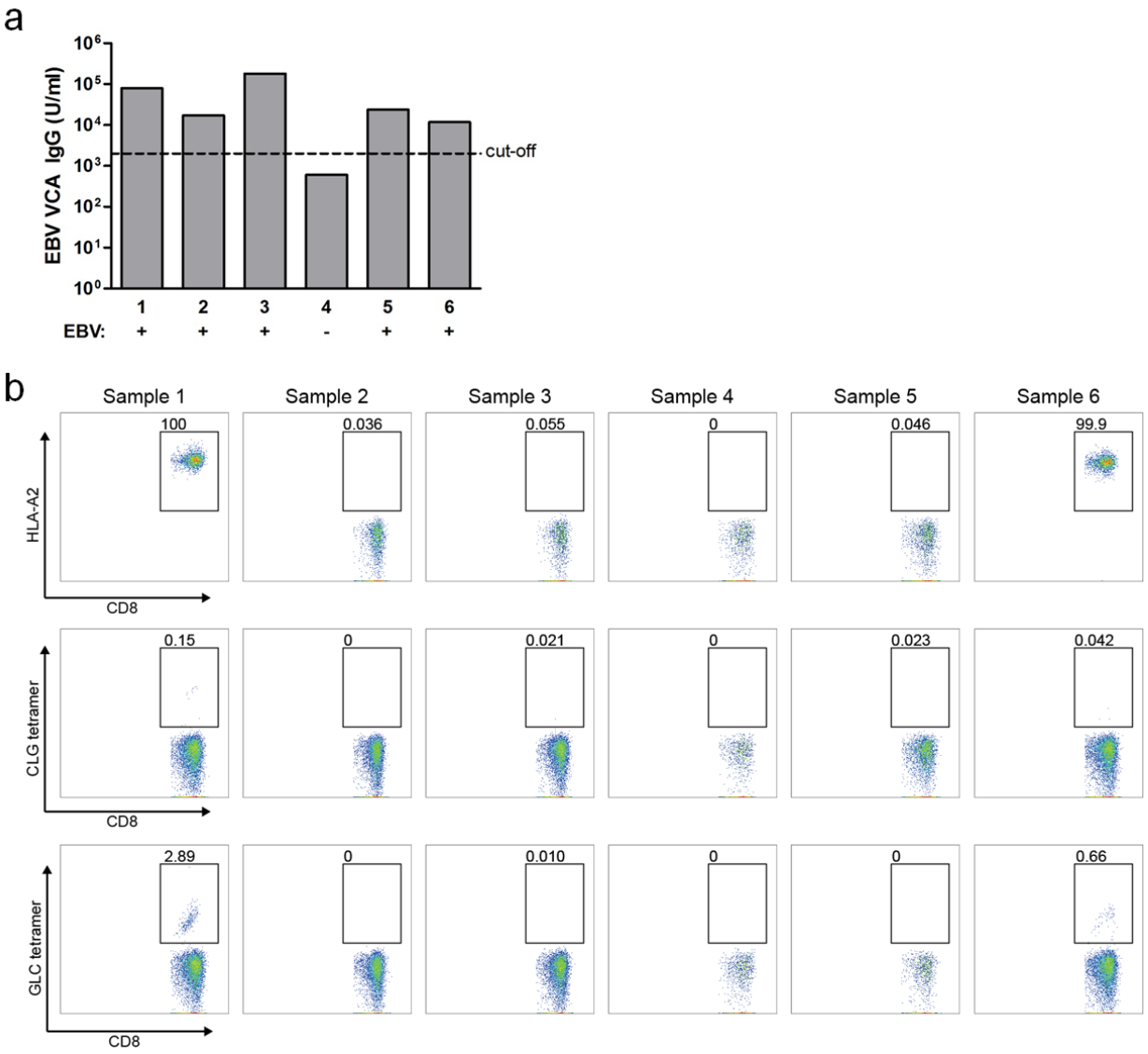

Figure A1. Evaluation of EBV-experience and HLA-A2 expression in human blood samples. (a) Quantification of anti-EBV viral capsid antigen (VCA) IgG in human serum samples via ELISA. Samples that had IgG levels higher than the cut-off, as defined by the manufacturer, were considered EBV-experienced. (b) Measurement of HLA-A2 expression on CD8+ T cells from human PBMC samples. Sample 6 is sample "A" in Tables 4.1-4.2, sample 1 is sample "B" in Tables 4.1-4.2.